ELECTRICAL CONDUCTION IN FERROMAGNETIC METALS

J. W. F. DORLEIJN

ELECTRICAL CONDUCTION IN FERROMAGNETIC METALS

PROEFSCHRIFT

TER VERKRIJGING VAN DE GRAAD VAN DOCTOR IN DE TECHNISCHE WETENSCHAPPEN AAN DE TECHNISCHE HOGESCHOOL DELFT, OP GEZAG VAN DE RECTOR MAGNIFICUS, PROF. IR. L. HUISMAN, VOOR EEN COMMISSIE AANGEWEZEN DOOR HET COLLEGE VAN DEKANEN TE VERDEDIGEN OP WOENSDAG 2 MAART 1977 TE 16.00 UUR

DOOR

JAN WILLEM FREDERIK DORLEIJN

NATUURKUNDIG INGENIEUR
GEBOREN TE DELFT

DIT PROEFSCHRIFT IS GOEDGEKEURD DOOR DE PROMOTOR
PROF. DR. J. J. VAN LOEF

Dankwoord

Het hier beschreven onderzoek is verricht in het Natuurkundig Laboratorium van de N.V. Philips' Gloeilampenfabrieken. De directie van dit laboratorium ben ik erkentelijk voor de gelegenheid welke zij mij bood om dit proefschrift te bewerken.

Graag betuig ik mijn dank aan allen die aan het hier beschreven onderzoek een bijdrage hebben geleverd.

CONTENTS

GUIDE TO MAJOR TABLES

The work described in this thesis may be referred to as:

J. W. F. Dorleijn, Philips Res. Repts **31**, 287, 1976.

1. INTRODUCTION

This paper reports an extensive experimental investigation of electrical-transport properties in alloys based on either nickel or iron, as representatives of the ferromagnetic metals.

Electrical conduction is phenomenologically different in ferromagnetic metals as compared to non-magnetic metals. In the first place the residual resistivities due to small amounts of two metals dissolved in iron or nickel cannot be simply added in order to derive the total resistivity of the corresponding ternary alloy. In a ferromagnetic solvent deviations from this rule of additivity, Matthiessen's rule, can easily be as large as a factor two.

A phenomenon that is characteristic of ferromagnetic metals and does not occur in non-magnetic metals is the resistivity anisotropy. The effect is illustrated in fig. 1.1. Two extreme situations can be distinguished for the resistivity, in

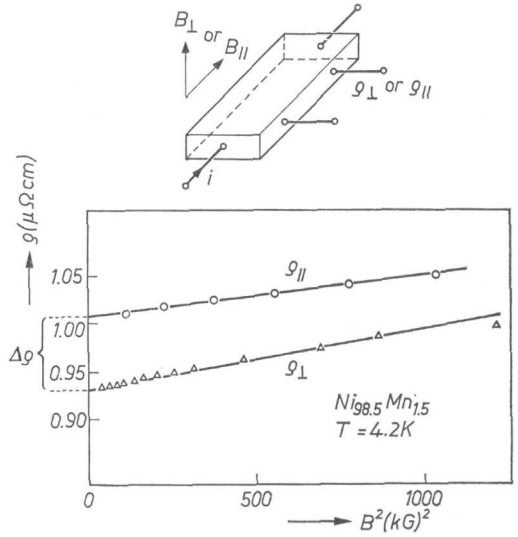

Fig. 1.1. The resistivity of a sample of $Ni_{98.5}Mn_{1.5}$ at 4.2 K as a function of B^2 for the two extreme cases $B \parallel i$ and $B \perp i$. We define $B = H_{ext} + H_{dem} + 4\pi M_s$. The anisotropy effect is defined as the ratio $\Delta\varrho/\varrho_{\parallel}$ at $B = 0$.

which the saturation magnetization of the ferromagnetic metal is either parallel or perpendicular to the electrical current. The resistivity anisotropy is defined as $(\varrho_{\parallel} - \varrho_{\perp})/\varrho_{\parallel}$, in which the ϱ values are obtained from the values measured in external magnetic fields, sufficiently high to saturate the sample magnetically by extrapolation to zero induction B (see fig. 1.1). At low temperatures the anisotropy effect can be quite large (13.5% in NiCo alloys, 11% in FeV alloys). At room temperature the effect can still be considerable, up to 6% in concen-

trated NiCo alloys [1]) and has been found of technical interest in the field of magnetic recording [2,3,4]).

The Hall effect of ferromagnetic metals is also quite different as compared to non-magnetic metals. In non-magnetic metals the Hall voltage V_H is simply proportional to B. In a ferromagnetic metal there is an additional contribution to the Hall effect, which contribution does not vary with B. Its magnitude is established by extrapolating to $B = 0$ the values of the Hall effect experimentally observed in fields that are sufficiently high to saturate the samples magnetically (see fig. 1.2). Contrary to the normal Hall effect the anomalous effect varies

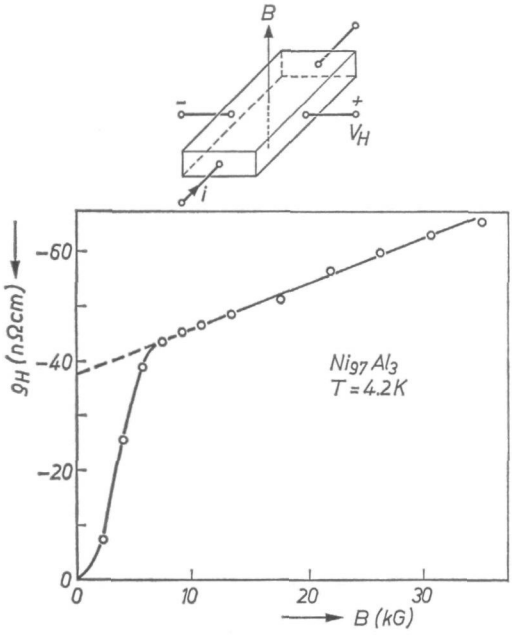

Fig. 1.2. The Hall resistivity ϱ_H as a function of B; ϱ_H is obtained from the Hall voltage V_H according to $\varrho_H = V_H\, d/I$ where d is the thickness of the sample and I is the total current.

markedly with resistivity. As a consequence, the anomalous Hall effect tends to zero in pure ferromagnetic metals at zero temperature while in ferromagnetic alloys it depends both on the concentration and the kind of the solute metal.

Although the above peculiar effects have been known to exist in ferromagnetic metals for a long time, the fundamental understanding of their origin has remained far from complete. This is at least partially due to the lack of an extensive coherent set of experimental data. There is a relatively large number of papers (see below) dealing with experimental studies of electrical transport in ferromagnetic metals. In most cases, however, the relevant properties were not measured in the same alloys which makes it difficult to obtain an overall

picture. In addition in many studies the influence of impurities on the transport properties was examined by studying their temperature dependence. In those studies a fairly detailed model is required to take scattering by phonons into account. In these scattering processes the spin direction of the current carriers is not necessarily conserved.

We have obtained a coherent set of experimental data on the electrical-transport properties of nickel- and iron-based alloys at low temperatures which can be analysed without making assumptions on scattering by phonons or spin waves. About 475 binary and ternary alloys representing practically all elements that can be dissolved in nickel or iron up to concentrations of 3 at%, were investigated. At low temperature the resistivity, the resistivity anisotropy, the normal and the anomalous Hall effect of all these alloys was measured in magnetic fields up to about 50 kOe. Details of the experiments are given in chapter 3.

The resistivity of elements dissolved in iron or nickel is insufficiently characterized by their residual resistivity in $\mu\Omega$cm/at%. It turns out that the residual resistivity produced by a given impurity should preferably be resolved into two components, representing the two residual resistivities in a two-current model. Here the two currents are the charge carriers with magnetic moment either parallel or antiparallel to the magnetization of the ferromagnetic metal. The principle of two-current conduction in ferromagnetics has been proposed by Mott in 1936 [5,6,7]). Recently its usefulness has been amply demonstrated as, for instance, in a review by Fert and Campbell [8]). The two-current model is also essential in a description of the thermo-electric power (see Cadeville and Roussel [9]) and further references given there).

In nearly all investigations the two residual resistivities for a given impurity were derived from an analysis of the temperature dependence of the resistivity of the corresponding binary alloy. Temperature-dependent deviations from Matthiessen's rule were observed in binary Fe-based alloys by Campbell et al.[10]) and by Schwerer et al.[11]). Deviations from Matthiessen's rule as a function of temperature have been studied by Loegel and Gautier [12]) for Co-based alloys, by Durand and Gautier [13]) and Hugel [14]) for both Co- and Ni-based alloys, and by Price and Williams [15]) for Fe-, Co- and Ni-based alloys. Similar studies for Ni-based alloys have been made by Fert and Campbell [16]), Farrell and Greig [17]), Gautier and Loegel [18]) and Schwerer and Conroy [19]).

A more direct method to derive sub-band residual resistivities consists in analysing the low-temperature resistivities of ternary alloys. In the past this method has been applied in a few cases only, mainly because of the large amount of preparative work involved. This method was used by, for example. Fert and Campbell [16]) in an analysis of NiCrMn alloys, Leonard et al.[20]) for NiCoCr alloys and Fert and Campbell [8]) for NiCoV and NiFeV alloys. Hugel [14]) analysed NiCoGe, NiCoGa and NiCrGe alloys. The same method

has been used by Durand and Gautier [13]) for CoIrRe alloys and by Loegel and Gautier [12]) for CoIrFe, CoRuFe and CoOsFe alloys. Deviations from the rule of additivity of individual impurity resistivities at 4.2 K in ternary iron-based alloys were observed by Campbell et al.[10]).

We opted for this method to derive the two residual resistivities for impurity metals in general. By combining a given element with different partners, e.g. Cr in NiCrAl, NiCrFe, NiCrMn or NiCrTi, the validity of the description of the resistivity due to Cr in nickel in terms of two residual resistivities can be investigated (see chapters 2 and 4).

The dependence of the resistivity of a ferromagnetic metal on the angle between magnetization and current (resistivity anisotropy) was first described as long ago as 1858, by Thomson (Phil. Mag. IV, **15**, p. 469), but a hundred years passed before the first systematic investigations of the effect were carried out by Smit [21]), Van Elst and Gorter [22]), Van Elst [1]) and Berger [23]). More recently the effect has been studied by Campbell [24]), Campbell et al.[25]), Vasilyev [26]), Campbell [27]), Dedić [28]) and Jaoul and Campbell [29]).

To understand the origin of the resistance anisotropy it would be desirable to have a fairly complete knowledge of the magnitude of the effect due to a large variety of solutes. This means experiments on dilute binary alloys at low temperatures for all impurity metals that can be dissolved in a given ferromagnetic metal at a sufficiently high concentration. At the start of the present investigation extensive experimental information was available only for nickel-based alloys. See for a survey of numerical data McGuire and Potter [30]) and Jaoul [31]). The information concerning iron-based alloys was scarce. A small effect was known to exist in pure iron at room temperature [32]) and a large effect in FeV alloys at low temperature [33]). We investigated the effect for practically all metals that can be dissolved in iron and nickel in maximum concentrations of about 5 at%. The observations could in a consistent way be described in the two-current model (see chapters 2 and 5).

The anomalous Hall effect, too, has a long history. One of the first descriptions was given by Kundt [34]) in 1893. A vast amount of experimental information on this effect is available for the case of concentrated ferromagnetic alloys. A review is given by Hurd [35]); see also Cohen et al.[36]). Much less information, however, is available on dilute alloys at low temperatures. Such information is preferred because the source of scattering is well defined. Investigations of this type have been performed by Jaoul [31]), Fert and Jaoul [37]), Huguenin and Rivier [38,39,40,41]), Rivier [42]) and Rivier and Huguenin [43]) on dilute nickel-based alloys and that by Majumdar and Berger [44]) on two binary iron-based alloys. It appears from these investigations that the anomalous Hall resistivity ϱ_{aH} can be resolved into two contributions which depend linearly and quadratically, respectively, on the resistivity $\varrho_{\perp}$

$$\varrho_{aH} = \varphi_{sk}\,\varrho_{\perp} + b\,\varrho_{\perp}^{2}. \tag{1.1}$$

We investigated both φ_{sk} and b in great detail for both iron and nickel alloys and find that φ_{sk} and b depend on the impurity. Furthermore, the values of φ_{sk} and b can be described quite satisfactorily in terms of the two-current model.

The two-current model is used throughout this paper in the analysis of our measurements. The model is introduced in chapter 2, where the main body of data is presented also in order to demonstrate the relevance of the model. Chapter 2 in fact is the central part of the paper. In the succeeding chapters we give more details concerning the analysis of experimental data and the accuracy of the results. We also give an extensive comparison between the present results and the experimental and theoretical work reported in the literature.

One of the conclusions of this paper is that the theory of electrical transport properties of ferromagnetic metals is still far from satisfactory. It is thus important to have the bare experimental data accessible for future (alternative) interpretation. Our data can be found in the appendix.

2. THE TWO-CURRENT MODEL FOR IRON AND NICKEL ALLOYS

2.1. Electrical conduction in ferromagnetic metals

The electrical conduction in ferromagnetic metals such as iron and nickel differs from that in ordinary metals such as aluminium or copper for two reasons: iron and nickel are transition metals and they are ferromagnetic.

In ordinary metals the electrons can be devided into core electrons and valence electrons. Core electrons have a large probability density near the center of the atom and a very small one at the boundaries of the Wigner–Seitz atomic cells. As a consequence core electrons hardly contribute to the cohesive energy of the solid metal. If treated in a band model they are housed in fully occupied narrow bands. Valence electrons on the contrary are divided approximately uniformly throughout the crystal. They occupy a broad conduction band which is not very different from a parabolic one ($\varepsilon \propto k^2$), see fig. 2.1.

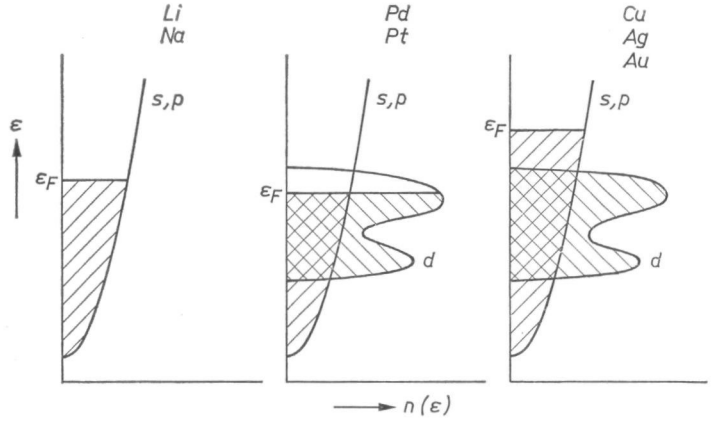

Fig. 2.1. The conduction-band density of states $n(\varepsilon)$ as a function of the energy ε for simple metals, transition metals and the noble metals; ε_F is the Fermi energy. The drawing is schematical i.e. the width of the d band is not necessarily always the same.

For such a parabolic band of nearly free electrons the electrical conductivity can be expressed in terms of the electronic charge e, an effective electron mass m^*, a relaxation time τ and the density of electrons n as

$$\sigma = n\, e^2\, \tau / m^*. \tag{2.1}$$

Transition metals are metals belonging to groups IIIB, IVB, VB, VIB, VIIB and VIII of the Periodic Table. They are special because the electrons of the partially filled d shell cannot easily be classified as either core or valence electrons. They differ from valence electrons as their spatial distribution is far from uniform. Consequently bands formed from d electrons are much narrower than a normal conduction band. Neither are they core electrons, since the d bands

are not completely full and d electrons have an important probability density in the region between neighbouring atoms. The latter is clearly reflected in the high cohesive energies or boiling points of transition metals (see table 2-I).

The difference between a non-transition metal and a paramagnetic transition metal can be schematically illustrated by means of fig. 2.1. The strict separation of s, p and d electrons in the range of energies that the two bands have in common is rather artificial since hybridization will occur.

In fig. 2.1 we have also sketched the band filling for the noble metals Cu, Ag and Au. There is a d band and hence a contribution to the cohesive energy but, in contrast to the situation in transition metals, this band of d electrons is filled up.

The effect on the electrical conduction of adding d electrons to a metal in which conduction takes place by s-like carriers can be understood qualitatively using relationship (2.1). On the one hand additional d electrons will increase the conductivity via the increase in n. The effect of increasing n is only moderate since m^* is large for d electrons (m^* is connected with the curvature of the band: $m^* = \hbar^2/(\partial^2\varepsilon/\partial k^2)$). On the other hand the conductivity is decreased since the introduction of d states enhances the density of states at the Fermi surface $n(\varepsilon_F)$, which directly influences the characteristic time for scattering τ; this relaxation time τ will be shorter when the number of states into which an electron can be scattered becomes greater. The increase of $n(\varepsilon_F)$ expected from fig. 2.1 is clearly demonstrated in table 2-I where we have collected values for the coefficient γ of the linear term in the low-temperature heat capacity. It will be seen that as a rule γ, which is approximately proportional to $n(\varepsilon_F)$, has a considerably larger value for transition metals than for other metals. Assuming that the relaxation time τ is inversely proportional to the number of states into which a charge carrier can be scattered, it becomes plausible that the electrical resistivity of transition metals exceeds that of noble metals. In table 2-I this is qualitatively demonstrated by the resistivities of metals at a comparable temperature, i.e. the Debije temperature (ϑ_D).

For the electrical-conduction properties of iron and nickel it is important not only that they are transition metals but also that they are ferromagnetic. In ferromagnetic metals it is appropriate to distinguish the electrons according to the direction of their magnetic moment, either parallel or antiparallel to the total magnetization. In this paper we will indicate the charge carriers with magnetic moment parallel to the total magnetization, i.e. the majority-spin band, with "up" or ↑. Charge carriers in the minority-spin band are indicated with "down" or ↓. Throughout this work we will use the word spin in the sense of magnetic moment, regardless of the negative g value of the electron. This division according to spin direction leads to a picture like that in fig. 2.2, where the two bands are shifted over some distance as regards energy. Now the two bands will not be filled equally, leading to a non-zero magnetization.

TABLE 2-I

IA												IIIA	IVA	VA	VIA	VIIA	VIIIA
H 20																	He 4.2
	IIA																
Li 1615 1.63 10.9	Be 2745 0.17 15.9											B 4275	C 4100	N 77	O 90	F 85	Ne 27
Na 1156 1.38 2.54	Mg 1363 1.3 5.83	IIIB	IVB	VB	VIB	VIIB	transition metals VIII			IB	IIB	Al 2793 13.5 3.98	Si 3540	P 550(w)	S 718	Cl 239	Ar 87
K 1032 2.08 2.22	Ca 1757 2.9 2.81	Sc 3104 10.7 57.1	Ti 3562 3.35 61.4	V 3682 9.26 25.6	Cr 2945 1.40 27.5	Mn 2335 9.20 193	Fe 3135 4.98 15.6	Co 3201 4.73 8.75	Ni 3187 7.02 10.7	Cu 2836 0.695 1.98	Zn 1180 0.64 6.56	Ga 2478 0.596 16.1	Ge 3107	As 876 0.19	Se 958	Br 332	Kr 120
Rb 961 2.41 2.37	Sr 1650 3.6 10.7	Y 3611 10.2 55.5	Zr 4682 2.80 41.8	Nb 5017 7.79 13.5	Mo 4912 2.0 8.08	Tc (4538)	Ru 4423 3.3 15.1	Rh 3970 4.9 7.81	Pd 3237 9.42 9.75	Ag 2436 0.646 1.23	Cd 1040 0.688 5.15	In 2346 1.69 3.20	Sn 2876 1.78 7.46	Sb 1860 0.11 29.5	Te 1261	I 458	Xe 165
Cs 944 3.20 2.58	Ba 2171 2.7 14.5	La 3730 10.0 38.0	Hf 4876 2.16 26.1	Ta 5731 5.9 10.7	W 5828 1.3 7.19	Re 5869 2.3 27.1	Os 5285 2.4 15.4	Ir 4701 3.1 7.26	Pt 4100 6.8 8.46	Au 3130 0.729 1.23	Hg 630 1.79	Tl 1746 1.47 4.36	Pb 2023 2.98 7.47	Bi 1837 0.003 46.8	Po	At	Rn 211
Fr	Ra	Ac															

key

Ni
3187 → boiling point in K at 1 atm, data from Hultgren et al.[60]).
7.02 → electronic heat capacity constant γ in mJ/(mol K^2), data from Kittel [61]).
10.7 → resistivity in $\mu\Omega$cm at the Debije temperature, calculated from data given by Kittel[61]).

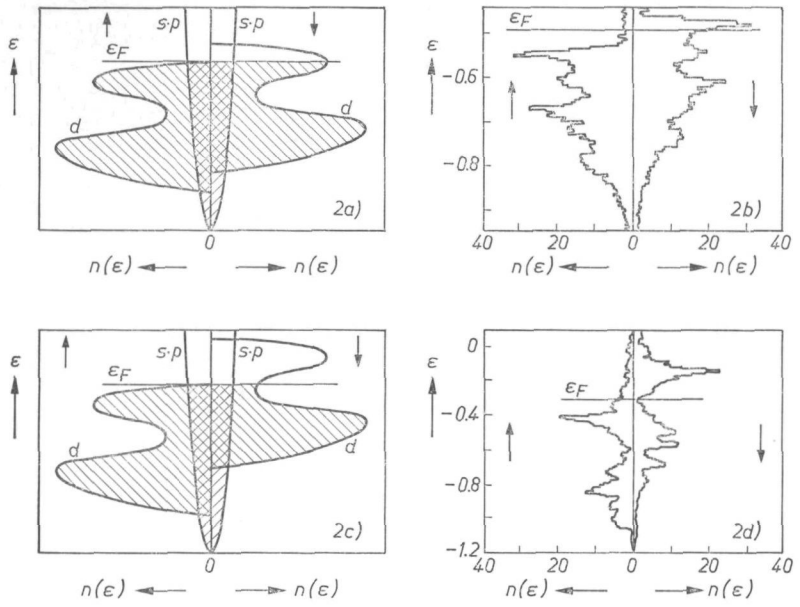

Fig. 2.2. Density of states curves for ferromagnetic nickel top and iron (bottom). Curves on the left are purely schematic, those on the right are results of band-structure calculations by Langlinais and Callaway [45]) for nickel and by Duff and Das [46]) for iron, in the form of summations over the Brillouin zones. A quantitatively similar result for iron was obtained by Tawil and Callaway [51]).

Moreover, the densities of states may be quite different for majority (↑)- and minority(↓)-spin bands. For nickel the resulting difference in $n(\varepsilon_F)$ is very large since the majority d band becomes practically filled. The schematic band pictures in fig. 2.2 have been drawn in accordance with density of states histograms obtained in band-structure calculations such as those of Langlinais and Callaway [45]) for nickel, and those of Duff and Das [46]) for iron. In the band-structure calculations only the total density of states can be given for each spin direction. The s-band density of states, however, is apparent at both low and high energies; in the intermediate energy region the separation into s, p or d electrons is arbitrary. Since in the schematic representation the density of states of s and p electrons is relatively small, the question of whether or not there is a magnetic polarization of s and p electrons is of little importance here.

The separation of electrons into two spin bands is of central importance to the electrical conduction at low temperatures. As was suggested by Mott [5,6,7]) scattering events with conservation of spin direction become much more probable at low temperature (i.e. temperatures much lower than the Curie temperature) than scattering events in which the spin direction is changed. Mott's suggestions lead to a description of conduction by two independent currents in parallel (fig. 2.3). Since the Fermi surfaces for majority (↑) and minority (↓)

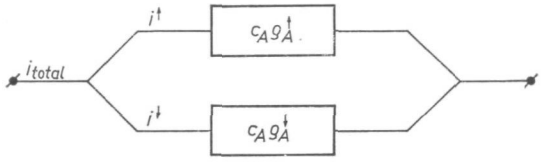

Fig. 2.3. The two-current model for ferromagnetic metals at low temperatures. An impurity A is characterized by two specific residual resistivities $\varrho_A{}^{\uparrow}$ and $\varrho_A{}^{\downarrow}$.

electrons can be very different there is no reason to assume equal relaxation times or conductivities for the two spin currents.

A division of charge carriers according to the direction of their magnetic moment may seem somewhat arbitrary in view of the many other subdivisions that can imagined (e.g. electrons versus holes, s versus d electrons, carriers with different τ values). It will be found that Mott's suggestion on its own offers a simple and fairly complete explanation of the experimental data. The consequences of this first subdivision according to spin direction will prove to be much more important than further refinements can be, mainly because of the larger differences in densities of states and hence in relaxation times that can be accounted for in a two-spin-current description.

2.2. The residual resistivity of dilute ternary alloys

If two impurity metals A and B, are dissolved simultaneously at concentrations c_A and c_B in an ordinary metal, e.g. copper, the electrical resistivities caused by the impurities can be simply added. This is Matthiessen's rule:

$$\varrho = c_A \varrho_A + c_B \varrho_B, \tag{2.2}$$

where ϱ_A and ϱ_B are the specific residual resistivities (in $\mu\Omega$cm/at%) measured in the corresponding binary alloy. Relation (2.2) presupposes that the impurities scatter independently. For instance it is required that the concentration of the impurities is small enough for the resistivity of corresponding binary alloys to be linearly dependent on the concentration.

In the same range of concentrations, however, relation (2.2) does not apply to ferromagnetic alloys, which is a consequence of the two-current model introduced above. In the two-current model the residual resistivity due to a given impurity (A) is characterized by two numbers giving the specific resistivity ($\varrho_A{}^{\uparrow}$ or $\varrho_A{}^{\downarrow}$) for each of the two currents. This immediately leads to the schematic representation of the resistivity in dilute ternary alloys given in fig. 2.4. It shows that Matthiessen's rule applies to each current separately but not to the total resistivity. The model in fig. 2.4 leads to

$$\varrho = \frac{(c_A \varrho_A{}^{\uparrow} + c_B \varrho_B{}^{\uparrow})(c_A \varrho_A{}^{\downarrow} + c_B \varrho_B{}^{\downarrow})}{c_A \varrho_A{}^{\uparrow} + c_B \varrho_B{}^{\uparrow} + c_A \varrho_A{}^{\downarrow} + c_B \varrho_B{}^{\downarrow}}. \tag{2.3}$$

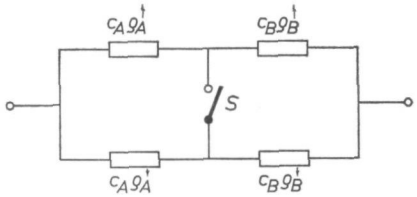

Fig. 2.4. The low-temperature resistivity of a ferromagnetic metal containing two different types of solutes. Matthiessen's rule would be valid if the switch S were closed.

If relation (2.2) were valid the total resistivity should, at low temperatures, equal

$$\varrho = c_A \frac{\varrho_A{}^{\uparrow}\,\varrho_A{}^{\downarrow}}{\varrho_A{}^{\uparrow} + \varrho_A{}^{\downarrow}} + c_B \frac{\varrho_B{}^{\downarrow}\,\varrho_B{}^{\uparrow}}{\varrho_B{}^{\uparrow} + \varrho_B{}^{\downarrow}}. \tag{2.4}$$

It will be readily seen that relation (2.3) leads to a higher value for ϱ than relation (2.4). We demonstrate this by means of the switch in fig. 2.4; the situation leading to relation (2.4) can be obtained by closing the switch, which is open if relation (2.3) applies. Since closing the switch can only lower the resistivity it follows that in the two-current model only positive (or zero) deviations from Matthiessen's rule are to be expected.

The deviations from Matthiessen's rule can in principle be very large, as can be seen from the following numerical example. Suppose we have a ternary alloy $Ni_{99}A_{0.5}B_{0.5}$ for which the specific residual resistivities of metal A are $\varrho_A{}^{\downarrow} = 10$ and $\varrho_A{}^{\uparrow} = 1$ (in $\mu\Omega$cm/at%) and those of metal B are simply the reverse $\varrho_B{}^{\downarrow} = 1$ and $\varrho_B{}^{\uparrow} = 10$. The residual resistivities of the binary alloys $Ni_{99}A$ and $Ni_{99}B$ are equal: 10/11 $\mu\Omega$cm. Matthiessen's rule, relation (2.2), would predict $\varrho = 10/11$ for the resistivity of all alloys $Ni_{99}A_{1-x}B_x$. In the two-current model, however, relation (2.3) yields $(10 + 1)/2 = 5.5$ $\mu\Omega$cm for both $\varrho^{\uparrow}$ and $\varrho^{\downarrow}$ in $Ni_{99}A_{0.5}B_{0.5}$. Thus the total resistivity is 2.75 $\mu\Omega$cm, which is very different from 10/11 $\mu\Omega$cm. The differences at other concentrations are

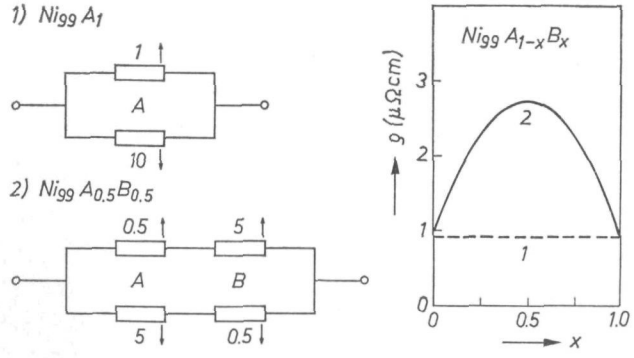

Fig. 2.5. Deviations from Matthiessen's rule for the resistivity of an alloy $Ni_{99}A_{1-x}B_x$ for which $\varrho_A{}^{\downarrow}/\varrho_A{}^{\uparrow} = 10$ and $\varrho_B{}^{\downarrow}/\varrho_B{}^{\uparrow} = 0.1$. The broken line (curve 1) is drawn according to Matthiessen's rule, the drawn curve (2) is in agreement with the two-current model.

shown in fig. 2.5. This numerical example may seem highly exaggerated. Deviations of a comparable magnitude nevertheless occur in experiments, as we show in fig. 2.6 for NiCoRh and FeCoV alloys.

Owing to the fact that there are large deviations from Matthiessen's rule in the two-current model, an obvious method to derive the sub-band residual resistivities for impurity metals in a ferromagnetic matrix is to fit numerically relation (2.3) to experimentally obtained points such as those in fig. 2.6. In this

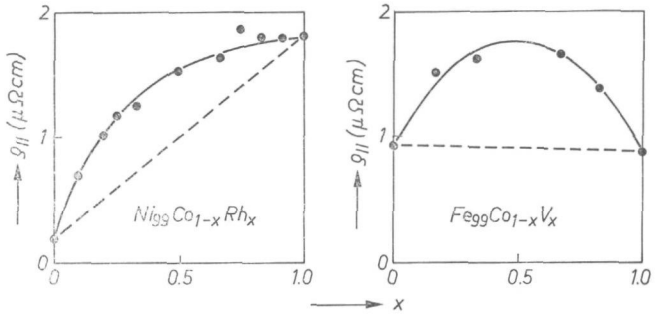

Fig. 2.6. The residual resistivities in $\mu\Omega$cm of a set of ternary alloys $Ni_{99}Co_{1-x}Rh_x$ and $Fe_{99}Co_{1-x}V_x$ as a function of x. The broken line is in agreement with Matthiessen's rule. The solid curve for $Ni_{99}Co_{1-x}Rh_x$ is identical to the one given in the appendix, fig. A.5. The curve for $Fe_{99}Co_{1-x}V_x$ differs from the one in fig. A.28 since here we fitted the theoretical curve of the two-current model to the experimental points of this set of alloys only.

investigation $\varrho_A{}^{\uparrow}$ and $\varrho_A{}^{\downarrow}$ were determined for a large number of impurity metals A in nickel and iron by studying the resistivity of ternary alloys (19 systems on the basis of nickel and 16 systems based on iron, see appendix).

The necessary condition for the above analysis to be applicable is that the resistivity of binary alloys of the impurities considered depends linearly on their concentration in the range of concentrations studied. For a few examples — NiRu, NiCo, FeAl and FeV — this can be seen from fig. 2.7; the specific residual resistivity ϱ (in $\mu\Omega$cm/at%) is obtained from the slope of the straight lines drawn through the experimental points. Similar measurements have been reported earlier for many more systems (Arajs et al.[47,48]), Chen [49]) and Cadeville and Durand [50]), see also table 4-I). In all cases the linear dependence *) on the concentration is observed for concentrations up to at least 5 at%.

Investigations into different ternary alloy systems $Ni_{99}A_{1-x}B_x$, in which the element A is the same and in which element B is different for different ternaries, offer the possibility to assess the validity of the two-parallel-current description. If the model were rigorously valid (and there were no experimental uncertainties involved), the values for $\varrho_A{}^{\uparrow}$ and $\varrho_A{}^{\downarrow}$ derived from different sets of alloys would

*) The possibility that for very dilute alloys, say a few p.p.m. of impurity, the behaviour of the residual resistivity is similar to that of Kondo alloys (dilute alloys of magnetic impurities in a non-magnetic matrix) cannot be excluded. In this work dilute alloys mean concentrations higher than 0.1 at% and lower than 3 at%.

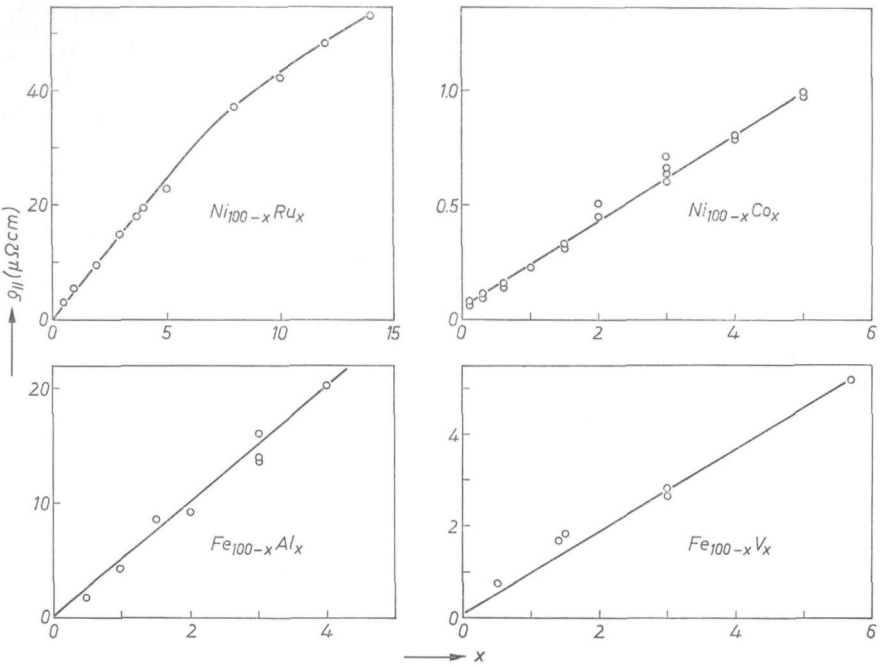

Fig. 2.7. The residual resistivity in the orientation $B \parallel i$ (at $B = 0$) as a function of the nominal solute concentration for different binary alloys based on nickel or iron. The concentration x is in at%.

TABLE 2-II

Validity of the two-current model. The specific sub-band resistivities ($\mu\Omega$cm/at%) in the parallel configuration at 4.2 K, determined in the two-current model for different solute elements in nickel or in iron with various partners.

alloy	$\varrho_{Cr}{}^{\uparrow}$ ($\mu\Omega$cm/at%)	$\varrho_{Cr}{}^{\downarrow}$ ($\mu\Omega$cm/at%)
NiCrAl	29	6.1
NiCrFe	40	5.5
NiCrMn	22	6.5
NiCrTi	25	6.3

alloy	$\varrho_{Co}{}^{\downarrow}$ ($\mu\Omega$cm/at%)	$\varrho_{Co}{}^{\uparrow}$ ($\mu\Omega$cm/at%)
FeCoMo	6.6	1.1
FeCoOs	11	1.0
FeCoRu	3.4	1.3
FeCoV	5.8	1.1

not depend on the alloying partner B. The actual results of experiments of this kind are quite satisfactory as can be seen from table 2-II where results derived for Cr in nickel with Al, Fe, Mn or Ti as partners are compared. The same has been done for Co in iron. The differences in the results derived from different

sets of alloys are of the order of those expected from the experimental uncertainties (see chapter 3); we therefore concluded that it is meaningful to attribute one set of $\varrho^{\uparrow}$ and $\varrho^{\downarrow}$ values to each solute metal, independent of the alloying partner. These two resistivities were obtained by fitting all resistivity data simultaneously (see chapter 4); the results are given in table 2-III. The resistivity depends on the orientation of the current density with respect to the saturation magnetization. The resistivities $\varrho_A{}^{\uparrow}$ and $\varrho_A{}^{\downarrow}$ for an impurity element A correspond to parallel orientation of i and M_s. The ratio $\varrho_A{}^{\downarrow}/\varrho_A{}^{\uparrow}$ is denoted by the parameter α. It follows then that the parameter β denoting the fraction of the current, $i^{\uparrow}/i_{\text{total}}$, transported by carriers with spin $\uparrow$ in the corresponding binary alloy at low temperatures, equals $\alpha/(1 + \alpha)$.

Apart from studying ternary alloys there is another way to obtain values for $\varrho^{\uparrow}$ and $\varrho^{\downarrow}$, which consists in analysing the temperature dependence of the

TABLE 2-III

The specific sub-band resistivities at 4.2 K calculated in the two-current model for different solute elements in nickel or in iron. The configuration is the parallel one with $M_s \parallel i$. Values of $\varrho^{\uparrow}$ and $\varrho^{\downarrow}$ were estimated for asterisked iron-based alloys; see chapter 4.

alloys based on nickel			
solute element	$\varrho^{\uparrow}$ ($\mu\Omega$cm/at%)	$\varrho^{\downarrow}$ ($\mu\Omega$cm/at%)	$i^{\uparrow}/i_{\text{total}}$
Al	3.4	5.8	0.63
Au	0.44	2.6	0.86
Co	0.20	2.6	0.93
Cr	29	6.1	0.17
Cu	1.3	3.8	0.74
Fe	0.44	4.8	0.92
Ir	21	5.0	0.19
Mn	0.83	5.2	0.86
Pt	3.6	0.85	0.19
Re	24	7.5	0.24
Rh	8.0	2.3	0.23
Ru	72	5.4	0.07
Si	5.0	6.4	0.56
Sn	4.4	7.2	0.62
Ti	7.6	7.2	0.49
V	14	6.4	0.31
Zn	1.3	2.9	0.70

TABLE 2-III (cont.)

alloys based on iron			
solute element	$\varrho^{\downarrow}$ ($\mu\Omega$cm/at %)	$\varrho^{\uparrow}$ ($\mu\Omega$cm/at %)	$i^{\downarrow}/i_{\text{total}}$
Al	48	5.6	0.11
Be *	29	4.7	0.14
Co	4.5	1.2	0.21
Cr *	2.6	7.0	0.73
Ga *	44	5.4	0.11
Ge *	49	7.9	0.14
Ir *	20	2.2	0.10
Mn	1.5	8.5	0.85
Mo	2.3	11	0.83
Ni	17	2.4	0.13
Os	4.3	13	0.75
Pt *	12	1.5	0.11
Re	2.7	8.7	0.77
Rh	6.4	1.1	0.15
Ru	2.8	7.3	0.72
Si	36	6.4	0.15
Ti *	4.4	6.6	0.60
V	1.0	7.5	0.88
W *	1.8	7.5	0.81
Zn *			0.35

resistivity of binary nickel- and iron-based alloys. In a sense binary alloys at non-zero temperatures can also be considered as ternary alloys; the phonons can be treated as one of the impurity elements in a ternary alloy, the concentration of which increases with increasing temperature. We have used deviations from Matthiessen's rule at room temperature to determine the sub-band resistivities of the asterisked elements in table 3-III. For details see chapter 4. A complication which is inherent in the analysis of the temperature dependence of resistivities is the occurrence of spin-flip processes (due for instance, to long-wavelength spin-waves) tending to equalize the two currents. Also, it is not evident a priori that the impurity resistivity does not change with temperature. Another, more practical, disadvantage of most of the temperature-dependence investigations reported is that the direction of the spontaneous magnetization is not specified.

In practice the two methods for deriving $\varrho^{\uparrow}$ and $\varrho^{\downarrow}$ compare favourably with each other in spite of these additional problems (see the discussion in chapter 4).

It will be clear, however, that if values for $\varrho^{\uparrow}$ and $\varrho^{\downarrow}$ derived from experiments on ternary alloys are available for a given impurity metal, these values are to be preferred.

The convention of associating the $\uparrow$ or $\downarrow$ direction of the magnetic moment of the electrons with the two residual resistivities of a given solute element is, to some extent, only a matter of taste. In the case of nickel an argument advanced for the choice made has been that with this convention the resistivity due to phonons is smaller in the $\uparrow$ band, i.e. the majority band with the smaller density of states, than the phonon resistivity in the $\downarrow$ band. Once this choice for α_{phonon} has been made, the convention as to which resistivity represents $\uparrow$ and which represents $\downarrow$ is completely decided for all solute elements. A satisfactory aspect of this convention is that Co as a solute metal in nickel has its expected value for $\alpha > 1$, the $d^{\uparrow}$ states in cobalt metal, too, being fully occupied (see also discussion in sec. 4.3).

For iron the situation is less clear as far as the phonon resistivities are concerned. The differences in densities of states at ε_F, as obtained in band-structure calculations, do not differ much. Furthermore, calculations of different authors do not agree quantitatively (cf. Tawil and Callaway [51]) and Duff and Das [46])). Our choice is based on the connection that can be made between experimental information on the magnetic moment of solute atoms in iron (from neutron diffraction or NMR experiments) and our results for the two sub-band resistivities. For details we refer to sec. 4.3.

2.3. The resistivity anisotropy

In this section we consider the resistivity anisotropy in terms of the two-current model. We define the resistivity anisotropy in poly-crystalline alloys as

$$\Delta\varrho/\varrho_{\parallel} = (\varrho_{\parallel} - \varrho_{\perp})/\varrho_{\parallel}, \tag{2.5}$$

where $\parallel$ and $\perp$ stand for the orientation of the saturation moment with respect to the current direction and ϱ is extrapolated to zero magnetic induction B.

A first observation is that for a given solute metal the anisotropy effect in principle does not depend on the concentration. It can, however, be very different for different impurities. This can be seen from table 2-IV where values for $(\Delta\varrho/\varrho_{\parallel})$ for a number of iron- and nickel-based alloys are listed for different solutes at concentrations between 1 and 5 at%. For concentrations lower than 1 at% the parasitic impurities causing the residual resistivity of our nominally pure nickel may start to interfere *). Large positive values of $\Delta\varrho/\varrho_{\parallel}$ result from Co and Fe solutes in nickel-based alloys and from Mo in iron-based alloys.

*) As a result the experimental values of the effect in, for instance, NiCo alloys decreases at Co concentrations near 0.1 at% (Co is the metal that causes the lowest residual resistivity in Ni). Jaoul and Campbell [29]) attributed this effect to the occurrence of spin-flip scattering even at very low temperatures, becoming considerable if the electron mean free path for impurity scattering becomes long.

TABLE 2-IV

The resistivity anisotropy for some alloys with different solute concentrations at 4.2 K

alloy	$\Delta\varrho/\varrho_{\parallel}$ (%)
$Ni_{95}Co_5$	+14.2
$Ni_{96}Co_4$	+13.0
$Ni_{97}Co_3$	+14.2
$Ni_{98}Co_2$	+12.3
$Ni_{98.5}Co_{1.5}$	+12.4
$Ni_{99}Co_1$	+10.2
$Ni_{95}Fe_5$	+12.7
$Ni_{96}Fe_4$	+12.5
$Ni_{97}Fe_3$	+11.9
$Ni_{98}Fe_2$	+11.7
$Ni_{99}Fe_1$	+10.8
$Ni_{95.5}Co_{3.6}Rh_{0.9}$	+4.6
$Ni_{97}Co_{2.4}Rh_{0.6}$	+5.2
$Ni_{98.5}Co_{1.2}Rh_{0.3}$	+4.4
$Ni_{97}Si_3$	+2.6
$Ni_{98.5}Si_{1.5}$	+2.1
$Ni_{95}Ru_5$	—0.4
$Ni_{96}Ru_4$	—1.1
$Ni_{97}Ru_3$	—0.5
$Ni_{98}Ru_2$	—0.6
$Ni_{99}Ru_1$	—0.7

alloy	$\Delta\varrho/\varrho_{\parallel}$ (%)
$Fe_{97}Mo_3$	+8.3
$Fe_{98}Mo_2$	+8.4
$Fe_{98.5}Mo_{1.5}$	+8.5
$Fe_{99}Mo_1$	+8.9
$Fe_{96}Al_4$	—0.2
$Fe_{97}Al_3$	0.0
$Fe_{98}Al_2$	—0.8
$Fe_{98.5}Al_{1.5}$	—0.2
$Fe_{99}Al_1$	—0.1
$Fe_{99.5}Al_{0.5}$	—0.3

Small negative values of $\Delta\varrho/\varrho_{\parallel}$ are found for Ru in nickel and for Al in iron. For completeness' sake we also include data on ternary NiCoRh to illustrate that in ternary alloys with the same relative concentration of solute metals but varying total concentration, the anisotropy effect is a constant.

A number of data for $\Delta\varrho/\varrho_{\parallel}$ in nickel have been reported in previous investigations, e.g. Van Elst [1]), Jaoul [31]) and Jaoul and Campbell [29]). We compare these values with the present ones in chapter 5. For iron-based alloys there is experimental information for FeV alloys (Sueda and Fujiwara [33])).

One of the reasons why the effect for iron was not investigated more extensively in the past is probably that, on theoretical speculations (Campbell [27]), large effects such as those we report in table 5-II were not expected for iron alloys.

As a consequence of the two-current model the anisotropy in the total resistivity can be resolved into the resistivity anisotropies of the two spin currents. In terms of the two-current model the total conductivity is written as

$$\sigma_{\parallel} = \sigma_{\parallel}{}^{\uparrow} + \sigma_{\parallel}{}^{\downarrow}. \tag{2.6}$$

When the magnetization is rotated from $M_s \parallel i$ to $M_s \perp i$ the conductivities will change by $\Delta\sigma$, $\Delta\sigma^{\uparrow}$ and $\Delta\sigma^{\downarrow}$:

$$\Delta\sigma = \Delta\sigma^{\uparrow} + \Delta\sigma^{\downarrow}. \tag{2.7}$$

Rewriting this expression in terms of the resistivities $\varrho = \sigma^{-1}$ we obtain

$$\Delta\varrho/\varrho_{\parallel}{}^2 = \Delta\varrho^{\uparrow}/(\varrho_{\parallel}{}^{\uparrow})^2 + \Delta\varrho^{\downarrow}/(\varrho_{\parallel}{}^{\downarrow})^2. \tag{2.8}$$

Multiplying by $\varrho_{\parallel}$ and replacing $\varrho_{\parallel}/\varrho_{\parallel}{}^{\uparrow}$ by $(i^{\uparrow}/i_{\text{total}})_{\parallel}$ we obtain

$$\Delta\varrho/\varrho_{\parallel} = (i^{\uparrow}/i_{\text{total}})_{\parallel}\,(\Delta\varrho/\varrho_{\parallel})^{\uparrow} + (i^{\downarrow}/i_{\text{total}})_{\parallel}\,(\Delta\varrho/\varrho_{\parallel})^{\downarrow}. \tag{2.9}$$

In the description of the resistivity anisotropy in a binary alloy we have to deal with two parameters $(\Delta\varrho/\varrho_{\parallel})_A{}^{\uparrow}$ and $(\Delta\varrho/\varrho_{\parallel})_A{}^{\downarrow}$ that characterize the solute metal A in the matrix under consideration. The introduction of these two new parameters in fact means that it is not easy to predict the total effect $\Delta\varrho/\varrho_{\parallel}$ for a given impurity. If, however, it is assumed that $(\Delta\varrho/\varrho_{\parallel})^{\uparrow}$ and $(\Delta\varrho/\varrho_{\parallel})^{\downarrow}$ are quantities that characterize the spin currents rather than the solute metals, relation (2.9) predicts a linear relation between $\Delta\varrho/\varrho_{\parallel}$ and $(i^{\uparrow}/i_{\text{total}})_{\parallel}$. The experiments demonstrate that the above assumption is at least approximately correct. In figures 2.8 and 2.9 we have plotted the observed values of $\Delta\varrho/\varrho_{\parallel}$ as a function of $(i^{\uparrow}/i_{\text{total}})_{\parallel}$ and $(i^{\downarrow}/i_{\text{total}})_{\parallel}$ for binary nickel and binary iron alloys, respectively. For iron in particular, the data agree quite well with a straight line i.e. $(\Delta\varrho/\varrho_{\parallel})^{\uparrow} = +10\%$, $(\Delta\varrho/\varrho_{\parallel})^{\downarrow} = -2\%$ for nickel; $(\Delta\varrho/\varrho_{\parallel})^{\downarrow} = +9\%$, $(\Delta\varrho/\varrho_{\parallel})^{\uparrow} = -1\%$ for iron alloys.

As a matter of fact, the actual values of $(\Delta\varrho/\varrho_{\parallel})^{\uparrow}$ and $(\Delta\varrho/\varrho_{\parallel})^{\downarrow}$ for solute elements can be derived individually, too. In the same way *) as we determined sub-current resistivities for impurity metals for the situation $M_s \parallel i$, we can also determine these resistivities for the case of $M_s \perp i$. The results are collected in table 2-V for nickel alloys and in table 5-II for iron alloys, where $(\Delta\varrho/\varrho_{\parallel})_A{}^{\uparrow}$ and $(\Delta\varrho/\varrho_{\parallel})_A{}^{\downarrow}$ are given for different impurities A arranged according to their values for $(i^{\uparrow}/i_{\text{total}})_{\parallel}$. Indeed the anisotropy in nickel-based alloys

*) Strictly speaking, the determination of $\varrho^{\uparrow}$ and $\varrho^{\downarrow}$ from an analysis of resistivities of ternary alloys is less straight-forward in the case of $M_s \perp i$. Hall voltages produced by the two subcurrents individually will tend to couple the two currents. Since the experimentally observed Hall angles for our alloys do not exceed 2%, this coupling is not expected to be important.

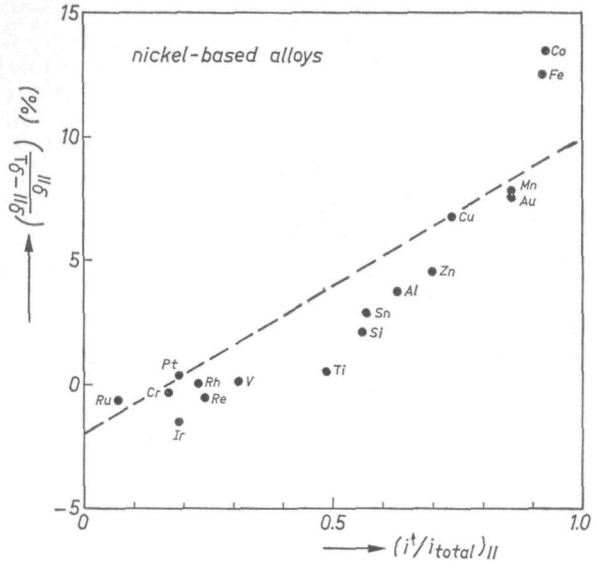

Fig. 2.8. The resistivity anisotropy for various solute metals in binary Ni-based alloys as a function of the fraction of the current carried by spin-up electrons. If $(\Delta\varrho/\varrho_{11})^{\uparrow}$ and $(\Delta\varrho/\varrho_{11})^{\downarrow}$ were constants independent of the impurity, the relation would be linear.

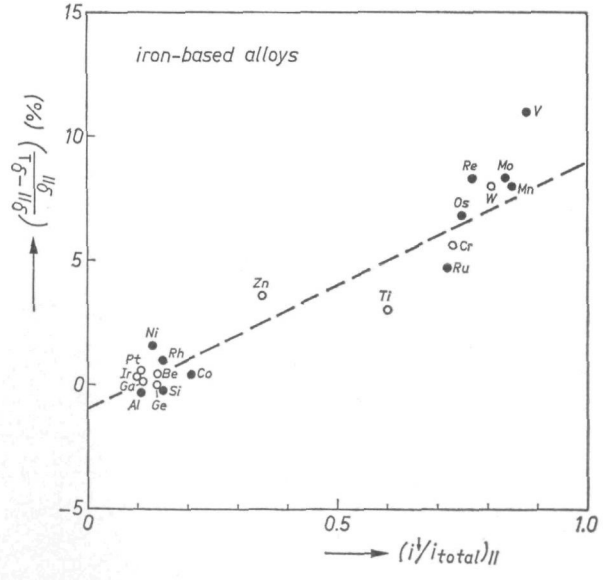

Fig. 2.9. As fig. 2.8 but now for solute metals in Fe. For the filled circles we derived $i^{\downarrow}/i_{\text{total}}$ from experiments on ternary alloys. For the open circles $i^{\downarrow}/i_{\text{total}}$ is estimated from temperature-dependent resistivity measurements.

TABLE 2-V

The resistivity anisotropy for nickel alloys. The effects for the two spin directions were determined separately. Since the effect is positive in the up band and is negative in the down band, the total effect correlates with $i^{\uparrow}/i_{\text{total}}$.

solute element	$(i^{\uparrow}/i_{\text{total}})_{\parallel}$	$\Delta\varrho/\varrho_{\parallel}$ (%)	$(\Delta\varrho/\varrho_{\parallel})^{\uparrow}$ (%)	$(\Delta\varrho/\varrho_{\parallel})^{\downarrow}$ (%)
Co	0.93	+13.5	+14.4	−1.5
Fe	0.92	+12.5	+14.0	−2.2
Mn	0.86	+ 7.8	+ 9.6	−3.3
Au	0.86	+ 7.5	+ 8.1	−2.2
Cu	0.74	+ 6.8	+ 9.7	−2.1
Zn	0.70	+ 4.6	+ 7.8	−2.9
Al	0.63	+ 3.8	+ 7.3	−2.3
Sn	0.62	+ 2.9	+ 6.3	−2.7
Si	0.56	+ 2.1	+ 6.2	−3.2
Ti	0.49	+ 0.55	+ 4.2	−3.2
V	0.31	+ 0.15	+ 7.9	−3.1
Re	0.24	− 0.50	+ 6.5	−2.4
Rh	0.23	+ 0.05	+ 7.8	−2.3
Ir *)	0.19	− 1.48	− 2.5	−1.4
Pt	0.19	+ 0.40	+ 5.8	−0.8
Cr	0.17	− 0.35	+ 5.8	−1.7
Ru	0.07	− 0.60	+ 7.6	−1.1

*) From Jaoul et al.[103]) we learned that Ir was an exception to the rule of a "constant effect" for the spin-up and the spin-down bands which we published earlier (Dorleijn and Miedema [115])). We checked this exception by also investigating the NiAuIr system. The results show that Jaoul et al. are correct.

has (apart from a single exception Ir) one sign for the ↑ current and the other sign for the ↓ current. So for practically all alloys investigated, including both binary and ternary nickel-based alloys, the resistivity of the ↑ band decreases while that of the ↓ band increases when the magnetization is rotated from $M_s \parallel i$ to $M_s \perp i$.

As we shall demonstrate in chapter 5, table 5-II, the results for iron-based alloys show a similar pattern. In the spin-down band the anisotropy effect is large and positive (with one exception out of 11 solutes, i.e. Al) while it is varying around zero for the opposite spin direction.

A simple result as we obtained here for the resistivity anisotropy due to different solutes in nickel or iron has not been predicted theoretically. The present experimental result leads to the following picture. As far as their

effective cross-section for scattering is concerned impurities look like oblate ellipsoids with their short axes parallel to the magnetization direction in both the majority-spin band in nickel and the minority-spin band in iron. Contrarily, as seen by the charge carriers of the minority band in nickel or the majority band in iron impurities look like prolate ellipsoids. A discussion of possible explanations will be given in chapter 5.

2.4. The anomalous Hall effect: skew scattering and side displacement

The anomalous Hall effect is obtained by subtracting the normal Hall voltage from the observed voltage, see fig .1.2. Written in terms of the Hall resistivity ϱ_H we have

$$\varrho_H = \varrho_{aH} + \varrho_{nH}. \tag{2.10}$$

If the normal Hall coefficient R_0 is independent of the field B the subtraction is easy since $\varrho_{nH} = R_0 B$. An example of such a case is the alloy $Ni_{97}Al_3$ in fig. 1.2. In practice, however, there are a number of nickel alloys and many iron-based alloys for which R_0 is not independent of the field, in the fields $B > 4\pi M_s$ in which the actual measurements are made. By way of example in fig. 2.10 we show the experimental data plotted as the Hall angle $\varphi_H = \varrho_H/\varrho_\perp$ versus the

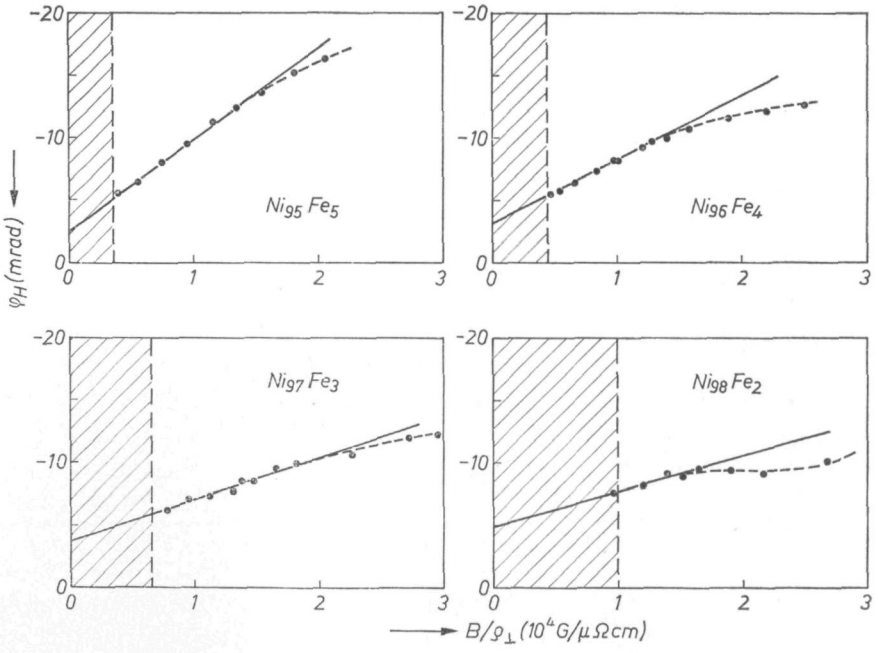

Fig. 2.10. The Hall angle $\varphi_H = \varrho_H/\varrho_\perp$ as a function of the reduced magnetic field $B/\varrho_\perp$ for a series of nickel and iron alloys. The hatched region defines fields for which $B < B_{sat.}$. It can be seen that, as expected, the region of a field-independent normal Hall coefficient extends to about the same value of $B/\varrho_\perp$ for all four cases.

reduced magnetic induction $B/\varrho_\perp$ for a number of NiFe alloys. It will be observed that the Hall coefficient starts to depend on the field at $B/\varrho_\perp \approx 20$ kG/($\mu\Omega$cm). At this field the transverse Kohler magnetoresistivity is about 3%, see fig. 4.2*a*. The value of the normal Hall angle is not a sufficient criterion for deciding whether or not one is in the low-field Hall region. In cases of a nearly compensated Hall effect, as in NiFe alloys, an additional criterion for the presence of a low-field Hall region is a small value of the Kohler magnetoresistivity. The value of 3% indicates that one is in the transition region from low-field to high-field Hall effect. It is not possible to perform measurements in fields below saturation, i.e. in the hatched region in fig. 2.10. A concentration of about 2 at% Fe in nickel is the smallest that can be studied *).

Experiments on a large number of binary and ternary nickel-based alloys show that the anomalous Hall angle is a linear function of the concentration of the solute metals. Since the concentration and the residual resistivity for a given impurity are proportional to each other we can write

$$\varphi_{aH} = \varphi_{sk} + b\,\varrho_\perp. \tag{2.11}$$

The validity of this relation is demonstrated in fig. 2.11 for NiRu, NiFe, FeAl and Ni($Cu_{0.61}Rh_{0.39}$). Relation (2.11) is generally obeyed for concentrations up to about 5 at%. The parameter φ_{sk} is found by extrapolating the straight line to $\varrho_\perp = 0$. The slope of the line corresponds to the value of b. It may be noted that different signs for both φ_{sk} and b occur for different nickel-based alloys.

Relation (2.11) means that the anomalous Hall resistivity tends to zero ($\varrho_{aH} = \varphi_{aH}\,\varrho_\perp$) in pure iron and nickel at low temperatures. This was verified experimentally several years ago by Smit and Volger [52]) for nickel and by Jan and Gijsman [53]) for iron.

A phenomenological picture of the anomalous Hall effect, and one which reproduces expression (2.11), was given by Berger [54]). We show his suggestion as fig. 2.12. The first term (φ_{sk}), called skew scattering, reflects the fact that on the average there is a correlation between the direction of motion of a charge carrier before and after scattering. The figure defines a deflection angle, characteristic of the source of scattering, which will lead to a linear relation between $\varrho_\perp$ and ϱ_{aH}. This skew-scattering mechanism was first proposed by Smit [55]). Berger suggests that in addition there may be a mechanism which he calls side displacement: on the average the electron trajectories before and after scattering will not cross at the impurity centre. Berger defines a displacement Δy which again characterizes the scattering centre. The corresponding

*) For alloys with low resistivity it is still possible to analyse the Hall effect in terms of normal and anomalous contributions provided the normal Hall effect shows a Kohler type behaviour i.e. $\varrho_{nH} = \varrho_{nH}(B/\varrho_\perp)$. However, for nickel alloys with $(i^\uparrow/i_{total})_\perp > 0.5$, e.g. nickel with Co, Fe, Mn, Au or Cu, the low-field Hall effect is found to vary with the concentration. See chapter 6 and the next section.

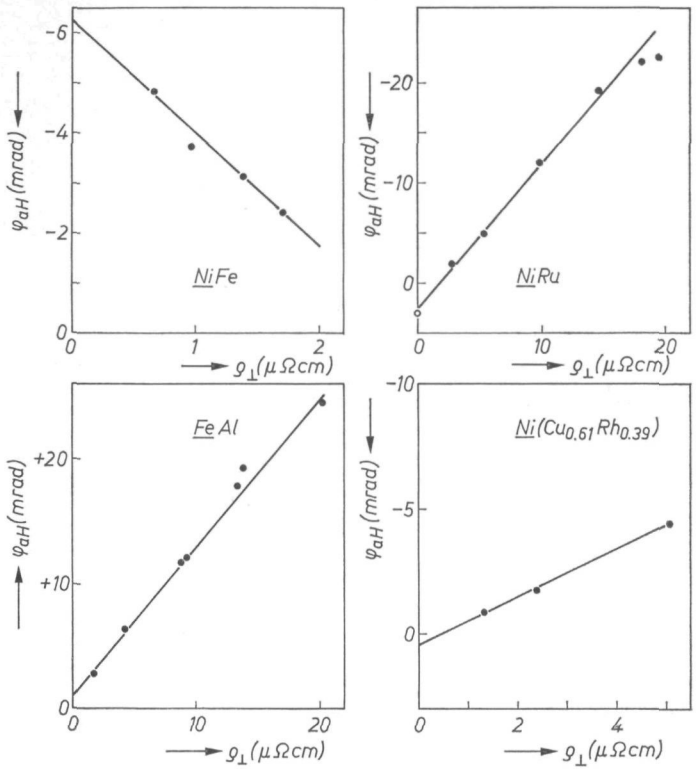

Fig, 2.11. The anomalous Hall angle as a function of the concentration of the solute metals. We take the resistviity $\varrho_\perp$ as a measure of the concentration. The straight lines drawn in correspond to relation (2.11). Note the positive sign of φ_{aH} for FeAl. The open point for NiRu is due to Jaoul [31]).

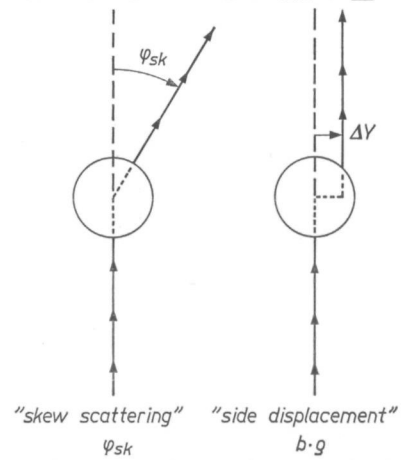

Fig. 2.12. Berger's phenomenological description of two contributions to the anomalous Hall effect. The average motion of an electron before and after scattering is shown. Scattering centres are represented by circles. The magnetization is perpendicular to the plane of the drawing. Generally both skew scattering and side displacement are present. The net current, owing to the influence of the electric Hall field, skew scattering and side displacement, will be in the vertical direction.

Hall angle will be proportional to $\Delta y/\bar{l}$, where $\bar{l}$ is the average distance between two successive scattering events, i.e. the average mean free path. Since $\bar{l}$ will be inversely proportional to $\varrho_\perp$ it follows that the mechanism of side displacement results in an anomalous Hall angle proportional to $\varrho_\perp$.

Systematic experimental investigations of the relation between ϱ_{aH} and the residual resistivity for a given impurity in nickel at low temperatures have previously been reported by Huguenin and Rivier [41]), Fert and Jaoul [37]) and Jaoul [31]). These experimental data concern the region of low concentration, less than 1 at%, with $\varrho_\perp$ smaller than 1 $\mu\Omega$cm, so that only the first term (φ_{sk}) in relation (2.11) is studied. A problem at these low resistivities is that the separation of normal and anomalous Hall effect is a complicated matter *). Because of this the present results for the φ_{sk} and b of solute metals in nickel with $\alpha = \varrho^\downarrow/\varrho^\uparrow > 1$ may be different from the values reported by other investigators. For solute elements in nickel with $\alpha < 1$ there are not such problems. For iron-based alloys the situation is more complicated because of the larger M_s value. Our results for iron are less complete than those for nickel, we discuss them in chapters 6 and 7.

Values for φ_{sk} and b obtained from our experiments on binary nickel-based alloys are collected in table 2-VI. The elements are arranged according to the ratio $(i^\uparrow/i_{total})_\perp$. This arrangement demonstrates a striking correlation between both φ_{sk} and b on the one hand and $(i^\uparrow/i_{total})_\perp$ on the other. For binary alloys in which the current is mainly carried by $\uparrow$ carriers φ_{sk} is negative and b is positive. For the opposite spin direction, i.e. $(i^\uparrow/i_{total})_\perp < 0.5$, φ_{sk} as well as b change signs. This suggests that spin-up charge carriers are characterized by an approximately constant negative value φ_{sk}, while spin-down carriers have an approximately constant positive value φ_{sk}.

This suggests the following relation:

$$\varphi_{sk} = (i^\uparrow/i_{total})_\perp \varphi_{sk}{}^\uparrow + (i^\downarrow/i_{total})_\perp \varphi_{sk}{}^\downarrow. \tag{2.12}$$

In fig. 2.13 we demonstrate that such a simple description holds remarkably well for nickel-based alloys. In this figure the straight line corresponds to relation (2.12) with $\varphi_{sk}{}^\uparrow = -7.5$ and $\varphi_{sk}{}^\downarrow = +4.5$ mrad. Only the result for Cu clearly deviates from this general relation.

Bearing in mind the analysis of the resistivity anisotropy of ternary alloys from which it was possible to derive $(\Delta\varrho/\varrho_{11})^\uparrow$ and $(\Delta\varrho/\varrho_{11})^\downarrow$ for each individual impurity, one might imagine that the same type of analysis could be used to derive $\varphi_{sk}{}^\uparrow$ and $\varphi_{sk}{}^\downarrow$ for individual impurities. In fact we measured the anomalous Hall effect as a function of the concentration for about 40 ternary alloys, keeping the ratio of the two solute concentrations the same. The determination

*) In our preliminary report on the anomalous Hall effect in dilute NiCo and NiFe alloys (Dorleijn and Miedema [56]), the field dependence of the Hall effect was not well anticipated, resulting in too high values for φ_{sk}.

TABLE 2-VI

Parameters characterizing the anomalous Hall effect in binary nickel-based alloys. The skew scattering is described by φ_{sk}, the side displacement by b.

solute element	$(i^{\uparrow}/i_{total})_{\perp}$	φ_{sk} (mrad)	b (mrad/$\mu\Omega$cm)
Co	0.94	− 6.2	+4.2
Fe	0.93	− 6.25	+2.25
Mn	0.88	− 6.5	+1.6
Au	0.87	− 4.8	+1.1
Cu	0.77	−10	+2.0
Al	0.65	− 3.7	−0.42
Sn	0.64	− 2.7	−0.90
Si	0.58	+ 1.1	−0.93
Ti	0.51	+ 1.5	−1.05
V	0.34	+ 3	−1.26
Re	0.25	+ 1	−1.25
Rh	0.25	0	−1.10
Pt	0.20	+ 1.7	−2.25
Ir	0.19	+ 3.2 *)	−1.17
Cr	0.18	+ 2.8	−1.3
Ru	0.08	+ 2.5	−1.43

*) Taken from Jaoul [31]).

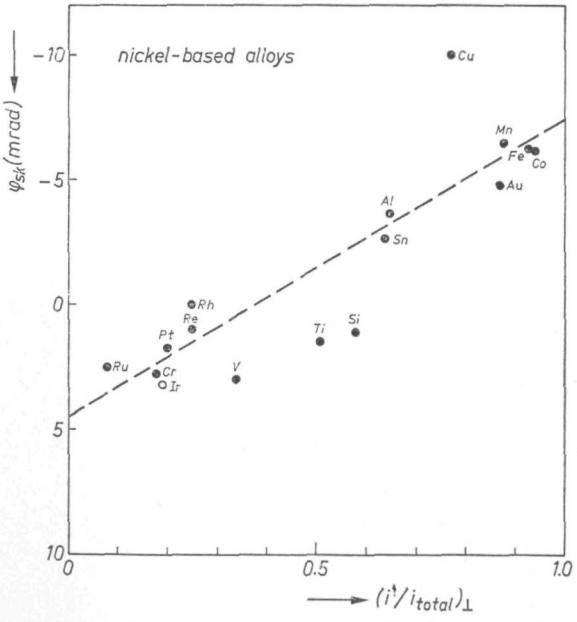

Fig. 2.13. The linear relation between φ_{sk}, the parameter for skew scattering, and the fraction of the current carried by spin ↑ charge carriers. The open point for Ir is due to Jaoul [31]).

of φ_{aH} at low resistivities remains somewhat uncertain and because of that the accuracy of φ_{sk} is not better than about 1 mrad. Still, having a large amount of data on ternary alloys, an analysis in terms of $\varphi_{sk}{}^{\uparrow}$ and $\varphi_{sk}{}^{\downarrow}$ is possible. Details are given in chapter 7. The results are shown in table 2-VII. One may see that indeed $\varphi_{sk}{}^{\uparrow}$ has the negative sign for all impurities while $\varphi_{sk}{}^{\downarrow}$ always has the positive sign, with the exception of Sn.

Comparing formula (2.9) for the resistivity anisotropy and formula (2.12) for the skew scattering, it appears that for approximately constant $(\Delta\varrho/\varrho_{||})^{\uparrow}$, $(\Delta\varrho/\varrho_{||})^{\downarrow}$, $\varphi_{sk}{}^{\uparrow}$ and $\varphi_{sk}{}^{\downarrow}$ the two quantities depend on $i^{\uparrow}/i_{total}$ in the same way. We neglect here the difference between $(i^{\uparrow}/i_{total})_{||}$, used in (2.9), and $(i^{\uparrow}/i_{total})_{\perp}$, used in (2.12). One may eliminate ambiguities in the determination of $i^{\uparrow}/i_{total}$, due to uncertainties in the sub-band resistivities, by plotting directly $\Delta\varrho/\varrho_{||}$ versus φ_{sk} for all alloys. This is realized in fig. 2.14. A linear correlation is found indeed.

Considering the results for the side displacement term b in more detail, we learn from table 2-VI that for nickel alloys there is a clear relationship between b and $(i^{\uparrow}/i_{total})_{\perp}$. Including ternary alloys, too, this relation is given in a graphical form as shown in fig. 2.15 according to which the b values plotted versus $(i^{\uparrow}/i_{total})_{\perp}$ all fall on a single curve. We note that the experimental uncertainties in the derivation of b are much smaller than in that of φ_{sk}, owing

TABLE 2-VII

Results of an analysis of the skew scattering in terms of a two-current model. For each solute metal the resulting skew scattering angles, one for each spin band, are given in mrad. The negative sign indicates that the deflection angle is in the same direction as the normal Hall effect of electrons.

solute element	$(i^{\uparrow}/i_{total})_{\perp}$	$\varphi_{sk}{}^{\uparrow}$ (mrad)	$\varphi_{sk}{}^{\downarrow}$ (mrad)
Co	0.94	− 6.8	+2.4
Fe	0.93	− 7.2	+5.7
Cu	0.77	−14	+3.5
Al	0.65	− 7.3	+3.2
Sn	0.64	− 3.8	−0.06
Ti	0.51	− 3.4	+5.5
V	0.34	− 3.9	+6.3
Rh	0.25	− 1.4	+1.3
Pt	0.20	− 2.6	+2.8
Cr	0.18	− 3.0	+4.2
Ru	0.08	− 4.7	+3.1

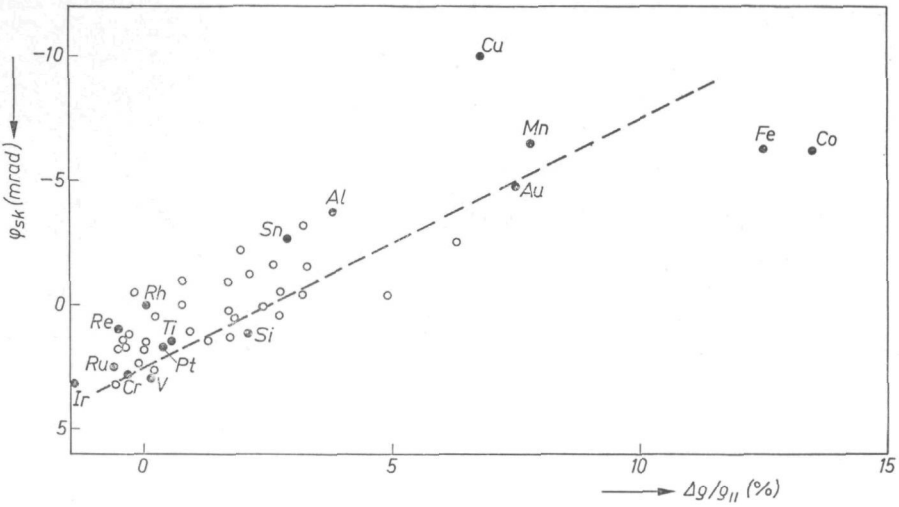

Fig. 2.14. The anomalous Hall angle for skew scattering φ_{sk} as a function of the resistivity anisotropy ($\Delta\varrho/\varrho_{\parallel}$) for binary (●) and ternary (○) nickel-based alloys at 4.2 K.

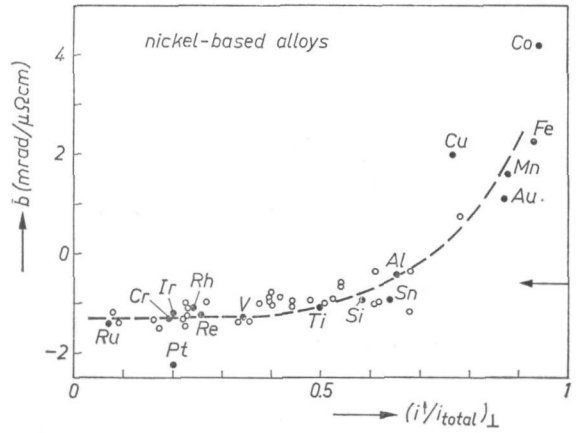

Fig. 2.15. The value for b in the relation $\varphi_{aH} = \varphi_{sk} + b\,\varrho_{\perp}$ for binary (●) and ternary (○) nickel-based alloys as a function of $(i^{\uparrow}/i_{total})_{\perp}$. The arrow indicates the value of b used by Jaoul [31]).

to the fact that alloys with a high resistivity now have a larger weight. It can be seen that the values for b derived for ternary alloys are fully consistent with those for the binary alloys.

In contradistinction to the relation of both φ_{sk} and $\Delta\varrho/\varrho_{\parallel}$ versus $i^{\uparrow}/i_{total}$ previously discussed, there is no a priori reason to expect a relation of comparable simplicity between b and $i^{\uparrow}/i_{total}$. Within the two-current model we have

$$\varphi_{side} = (i^{\uparrow}/i_{total})_{\perp}\,\varphi_{side}{}^{\uparrow} + (i^{\downarrow}/i_{total})_{\perp}\,\varphi_{side}{}^{\downarrow} \qquad (2.13)$$

and

$$\varphi_{\text{side}}{}^{\uparrow} = b^{\uparrow}\,\varrho_{\perp}{}^{\uparrow}; \qquad \varphi_{\text{side}} = b\,\varrho_{\perp}.$$

Since $(i^{\uparrow}\,\varrho^{\uparrow}/i_{\text{total}})_{\perp} = \varrho_{\perp}$ we immediately obtain

$$b = b^{\uparrow} + b^{\downarrow}. \tag{2.14}$$

In words: the anomalous Hall angle due to side displacement for a given spin current is larger according as the resistivity for this spin current is larger. With a larger resistivity, however, the carriers of that spin direction carry a smaller fraction of the current, so that the resulting Hall angle does not depend on the distribution of the current over the two spin directions.

It is still possible to subdivide the experimentally found value of b into the respective contributions $b^{\uparrow}$ and $b^{\downarrow}$ from the two spin currents.

For ternary alloys the total value of b is

$$\begin{aligned} b = {} & (c_{\text{A}}\,\varrho_{\text{A}\perp}{}^{\uparrow}\,b_{\text{A}}{}^{\uparrow} + c_{\text{B}}\,\varrho_{\text{B}\perp}{}^{\uparrow}\,b_{\text{B}}{}^{\uparrow})/\varrho_{\perp}{}^{\uparrow} + \\ & + (c_{\text{A}}\,\varrho_{\text{A}\perp}{}^{\downarrow}\,b_{\text{A}}{}^{\downarrow} + c_{\text{B}}\,\varrho_{\text{B}\perp}{}^{\downarrow}\,b_{\text{B}}{}^{\downarrow})/\varrho_{\perp}{}^{\downarrow}. \end{aligned} \tag{2.15}$$

The concentrations c_{A} and c_{B}, the specific sub-band resistivities $\varrho_{\text{A}\perp}{}^{\uparrow}$, $\varrho_{\text{A}\perp}{}^{\downarrow}$, $\varrho_{\text{B}\perp}{}^{\uparrow}$ and $\varrho_{\text{B}\perp}{}^{\downarrow}$, and the total resistivities $\varrho_{\perp}{}^{\uparrow}$ and $\varrho_{\perp}{}^{\downarrow}$ are known for ternary alloys, so that $b_{\text{A}}{}^{\uparrow}$, $b_{\text{A}}{}^{\downarrow}$, $b_{\text{B}}{}^{\uparrow}$ and $b_{\text{B}}{}^{\downarrow}$ can be found for those systems for which b is measured for a number of compositions with different ratios $c_{\text{A}}/c_{\text{B}}$. In fact, there are not four parameters b for a given ternary systems but only three since a given constant b may be added to both $b_{\text{A}}{}^{\uparrow}$ and $b_{\text{B}}{}^{\uparrow}$ provided that constant is simultaneously subtracted from $b_{\text{A}}{}^{\downarrow}$ and $b_{\text{B}}{}^{\downarrow}$. If this is done in relation (2.15) the result is

$$b \Rightarrow b + \frac{(c_{\text{A}}\,\varrho_{\text{A}\perp}{}^{\uparrow} + c_{\text{B}}\,\varrho_{\text{B}\perp}{}^{\uparrow})}{\varrho_{\perp}{}^{\uparrow}}\,b_0 - \frac{(c_{\text{A}}\,\varrho_{\text{A}\perp}{}^{\downarrow} + c_{\text{B}}\,\varrho_{\text{B}\perp}{}^{\downarrow})}{\varrho_{\perp}{}^{\downarrow}}\,b_0 = b. \tag{2.16}$$

Results for $b^{\uparrow}$ and $b^{\downarrow}$ are given in table 2-VIII for nickel alloys. As will be clear from relation (2.16), the values for b remain the same when values $b^{\uparrow}$ for all solute elements are increased by the same amount b_0 and at the same time values $b^{\downarrow}$ are decreased by b_0. Thus table 2-VIII represents a particular choice of this constant b_0. We have used the commonsense argument that if the specific residual resistivity for a given impurity and a given spin direction is small, the spatial extension of the scattering centre can also be expected to be small and hence the side displacement Δy in that case will be small too. We have chosen b_0 such that for Co and Fe in nickel, which have rather small specific resistivities in the $\uparrow$ band, the value of $b^{\uparrow}$ will be near zero. This assumption proves adequate to obtain a general correlation between $b^{\uparrow}$, $b^{\downarrow}$ and $\varrho_{\perp}{}^{\uparrow}$, $\varrho_{\perp}{}^{\downarrow}$, respectively, as can be seen from table 2-VIII and fig. 7.5. The correlation in fact means that the spin current, which is relatively unimportant for the resistance, the resistance

TABLE 2-VIII

The side-displacement term in the anomalous Hall effect of nickel-based alloys, broken down into the contribution of the separate spin currents

solute element	$(i^{\uparrow}/i_{\text{total}})_{\perp}$	$b^{\uparrow} + b_0$ (mrad/μΩcm)	$\varrho_{\perp}{}^{\uparrow}$ (μΩcm/at%)	$b^{\downarrow} - b_0$ (mrad/μΩcm)	$\varrho_{\perp}{}^{\downarrow}$ (μΩcm/at%)
Co	0.94	0.0	0.17	+4.2	2.6
Fe	0.93	−1.6	0.38	+3.9	4.9
Mn *)	0.88	−2.3	0.75	+3.8	5.4
Au *)	0.87	−3.0	0.41	+4.1	2.7
Cu	0.77	−2.1	1.2	+4.1	3.9
Zn *)	0.72	−4.1	1.2	+4.0	3.0
Al	0.65	−4.5	3.2	+4.2	5.9
Sn	0.64	−5.8	4.1	+4.9	7.4
Si *)	0.58	−5.4	4.7	+4.5	6.6
Ti	0.51	−5.0	7.3	+4.0	7.5
V	0.34	−5.8	13	+4.6	6.6
Re *)	0.25	−5.6	22	+4.4	7.7
Rh	0.25	−5.6	7.3	+4.4	2.4
Pt	0.20	−4.0	3.4	+1.7	0.86
Ir *)	0.19	−3.9	21	+2.6	5.1
Cr	0.18	−5.5	27	+4.2	6.2
Ru	0.08	−5.6	66	+4.2	5.5

*) For some solute elements we needed not only data on the concentration dependence of the anomalous Hall angle in ternary alloys but also ternary alloy data, for which only one concentration (3 at%) was studied. In these cases we estimated the skew-scattering angle from fig. 2.13 and calculated b directly from the Hall angle observed.

anisotropy and the skew scattering, dominates the side-displacement contribution to the anomalous Hall effect.

The combination of positive $\varphi_{\text{sk}}{}^{\downarrow}$ and $b^{\downarrow}$ values and negative $\varphi_{\text{sk}}{}^{\uparrow}$ and $b^{\uparrow}$ values leads to a simple picture that is related to a phenomenological description proposed by Hurd [35]). One considers the scattering centres as being intransparent for electrons, at least for part of their volume, see fig. 2.16. The connection of the sign of orbital moment to that of the spin moment will induce a preference to pass the impurity centre either on the right or on the left side, depending on the electron-spin direction. For this to be true it suffices that the incoming electron, which may have only little d character, resides for some time in an intermediate, more d-like, state. This leads to a side displacement of the order of the radius of the intransparent section of the impurity. Now the skew scattering has to do with the fact that for an outgoing electron,

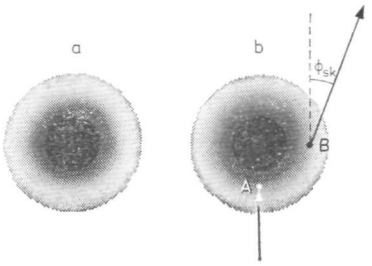

Fig. 2.16. (*a*) A simple picture of an impurity in a transition metal. The dark central region is considered to be intransparant for conduction electrons, i.e. the scattering probability for an electron travelling to that region is near 1. In the dotted region the scattering probability gradually decreases to zero with increasing radial distance.
(*b*) For a given spin direction of the incoming electron there is a preference to bypass the impurity on the right hand or the left hand side, which leads to a "side displacement". An outgoing electron, starting from B, cannot be emitted in the space angle, covered by the intransparant section of the impurity. An averaging leads to a non-zero "skew-scattering" angle φ_{sk}.

starting from point B in fig. 2.16, there is a forbidden space angle, i.e. the one covered by the intransparant impurity centre.

For iron-based alloys we have studied the concentration dependence of the anomalous Hall effect in binary alloys only. The results can be found in chapter 7. At this place it suffices to mention that a simple pattern as observed in nickel-based alloys does not exist in iron alloys. For instance φ_{sk} can be large and positive on both ends of the scale $(i^{\downarrow}/i_{total})_{\perp}$. This may have to do with the fact that the normal Hall effect has either sign in iron alloys, depending on the solute.

2.5. The normal Hall effect

In the two-current model it is assumed that the first step in the subdivision of the charge carriers is that according to the direction of their magnetic moment. From the resistivity of ternary alloys (sec. 2.2) it has been seen that this assumption is justified for both iron and nickel. If the two-current model were rigorously valid it would be possible to define two normal Hall coefficients $R_0{}^{\uparrow}$ and $R_0{}^{\downarrow}$ and two Kohler curves, one for each band, independent of the type of impurity. In the two-current model we obtain for the normal Hall coefficient R_0:

$$R_0 = (i^{\uparrow}/i_{total})_{\perp}{}^2 \, R_0{}^{\uparrow} + (i^{\downarrow}/i_{total})_{\perp}{}^2 \, R_0{}^{\downarrow}. \tag{2.17}$$

This means that R_0 is quadratically related to $(i^{\uparrow}/i_{total})_{\perp}$ with $R_0{}^{\uparrow}$ and $R_0{}^{\downarrow}$ as parameters. If $R_0{}^{\uparrow}$ and $R_0{}^{\downarrow}$ are equal, then the Hall coefficient as $(i^{\uparrow}/i_{total})_{\perp} = 0.5$ is two times smaller than the value at $(i^{\uparrow}/i_{total})_{\perp} = 0$ or 1, see fig. 2.17. This is easy to understand since basically the Hall coefficient is inversely proportional to the number of current carriers. The corresponding

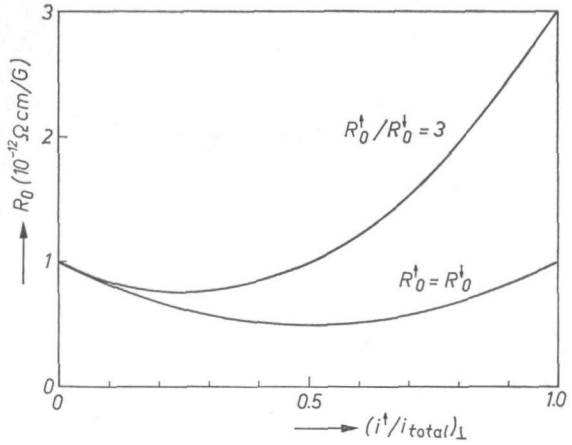

Fig. 2.17. The normal Hall coefficient in the two-current model for two cases.

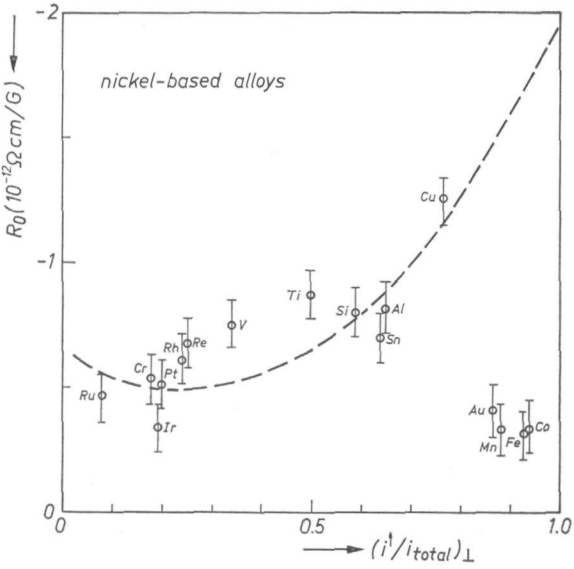

Fig. 2.18. The normal Hall coefficient for various solute elements in binary nickel alloys plotted versus the parameter of the two-current model ($i^{\uparrow}/i_{\text{total}}$). In principe the data represent the low-field condition and a solute concentration of 3 at %. The broken line would correspond to relation (2.17) with $R_0{}^{\uparrow}/R_0{}^{\downarrow} = 3$. In the present units $R_0 = -0.73$ would correspond to 1 electron per nickel atom in the free electron approximation. The error bars indicate our estimate of the experimental uncertainty.

plot for various nickel-based alloys is shown in fig. 2.18. The broken curve corresponds to $R_0{}^{\downarrow} = -0.65$ and $R_0{}^{\uparrow} = -1.95$ (10^{-12} Ωcm/G). The sign is that of electron-like charge carriers. The curve may represent the data for $(i^{\uparrow}/i_{\text{total}})_{\perp} < 0.8$, but at larger values of $(i^{\uparrow}/i_{\text{total}})_{\perp}$ there is a discrepancy (Au, Mn, Fe and Co).

The reason for this is the following. The Hall coefficient for a given band is not a constant. Firstly, it is a function of the magnetic field, i.e. if $B/\varrho_\perp$ is sufficiently large, the Hall effect may become a function of B; see fig. 2.10. For this reason, the Hall effects given in fig. 2.18, are values measured for 3 at% solute concentration so that we can be sure we are dealing with the low-field condition ($\omega_c \tau < 1$). Secondly, however, the Hall coefficient for the spin ↑ current is found to be a function of the resistivity, i.e. of the mean free path of the carriers. At first sight this seems highly surprising but information from completely different experiments gives similar indications. We are referring here to the work of Franse et al.[57,58]). Franse measured the magneto-crystalline anisotropy energy for single crystals of nickel and nickel-based alloys. At low temperatures in pure nickel the magnetocrystalline anisotropy energy shows a detailed structure as a function of the crystal direction and terms up to $(\cos \vartheta)^8$ are needed to describe the results. At high temperatures, and at low temperatures in alloys with 1% impurities, the detailed structure is lost; see fig. 2.19. Franse et al.[58]) were able to show that the effect that adding impurities has on the higher-order terms in the magnetocrystalline anisotropy energy is related to the impurity resistivity. When the mean free path of the current carriers is reduced the Fermi surface starts to loose details of its structure. Apparently

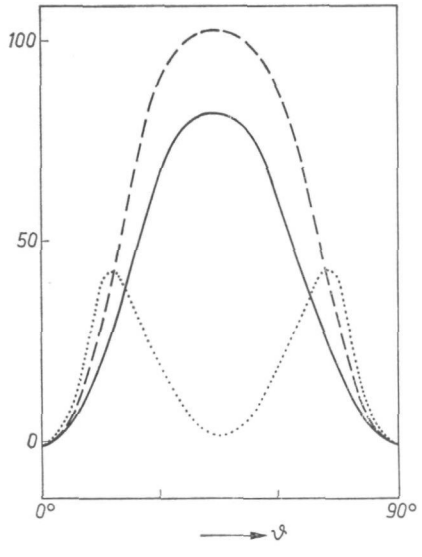

Fig. 2.19. A comparison of the contribution of higher-order constants to the torque curves in nickel crystals for pure and less pure nickel at 4.2 K, and for pure nickel at 77 K. In the vertical direction is plotted the torque between magnetization and field, in arbitrary units, in the horizontal direction the angular coordinate in the (100) plane of nickel. The drawn line is for pure nickel at 77 K. The broken line is for impure nickel at 4.2 K. The dotted line is for pure nickel at 4.2 K. Taken from Franse [57]). Impurities can be, for instance, Cu or Co, which have the same effect. It is suggested that a reduction of the mean free path blurs the detailed structure of the Fermi surface.

the magnetocrystalline anisotropy energy is a property which is highly sensitive to this loss of detail. We find the Hall effect for the ↑ band to be another such property.

We analysed our data on the Hall effect of nickel alloys in terms of the two-current formula (2.17) but have allowed the coefficients $R_0{}^{\uparrow}$ and $R_0{}^{\downarrow}$ to be dependent on the resistivity. For $R_0{}^{\downarrow}$ we find no systematic dependence on the resistivity $\varrho_{\perp}{}^{\downarrow}$, though the result for different impurities may differ somewhat. This can be seen in fig. 2.20 where values for $R_0{}^{\downarrow}$ are plotted, derived

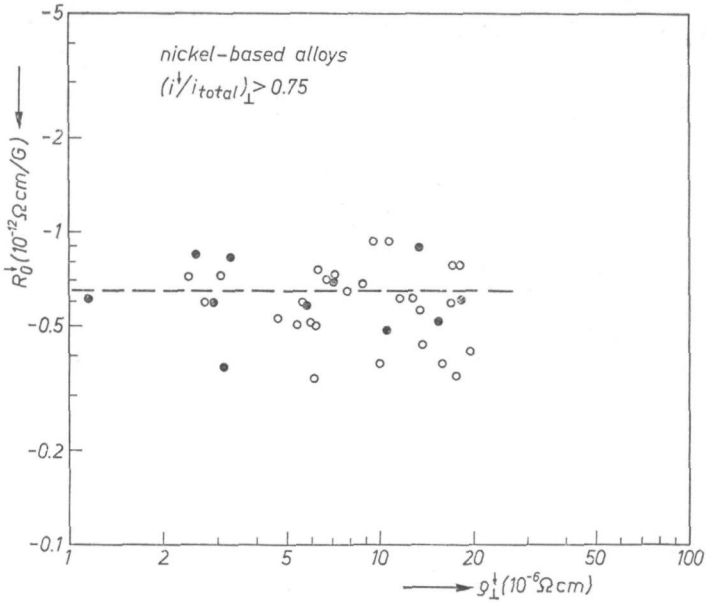

Fig. 2.20. The normal Hall effect of nickel-based alloys in the two-current model. The Hall coefficient for ↓ carriers is plotted vs the resistivity for these carriers $\varrho_{\perp}{}^{\downarrow}$. Filled circles (●) represent binary alloys, open circles (○) represent ternary alloys.

from alloy data for which $(i^{\downarrow}/i_{\text{total}})_{\perp} > 0.75$, i.e. alloys in which the Hall effect is dominated by ↓ carriers. $R_0{}^{\downarrow}$ is within the range $(0.65 \pm 0.30)10^{-12}$-Ωcm/G for all the alloys investigated.

The corresponding results for the up band derived from alloys with $(i^{\uparrow}/i_{\text{total}})_{\perp} > 0.5$ are shown in fig. 2.21. The results undoubtedly indicate a systematic variation of $R_0{}^{\uparrow}$ with $\varrho_{\perp}{}^{\uparrow}$ in the range of resistivities from 1 to 10 μΩcm. This explains the deviating behaviour of the four solute metals in fig. 2.18. For alloys with 3 at% of Mn, Au, Co or Fe the resistivity is about 1 μΩcm, which is much lower than for the other solute metals. We like to stress that the dependence of $R_0{}^{\uparrow}$ on $\varrho_{\perp}{}^{\uparrow}$ which we observe here is a real dependence on $\varrho_{\perp}{}^{\uparrow}$ and not a dependence on $B/\varrho_{\perp}{}^{\uparrow}$. The data are all within

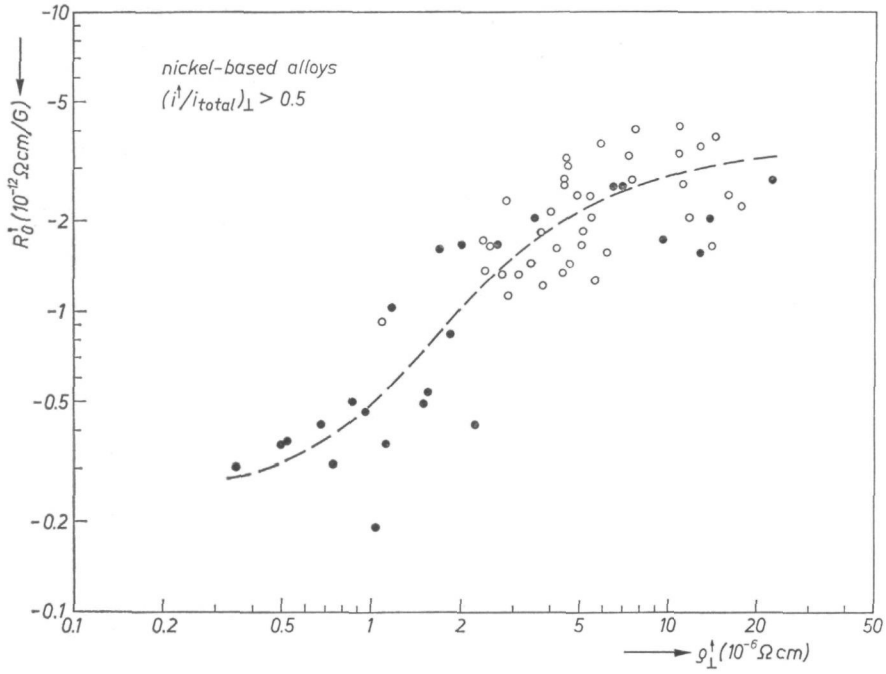

Fig. 2.21. The normal effect $R_0{}^{\uparrow}$ for ↑ carriers as a function of the relevant resistivity $\varrho_{\perp}{}^{\uparrow}$. Filled circles (●) represent binary alloys, open circles (○) ternary alloys. The Hall coefficient of nickel "up" carriers changes from a low value at low resistivity to the value expected for about 0.35 electron per atom at high resistivity. In view of our interpretation of this dependence of $R_0{}^{\uparrow}$ on $\varrho_{\perp}{}^{\uparrow}$ in terms of a blurring of the Fermi surface we opted for a representation of $\varrho_{\perp}{}^{\uparrow}$ on a logarithmic scale. If plotted linearly $R_0{}^{\uparrow}$ extrapolates to zero for low resistivities.

the low-field limit, which is the range of fields where the Kohler magnetoresistivity is never more than a few percent.

The remarkable behaviour of the Hall effect in nickel, i.e. low values of $R_0{}^{\downarrow}$ and $R_0{}^{\uparrow}$ dependent on the resistivity $\varrho_{\perp}{}^{\uparrow}$, can be understood in terms of a representation of the band structure in nickel given by Reed and Fawcett [59]). The essence is that there are small numbers of d-type holes in the up band while the contribution of d-type carriers to the down band is mainly electron-like. For details see chapter 6.

3. EXPERIMENTAL ARRANGEMENTS

In this chapter we describe the experimental set-up for measuring electrical resistivities and Hall effects at low temperatures. We also describe the preparation and the metallurgical treatment of our samples.

A primary objective in the organization of the experimental work, i.e. the method chosen and the inaccuracies that have been considered acceptable, was to make it possible for us to investigate a relatively large number of samples (about 475) in a reasonable time. The preparation of the samples had therefore, where possible, to fit into the standard procedures of our laboratory. Also, the experimental set-up had to permit easy replacement of the samples.

3.1. Measuring apparatus

In our investigations we measured rods measuring approximately $10 \times 2 \times 2$ mm and strips measuring approximately $30 \times 1.5 \times 0.15$ mm. A cross-section of the apparatus for measuring rods is given in fig. 3.1. The rods are mounted on a sample-holder of a synthetic-resin bonded fabric and positioned with clamps which also act as current contacts. The samples are pushed onto the voltage contacts which consist of platinum wires with rounded tips.

The apparatus for measuring strips is illustrated in fig. 3.2, where we give a sketch (3.2*a*) and a photograph (3.2*b*) of the apparatus. Its central part consists of a glass-fibre epoxy plate with a thickness of 1.6 mm carrying a pattern of

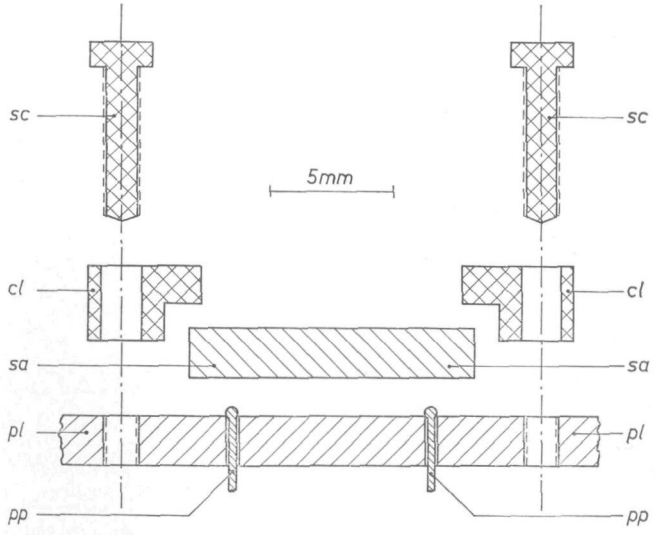

Fig. 3.1. Sketch of the cross-section of the sample holder for measuring rods. The sample (sa) is mounted with copper screws (sc) and brass clamps (cl) onto the base plate (pl). The current wires are soldered to cl, the potential wires are soldered to pp.

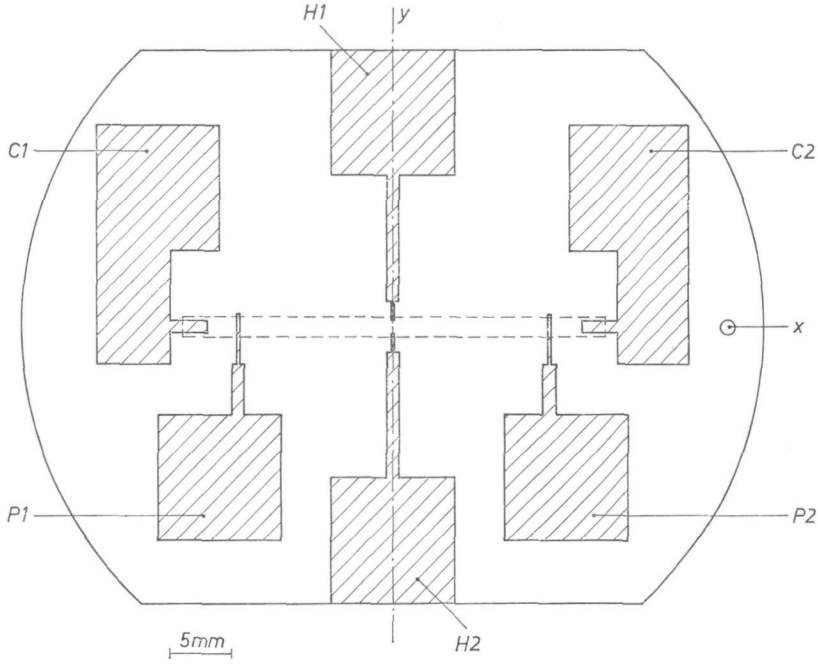

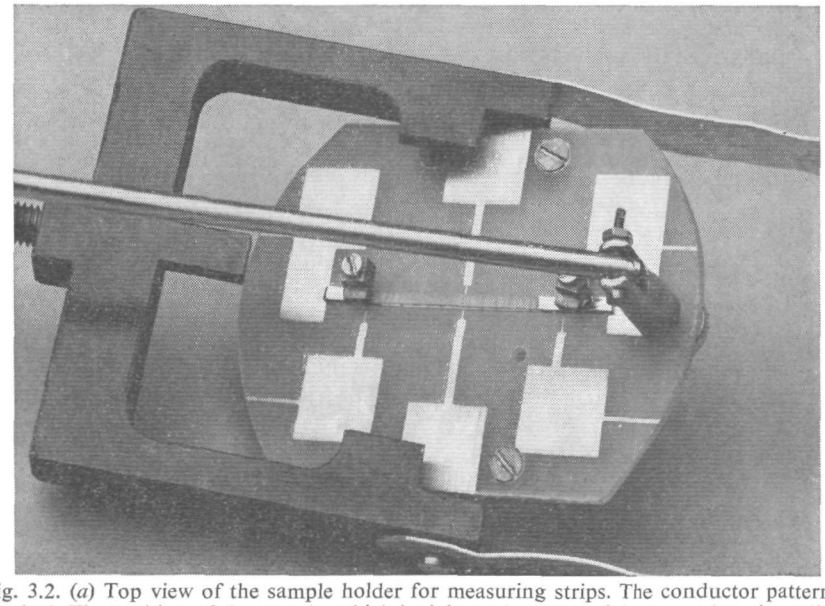

Fig. 3.2. (*a*) Top view of the sample holder for measuring strips. The conductor pattern is hatched. The position of the sample, which is tightened on top of the base plate, is outlined with a dashed line. The current wires are soldered to the bonding flaps C while the potential wires and the wires for the Hall voltage are soldered to the flaps P and H respectively. The plate can be tilted around the *y*-axis.
(*b*) Photograph of the sample holder.

copper conductors with a thickness of 30 μm. The conductors are coated with a 10 μm-thick gold layer. Six bonding flaps enable the connection of electric wiring, namely C1 and C2 for current contacts, P1 and P2 for potential probes and H1 and H2 for Hall probes. The plate shown in fig. 3.2*a* is mounted in a U-shaped holder (see photograph 3.2*b*) at the end of a stainless steel tube which can be moved up and down through the flange at the top of the cryostat. The sample-holder is immersed in liquid helium. In our experiments, in which the magnetic field produced by a super-conductive solenoid magnet was directed vertically, it was important to ensure that the sample could be oriented both horizontally and vertically. By means of a second tube connected to point x and working like a hinge, the sample can be changed from the position in which it is parallel to the magnetic field to the perpendicular position, by rotating the holder along the y-axis.

The magnetic field is produced by a superconductive solenoid magnet made by Thor Cryogenics Ltd. It has a clear bore of 63 mm and an overall length of 230 mm. The maximum central-field intensity is about 50 kOe. The central-field homogeneity is 0.2% over a cylinder with a diameter of 20 mm and a length of 50 mm. Since the magnetic field had to be changed frequently, a large helium consumption resulted from the heating of the superconductive switch with which the magnet was provided for measuring in the persistent current mode. We therefore removed this switch.

The cryostat consists of an outer and an inner glass vessel. The inner vessel has an internal diameter of about 120 mm and a length of 1 m. On top of the cryostat was a large-diameter safety valve, which opened at a gauge pressure of 0.1 atm to protect the cryostat against explosion upon quenching of the magnet.

The voltage along the specimen and the Hall voltage were recorded with a Keithley microvoltmeter (model 149) and a Keithley nanovoltmeter (model 148), respectively. One of the Hall probes was earthed, while the potential probes were kept floating. The output of the microvoltmeter was displayed on a Philips PM 2433 digital voltmeter; the Hall voltage was shown on an analogue scale. The current through the specimen was measured using a digital voltmeter, namely a Schneider Electronique VN 654, and a standard 1 Ω resistor (Bleeker). The correct operation of the electrical part of the experimental apparatus was checked by connecting standard voltages to the contacts of the sample-holder. The voltages measured were of the order of 10 mV for the resistivity and 10 μV for the Hall voltage. The readings of all meters were recorded manually.

The width of the samples was determined with an accuracy of about 2 μm by means of a microscope. The thickness was found by measuring the displacement of a mechanical probe electrically with an accuracy of about 2 μm. The distance between the potential contacts of the sample holder described in fig. 3.2 was 24.98 mm.

3.2. Preparation of the samples

The alloys were made in the form of 10-g buttons by melting the pure components in an arc melting furnace under argon pressure. The components were weighed with an accuracy of 0.5 mg. The nickel used was carbonyl nickel, produced by International Nickel, in which the main impurity was 0.01% iron. The iron used was electrolytic iron, produced by Johnson and Matthey. In both cases carbon was removed by heating the powder in a vacuum and subsequently reducing it in a hydrogen atmosphere after which the nickel was 99.99% pure and the iron 99.999% pure. All the solute elements had a purity of at least 99.99%. For all the alloys studied it was known (Hansen, Elliott and Shunk [114])) that the solid solubility was considerably greater than the concentration prepared.

The elements dissolved in nickel were chosen such that a representative cross-section of the Periodic Table would be obtained, resulting in 17 different solute elements. For the iron-based system we decided to prepare binary alloys of all elements (except As) that could be dissolved in iron at a concentration of at least 3 at%, resulting in 20 different binary alloy systems. In the choice of the ternary alloy systems we aimed at obtaining large deviations from Matthiessen's rule. For the nickel system our choice was based on information from the literature about the sub-band resistivities of solute elements. We therefore preferably combined elements with $\alpha > 1$ ($\alpha = \varrho^{\downarrow}/\varrho^{\uparrow}$) and elements with $\alpha < 1$ into one ternary alloy. Practically no information was available from literature with regard to deviations from Matthiessen's rule in iron-based alloys. Our choice in this case was based rather on trial and error. The relation between the different sets of ternary nickel and iron-based alloys is illustrated in fig. 3.3, where elements that were dissolved in a full set of ternary alloys (consisting of about 6 different compositions) are connected by a black band. Elements that were combined in only one or two ternary alloys are connected by a white band. As a rule the total solute concentration was 3 at%, thus providing residual resistivities and Hall effects that could be measured easily. At this solute concentration the influence of contaminations of the pure nickel (with a residual resistivity of about 0.04 $\mu\Omega$cm) and the pure iron (with a residual resistivity of about 0.1 $\mu\Omega$cm) is negligible as compared to the effect of the solutes.

In our first experiments we measured the resistivity and resistivity anisotropy of nickel rods with dimensions $11 \times 1.8 \times 1.8$ mm. These rods were obtained from the ingot buttons using a spark-erosion technique. This technique was time-consuming and to eliminate it we decided, after measuring the resistivity and the resistivity anisotropy of about 35 samples in the systems NiAuRh, NiCoRh, NiCuRh and NiZnRh, to prepare our samples by cold-rolling. The resistivity and the resistivity anisotropy of these 35 samples was measured on spark-eroded rods and on rolled samples. No systematic difference was found. The buttons were cold-rolled to bands about 0.15 mm thick. From these bands

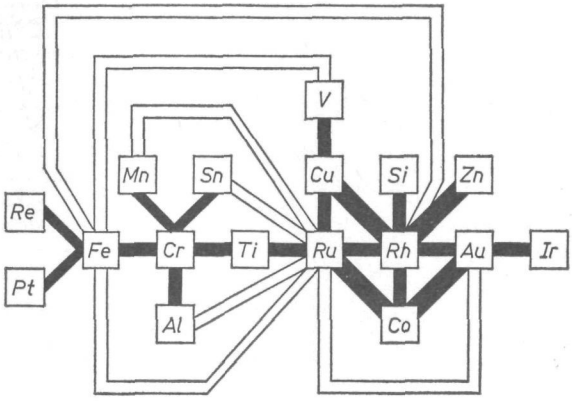

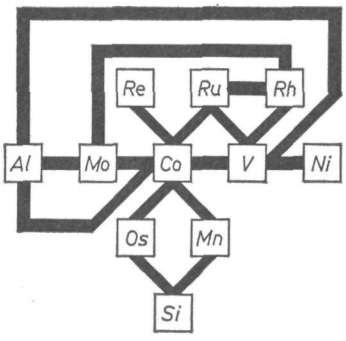

Fig. 3.3. The relation between different sets of ternary nickel- or iron-based alloys. Elements that were dissolved in a full set of ternary alloys (about 6 different compositions) are connected by a black band, a white band indicates a set consisting of one or two different compositions.

a piece with a length of about 5 cm was cut, then cleaned to remove lubricants. To remove possible surface contamination by iron introduced by the steel rollers, the nickel strips were cleaned in a solution of 65 cm^3 of nitric acid, 18 cm^3 of acetic acid and 17 cm^3 of water. They were subsequently annealed at 1000 °C in quartz tubes in a vacuum of about 10^{-5} Torr for at least 15h. The iron strips used in the second part of the investigation were treated in the same way except that they were not etched. The annealing temperature of most iron samples was 700 °C.

The resistivity and resistivity anisotropy of 37 binary and ternary iron-based alloys of composition FeAlMo, FeCoMo, FeCoOs, FeCoRu, FeCoV, FeNiV and FeRhV were measured on rods which were machined from the ingot but-

tons. Neither the spark-eroded nickel rods previously mentioned nor the machined iron rods were annealed.

3.3. Discussion of the experimental procedures

In each measurement of the Hall effect the electric current and the magnetic field were reversed separately, thus eliminating contributions due to misalignment of the Hall probes with respect to the magnetic field and the current density and contributions due to thermo-electric voltages. The resistance was calculated from the average of the voltage over the sample in these four situations. The resistance in the situation with $B \parallel i$ was obtained from the two values of the voltage by reversing the current through the sample, thus eliminating the influence of thermo-electric voltages. For each measurement the sample was precooled to the temperature of liquid nitrogen. The voltage across the sample at room temperature and that at the temperature of liquid nitrogen were recorded.

The point of contact between Hall probes and sample is vitally important for measurements of the Hall effect in a strip with the sample-holder shown in fig. 3.2. The way in which the strips are cut from the rolled bands introduces sharp edges at the long side of the samples, which are slightly bent to one side. It was found that the Hall probes made electrical contact at the extreme edges, as can be deduced from the results presented in table 3-I, in which we have collected Hall measurements on strips of different width cut from the same band. In calculating the Hall resistivity we took the width of the strips as the distance between the Hall probes. Since the results do not differ significantly for the various strips, it follows that our assumption was justified.

The current through the specimen was chosen as 700 mA. The magnetic field due to the current is perpendicular to the sample, so it will tend to orient the

TABLE 3-I

The anomalous Hall resistivity of strips of different widths cut from the same band of $Ni_{97}Ru_3$. We calculate ϱ_{aH} from $\varrho_{aH} = V_{aH}\, d/I$, where d is the thickness of the sample, I the total current and V_{aH} the anomalous Hall voltage (at $B = 0$).

width (mm)	ϱ_{aH} (nΩcm)
1.821	—272
1.492	—273
1.281	—272
1.257	—265
1.246	—267

magnetization perpendicular to the sample, thus influencing the measurement. In the direct neighbourhood of the sample this field was estimated to be about 10 Oe which is clearly too small to have any effect. We also varied the current intensity but did not find any indication that the current intensity influenced the galvanomagnetic properties of the samples investigated.

The total concentration of solutes in most alloys was 3 at%. This concentration may seem high as compared to values usually quoted in investigations of diluted alloys. The advantages of using such a concentration are that the residual resistivities can be measured relatively easily and that the effects due to dissolved elements are much larger than those due to possible contaminations of the nominally pure nickel or iron matrix (the Room-temperature Resistance Ratio of nickel was about 200; for iron we found RRR $\approx$ 100). The field-dependence of galvanomagnetic properties provides another reason to study samples with rather high resistivity, see chapter 6.

For all binary iron and nickel alloys, and a large number of ternary nickel alloys with the same ratio of solute elements, we checked the dependence of the residual resistivity on the total solute concentration up to at least 3 at%. A linear correlation was found between the residual resistivity and the total solute concentration for all solutes. This linear dependence was observed even for solutes with high specific residual resistivities such as Ru in Ni or Al in Fe, as can be seen in fig. 2.7. We concluded therefore that the alloys with a total concentration of up to 3 at% can still be considered as dilute for this study.

The chemical composition of our samples was checked in some cases of nickel-based alloys and more of iron-based alloys, usually by X-ray fluorescence techniques.

Owing to the better form factor (the thickness was reduced by a factor of 10 and the distance between the potential contacts was increased from 5 to 25 mm) both the voltage along the sample and the Hall voltage were much larger for rolled strips than for rods. A disadvantage of cold-rolling is the possibility of introducing textures.

Textures can be observed with X-ray techniques. An indication for the presence of textures was found in the large difference in X-ray intensities as compared to the intensities expected in an X-ray powder diffraction pattern. For our cold-rolled samples this difference was generally quite large. For this reason pole diagrams were made for a number of nickel and iron samples before and after annealing. A pole diagram gives information about the preferred orientation of grains. However, a quantitative statement about the amount of texture (How much differs the sample from a single crystal as far as the resistivity is concerned?) is difficult to give. For a sample $Ni_{99}Co_1$ it was found that the rolling direction becomes [1 1 1] while the [1 1 $\bar{2}$] direction is perpendicular to the strip. After annealing at 1000 °C the main difference with the not annealed sample turned out to be the grain size. For a $Ni_{96}Fe_4$ sample the

situation was very similar as was deduced from a (1 1 1) pole diagram *). An analysis of the annealed sample was very difficult because of the large grains: in this case there were indications for a more complex texture after annealing.

Since it is difficult to obtain a quantitative measure for the texture we considered our measurements on the galvanomagnetic properties decisive. The resistivity anisotropy basically depends on the direction of the electric current and the magnetization with respect to the crystallographic axes. For a cubic crystal one can express this orientation dependence in terms of the direction cosines $\alpha_{1,2,3}$ and $\beta_{1,2,3}$ with coefficients k_1, k_2, k_3 etc. Dedié [28]) has derived the 5 coefficients $k_1 \ldots k_5$ for a number of nickel-based alloys. His results make it possible to compare the resistivity anisotropy in a single crystal with an orientation which corresponds to our texture, with ideally polycrystalline material. From Dedié's result one expects a difference of a factor 1.5 for our NiFe samples (polycrystalline samples having a larger anisotropy effect than single crystals with the same orientation as the texture observed). However, we observed no difference in the resistivity anisotropy of rods, without texture, which were not annealed and foiles where textures were observed. We also checked that the resistivity and the resistivity anisotropy were the same in strips which were parallel and perpendicular to the rolling direction. It was therefore concluded that the influence of texture is still unimportant.

In iron-based alloys, too, textures were observed. A (1 1 0) pole diagram was constructed for $Fe_{97}Mo_3$ and $Fe_{97}Os_3$. Two kinds of textures could be identified. For both the rolling direction is the [1 1 0] direction. In the first texture the rolling plane is (0 0 1), in the other texture the rolling plane is (1 $\bar{1}$ 2). The main difference introduced by annealing in the b.c.c. phase ($Fe_{97}Mo_3$) is the larger grains. Upon annealing in the f.c.c. phase ($Fe_{97}Os_3$ at 1000 °C) a complicated pattern is obtained.

Also for iron we concluded that the presence of textures does not interfere much with our investigations of conduction properties. For a large number of binary alloys we checked that the resistivity anisotropy of cold-rolled and spark-eroded samples was the same. We verified that in $Fe_{99}Os_1$, $Fe_{97}Ni_3$ and $Fe_{97}Co_3$ the anomalous Hall effect was not different for samples annealed in the b.c.c. phase and in the f.c.c. phase.

*) I like to thank Mrs. C. Langereis and J. L. C. Daams for performing the X-ray analysis and constructing the pole diagrams.

4. THE RESIDUAL RESISTIVITY OF DILUTE IRON- AND NICKEL-BASED ALLOYS

4.1. Determination of the resistivity at 4.2 K

The definition of the electrical resistivity in ferromagnetic alloys is not as self-evident as in non-magnetic metals. The phenomena of resistivity anisotropy and field-dependent magnetoresistivity give rise to some complications.

In choosing between the two extreme configurations of the saturation magnetization with respect to the electric current, i.e. the perpendicular orientation, in which M_s is perpendicular to the current i, and the parallel configuration, in which M_s is oriented parallel to the current, we opted for the parallel configuration as the reference orientation. This choice was motivated by the consideration that a model of two independent currents cannot be rigorously correct for the perpendicular situation since the electric Hall field caused by the anomalous Hall effect will induce a coupling between the two currents.

Another problem is whether the unperturbed situation at low temperatures is reached at $B = 0$ or at $H = 0$. The magnetic induction B is equal to $B = H_{ext} - H_{dem} + 4\pi M_s$, with H_{ext} the external magnetic field and H_{dem} the demagnetizing field. De Haas–Van Alphen measurements by Joseph and Thorsen [72]) for nickel and by Anderson and Gold [73]) for iron have shown that the De Haas–Van Alphen oscillations are periodic in B^{-1}, proving that the effective field acting on the current carriers in a ferromagnet is B rather than H. In addition, the enhancement of the resistivity due to a magnetoresistance effect in the internal induction was studied for iron at low temperature by Berger and De Vroomen [74]) and for nickel by Schwerer and Silcox [75]). At low temperatures we therefore define as the reference situation for measurement of the resistivities of ferromagnetic metals that of $B = 0$ and the saturation magnetization parallel to the electric current *).

In the actual measurements an external field is needed to saturate the sample magnetically in the desired direction. The dependence of the resistivity at 4.2 K on the external field in the two configurations is shown in fig. 4.1 for two examples: $Ni_{98.5}Mn_{1.5}$ and $Fe_{97}Mn_3$. On the horizontal axis we plotted the magnetic induction B, taking $H_{dem} = 4\pi N M_s$ for the demagnetizing field, with N the demagnetization coefficient (Osborn [76])). Since the sample is saturated magnetically in fields $H_{ext} > H_{dem}$ an extrapolation over a distance $4\pi M_s$ is needed to correct for the Kohler magnetoresistance, which results in

*) At room temperature there is reason to adopt $H = 0$ rather than $B = 0$ as the reference state since part of the room-temperature resistivity is due to magnetic excitations (spin waves) which are suppressed by a magnetic field H. Here it has to be decided which magnetoresistance effect is more important: the suppression of spin waves by a magnetic field H or the curvature of the electron trajectories under the influence of the magnetic induction B.

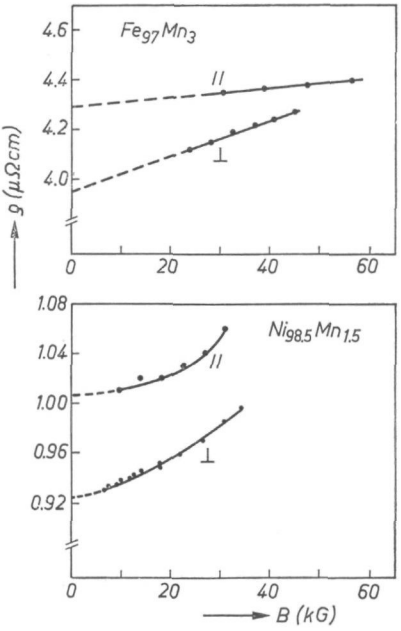

Fig. 4.1. The residual resistivity of an iron-based alloy (top) and a nickel-based alloy (bottom) as a function of the magnetic induction B in the two extreme configurations. In the nickel alloy a near quadratic behaviour of $\varrho = \varrho(B)$ is apparent (curves have been drawn to assist the eye), in contrast to the iron alloy where $\varrho = \varrho(B)$ is linear.

greater uncertainties for iron alloys where $4\pi M_s = 21.9$ kG than for nickel alloys where $4\pi M_s = 6.4$ kG.

The Kohler [77]) magnetoresistance curves for iron and nickel alloys are quite different as is shown in figs 4.2*a*, 4.2*b*, 4.3 and 4.4. $\varrho(B)/\varrho_0$ is plotted along the vertical axis and B/ϱ_0 along the horizontal one, $\varrho(B)$ being the value of the resistivity as a function of B and ϱ_0 being the value of the resistivity at $B = 0$. In the perpendicular orientation we have according to the definition of $\varrho_\perp$ given above $\varrho_0 = \varrho_\perp$, in the parallel configuration $\varrho_0 = \varrho_{||}$. Fig. 4.2*a* (for $B \perp i$) shows that the Kohler curves for binary nickel alloys with solutes Co, Fe, Mn, Ti, Al, V, Cr, Pt and Ru behave nearly quadratically at low values of B/ϱ_0. Exceptions which do not fit readily into this pattern are NiCu and NiAu alloys as given in fig. 4.2*b*.

It can be seen in fig. 4.3 that the longitudinal magnetoresistance for NiFe alloys is similar to but somewhat smaller than the transverse. In view of the nearly quadratic dependence of $\varrho(B)/\varrho_0$ on B we determined resistivities for our alloys from a plot of $\varrho(B)$ versus B^2 (see fig. 1.1). For iron alloys, too, the transverse and longitudinal magnetoresistance show a similar dependence on B, the longitudinal being smaller (for FeCo alloys see fig. 4.4). However, our measurements on iron alloys suggest, in contradistinction to nickel alloys, a

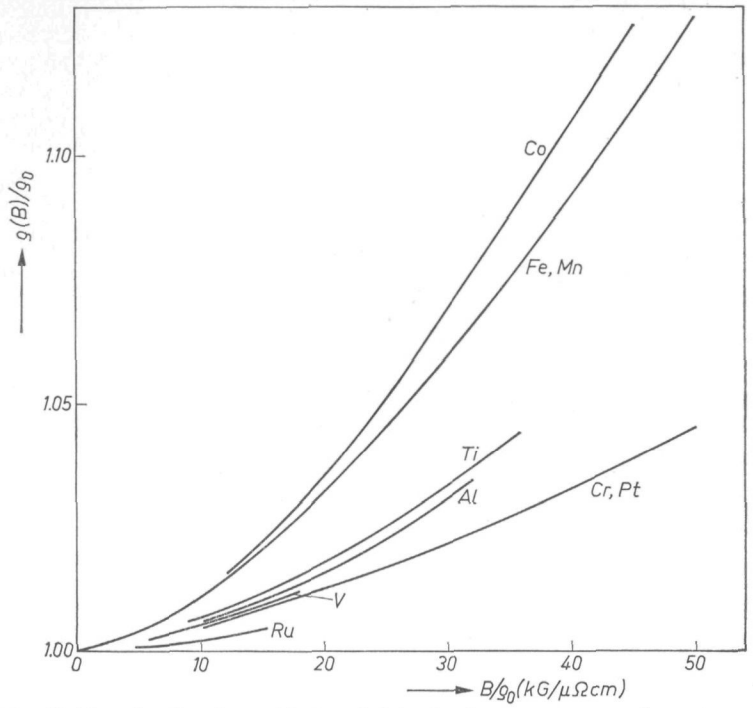

Fig. 4.2*a*. Kohler plot for the residual resistivity in the transverse configuration of some binary nickel-based alloys at 4.2 K.

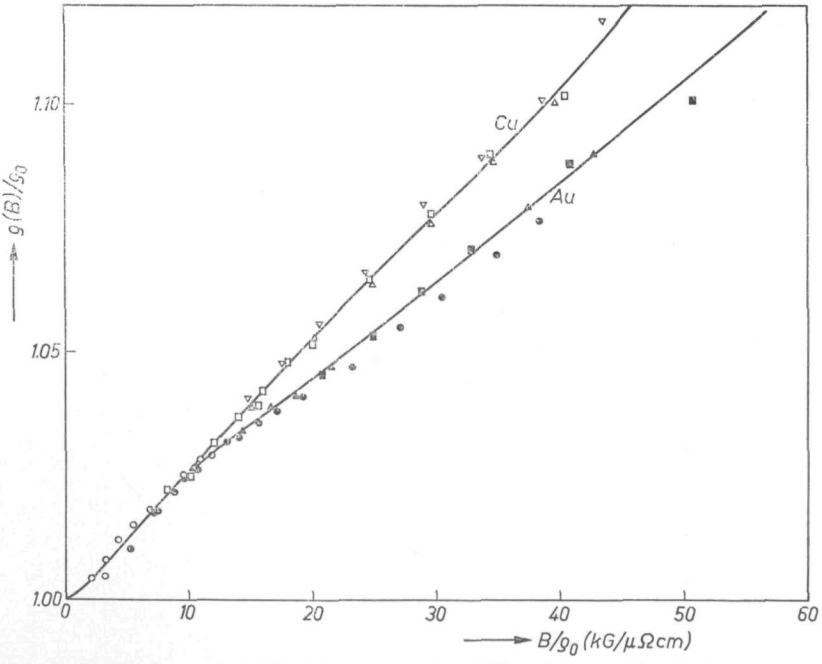

Fig. 4.2*b*. As fig. 2*a* but now for NiCu (white symbols) and NiAu (black symbols). The various symbols denote different alloys. The quadratic behaviour of the curves in fig. 2*a* is less apparent here.

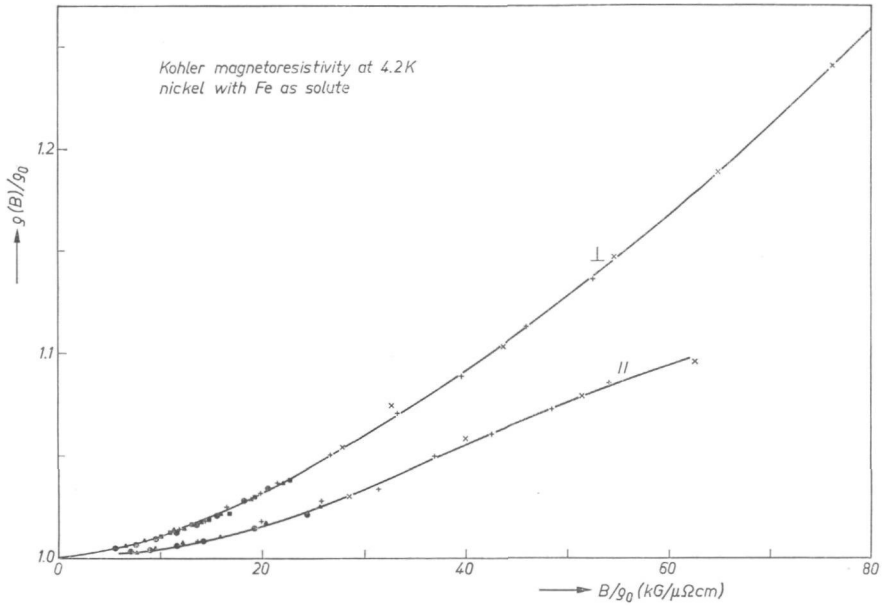

Fig. 4.3. Kohler plots for the residual resistivity in the transverse (⊥) and parallel (||) configuration of diluted nickel-based iron alloys (NiFe). The various symbols denote alloys with different Fe concentrations.

linear Kohler function for values of B/ϱ_0 between 5 and 20 kG/μΩcm. If there is a positive curvature of the Kohler plots for iron alloys similar to the curvature of the Kohler functions for nickel alloys, it will be at fields below $B/\varrho_0 = 5$ kG/μΩcm. Since the minimum value of $B = 22$ kG high resistivities of about 10 μΩcm would be needed in order to investigate the Kohler plots in that region, which means leaving the dilute alloy concentration range. It was therefore decided to plot the resistivity of iron-based alloys as a function of B and to extrapolate linearly to $B = 0$ *).

Taking the above considerations into account we estimate the resulting inaccuracies of the resistivities to be 0.3 and 0.7% in the transverse configuration and 0.1 and 0.3% in the parallel configuration for nickel- and iron-based alloys, respectively. This error is small compared to other errors as far as the actual resistivity is concerned. It is, however, the main source of inaccuracy in the resistivity anisotropy; see chapter 6. The main errors in our values for the resistivities are due to the form factor (i.e. the ratio of the distance between

*) It is conceivable that a coupling between the normal Hall effect and the anomalous Hall effect makes a contribution to the resistivity which is proportional to B, resulting in a Kohler function without a horizontal tangent at $B/\varrho_0 = 0$.

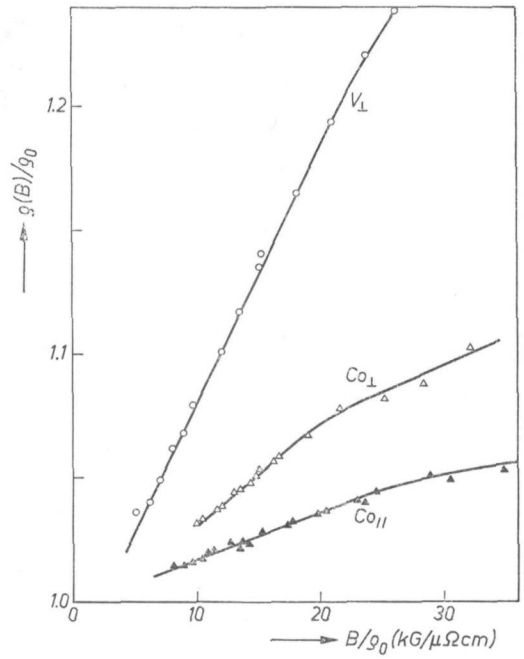

Fig. 4.4. Kohler plots for the resistivity at 4.2 K of some iron-based alloys: FeV is determined in the transverse configuration (indicated by $V_\perp$), FeCo in both the transverse ($Co_\perp$) and the parallel (Co_{II}) configuration.

the voltage probes and the cross-section of the sample) and deviations from the nominal composition. These errors can be assessed by considering fig. 2.7 where the resistivity ϱ_{II} is plotted versus the nominal composition. It is found that for the smaller values of ϱ_{II} (e.g. in the NiCo-alloys) the scatter in ϱ_{II} is up to a few %. Another way of assessing our results is to compare them with the results of other investigators; see table 4-IA and 4-IB for nickel- and iron-based alloys, respectively. Our data, given in these tables, refer to the parallel configuration at $B = 0$. The majority of authors do not specify the direction of the magnetization with respect to the current, their data referring in fact to a magnetically unsaturated state. All data included were obtained at low temperatures *).

Some of our values, notably for Fe, Co and Au in nickel, differ from the values we gave in an earlier publication [78]). This is due to the fact that more experimental data were used for the present results, thus reducing the uncertainties in the impurity concentrations. The residual resistivities were determined from at least three binary alloys with different solute concentrations.

*) Values for impurity resistivities quoted in textbooks have sometimes been derived from room-temperature data, assuming the validity of Matthiessen's rule of additivity. This assumption is not justified for ferromagnetic metals.

TABLE 4-IA

Specific residual resistivities of nickel-based alloys at 4.2 K. Resistivities are in $\mu\Omega$cm/at%.

solute element	present work	data from literature
Ti	3.7	3.3 [17]) 2.9 [8]) 3.4 [49])
V	4.4	4.2 [17]) 5.0 [47]) 4.5 [8]) 4.2 [49])
Cr	5.0	5.0 [19]) 4.8 [17]) 5.0 [49]) 4.5 [16]) 5.0 [20]) 5.0 [65])
Mn	0.72	0.79 [17]) 0.64 [8]) 0.7 [49]) 0.56 [16]) 0.75 [31])
Fe	0.39	0.33 [19]) 0.39 [17]) 0.32 [8])
Co	0.185	0.14 [17]) 0.13 [8]) 0.19 [16]) 0.20 [20]) 0.14 [65])
Zr	2.4	3.3 [13])
Nb		5.0 [47]) 4.9 [31])
Mo		7 [63]) 5.8 [13])
Ru	4.96	4.7 [50]) 5.0 [13]) 5.1 [31])
Rh	1.80	1.5 [50]) 1.9 [13]) 2.0 [31])
Pd		0.15 [17]) 0.2 [66]) 0.24 [70])
Hf	4.0	3.3 [13])
Ta		5.2 [64])
W		6.3 [1]) 6.9 [63]) 5.1 [13])
Re	6.0	5.5 [50]) 6.2 [13]) 6 [31])
Os		5.0 [50]) 5.8 [13]) 5.9 [31])
Ir	3.86	3.6 [50]) 3.8 [13]) 4.0 [31])
Pt	0.70	0.96 [17]) 0.7 [50]) 1.0 [13]) 0.8 [31])
Cu	0.98	1.0 [62]) 0.77 [17]) 0.77 [31])
Au	0.36	
Zn	0.91	1.1 [14])
Al	2.13	
Ga		1.9 [14])
C		3.5 [71])
Si	2.83	
Ge		2.8 [14])
Sn	2.78	3.0 [1]) 3.6 [63]) 3.5 [15])
As		4.5 [14])

TABLE 4-IB

Specific residual resistivities of iron-based alloys at 4.2 K. Resistivities are in $\mu\Omega$cm/at %.

solute element	present work	data from literature
Ti	2.6	3.0 [48] 2.5 [10] 2.9 [69]
V	0.88	1.2 [48] 1.4 [10] 1.4 [69]
Cr	1.90	2.1 [48] 2.5 [67] 2.6 [69] 2.5 [44]
Mn	1.30	1.4 [48] 1.44 [67] 1.7 [10] 1.7 [69]
Co	0.93	0.8 [48] 0.99 [67] 1.0 [69] 1.0 [44]
Ni	2.13	1.9 [48] 2.2 [67] 2.0 [10] 1.8 [69]
Mo	1.90	1.6 [48]
Ru	2.00	2.0 [48] 2.0 [67]
Rh	0.95	
Pd		1.7 [48]
Ta		2.5 [48]
W	1.5	1.7 [48] 1.6 [67]
Re	2.23	2.3 [48] 3.3 [10]
Os	3.08	4.0 [10]
Ir	2.0	
Pt	1.3	
Be	4.0	
Al	5.08	5.5 [48] 5.2 [10]
Ga	4.80	
C		4.9 [48]
Si	5.40	6.2 [48] 6.5 [67] 5.8 [10] 11.6 [68]
Ge	6.8	6.6 [48] 7.0 [67]
Sn		8.0 [48] 9.4 [15]

Exceptions to this rule are the residual resistivities of NiZr and NiHf, which were determined for a single alloy with a solute concentration of 0.5 at%, because of their low solubility in nickel. The residual resistivities of Ir and Zn, too, were determined from single NiIr and NiZn alloys.

4.2. Analysis of the resistivities

As pointed out in chapter 2, the resistivity due to solute elements in ferromagnetic alloys is insufficiently described by a single value for the specific

residual resistivity at low temperature as given in table 4-I. Deviations from the rule of additivity of individual impurity resistivities in dilute ternary alloys of the type $M_{99}A_{1-x}B_x$, where M stands for Ni or Fe and A and B are different solute elements, suggest a description in terms of a two-current model. The need for such a model also follows from an analysis of the temperature dependence of the resistivity of ferromagnetic metals, see sec. 4.4 of this chapter. In terms of a two-current model, with each current identified with a particular direction of the magnetic moment of the charge carriers, the residual resistivity of a particular solute element A is characterized by two specific resistivities $\varrho_A{}^{\uparrow}$ and $\varrho_A{}^{\downarrow}$, one for each spin current.

The specific sub-band resistivities were determined by fitting the residual resistivities of a set of ternary alloys of the type $M_{99}A_{1-x}B_x$, with various values of x with $0 \leqslant x \leqslant 1$, to the theoretical formula (2.3) with $c_A = 1 - x$ and $c_B = x$. The adjustable parameters are $\varrho_A{}^{\uparrow}$, $\varrho_A{}^{\downarrow}$, $\varrho_B{}^{\uparrow}$ and $\varrho_B{}^{\downarrow}$. The fitting was done by numerically minimizing the sum of the squares of the relative deviations. We used the Direct Search procedure as given by Hooke and Jeeves [79]) and modified by Bell and Pike [80]). By comparing the results for a particular element A as obtained from sets of alloys where a different element is taken for B in each different set, it is possible to obtain an impression of the validity of the two-current model. Results of this kind of experiment are given in table 2-II, where we consider Cr in nickel with different partners and Co in iron with different partners.

In assessing the validity of the two-current model from these numbers several aspects should be considered. The sub-division of current carriers according to the direction of their magnetic moment is not the only conceivable one. Other sub-divisions such as electrons and holes or s-like and d-like electrons could also be imagined. If, for a given spin direction, different groups of charge carriers were scattered by different types of impurities, then the result for $\varrho_A{}^{\uparrow}$ and $\varrho_A{}^{\downarrow}$ measured from a set of alloys $M_{99}A_{1-x}B_x$ would depend on the partner B. However, we did find from the analysis that the values $\varrho_A{}^{\uparrow}$ and $\varrho_A{}^{\downarrow}$ are to a good approximation independent of the partner B in the ternary alloy.

The main reason for the difference in results from different sets of alloys as shown in table 2-II is the limited accuracy. An impression of the influence of a different choice of adjustable parameters can be obtained from fig. 4.5. In fig. 4.5*a* we have plotted curves of the calculated two-current formula (2.3) for the resistivity of a set of alloys $M_{99}A_{1-x}B_x$ as a function of x. The residual resistivities of the binary alloys were kept the same, viz. $\varrho_A = \varrho_B = 1$. The ratio of the sub-band resistivities for A was assumed to be the reciprocal of the ratio for B: $\alpha_A = \varrho_A{}^{\downarrow}/\varrho_A{}^{\uparrow} = 1/\alpha_B$. The parameter for the different curves in fig. 4.5*a* is $\alpha_A = 1/\alpha_B$. The curves in fig. 4.5*b* were determined as in fig. 4.5*a* but now with $\varrho_A = 1$ and $\varrho_B = 2$. The curves in fig. 4.5*c* were calculated assuming $\alpha_A = 16\,\alpha_B$. The varying parameter for these curves is α_A. Owing to

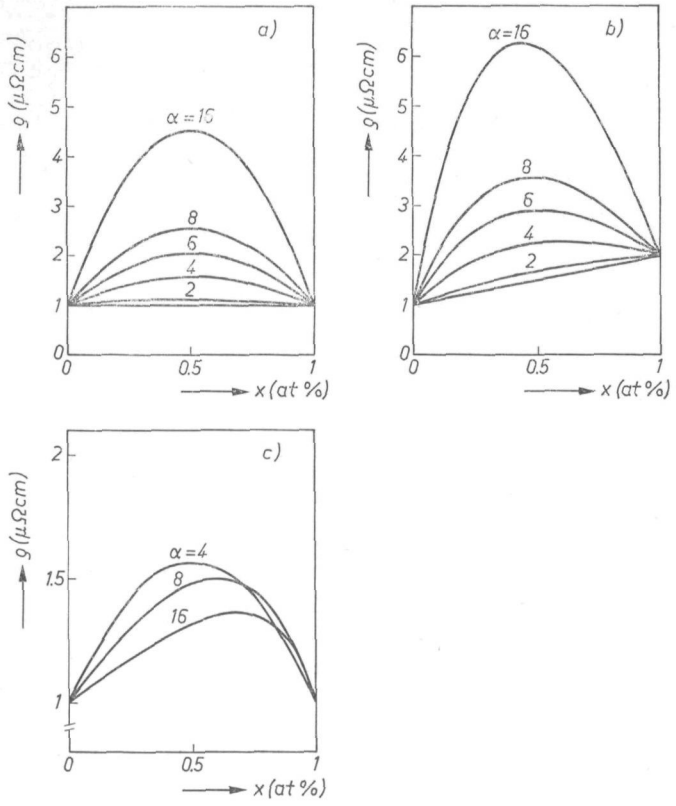

Fig. 4.5. Numerical examples of the resistivity of sets of ternary alloys $M_{99}A_{1-x}B_x$ as a function of x for different values of the parameter α:
(*a*) $\alpha_A = \alpha$; $\alpha_B = 1/\alpha$; $\varrho_A = \varrho_B = 1$ μΩcm
(*b*) $\alpha_A = \alpha$; $\alpha_B = 1/\alpha$; $\varrho_A = 1$ μΩcm; $\varrho_B = 2$ μΩcm
(*c*) $\alpha_A = \alpha$; $\alpha_B = \alpha/16$; $\varrho_A = \varrho_B = 1$ μΩcm.

the complex relationship between the sub-band resistivities and the residual resistivities of ternary alloys it is difficult to indicate in a clear-cut statement the uncertainty of the sub-band resistivities in connection with a given scatter in the experimental data. Clearly, the differences in α for the solute metals are more easily determined than the absolute values.

We decided to determine "average" values for the two residual resistivities by fitting all our experimental resistivity values of binary and ternary nickel- or iron-based alloys to relation (2.3) in a single computer fit. The experimental data used and the computer fit are recorded in the figures in the appendix. The black points (●) indicate that the actual value was determined from two or more (in most cases three) alloys with different total solute concentrations. The ratio of the concentrations of the solute elements was, of course, kept the same for these data points. The white circles (○) represent measurements on a single alloy, usually with a total solute concentration of 3 at%. All data

points plotted in the figures, whether plotted as ● or ○, were given equal weight in the fitting procedure. In the figures in the appendix all the resistivity data are reduced to a total solute concentration of 1 at%.

The number of data points for nickel-based alloys was 100 and the number of adjustable parameters 34, corresponding to 17 solute elements, each having a value for $\varrho^{\uparrow}$ and a value for $\varrho^{\downarrow}$. The corresponding numbers for iron-based alloys were 63 data points and 22 adjustable parameters. Data for binary alloys have got a larger weight, proportional to the number of sets of ternary alloys in which the corresponding solute occurred. The sum of the squares of the relative deviations was minimized with the previously mentioned Direct Search procedure. After this fitting the r.m.s. deviation was 4.3% for the nickel alloys and 4.1% for the iron alloys investigated, which agrees with our estimate of the experimental error. The sub-band resistivities thus found are recorded in table 2-III.

A computer fit in which all data points are included simultaneously has the obvious advantage that the influence of accidental errors, due to inaccuracies of the measurements, on the final result is reduced to a minimum. It is more important that, basically, the two-current model will only be an approximation and "average" values should preferably be obtained by combining a given solute with different solute metals as partners in different sets of ternary alloys. This advantage is absent when α values are based on the temperature-dependent resistivity of binary alloys or on detailed measurements on one ternary alloy system only (e.g. NiCoRh in fig. 2.6; NiCoCr in Leonard et al.[20]).

Inspection of the plots in the appendix shows that, as expected, large deviations from the rule of additivity occur in sets of ternary alloys in which one of the solute elements has $\alpha = \varrho^{\downarrow}/\varrho^{\uparrow} > 1$ and the other has $\alpha < 1$, e.g. $Ni_{99}Au_{1-x}Rh_x$, $Ni_{99}Co_{1-x}Ru_x$, etc. However, the presence of sets of alloys with small deviations from the rule of additivity is important since it confirms that either both solute elements have $\alpha > 1$, as in $Ni_{99}Au_{1-x}Co_x$ or both solute elements have $\alpha < 1$, as in $Ni_{99}Rh_{1-x}Ru_x$.

It is of interest to note that our analysis is incapable of determining which ϱ value is to be associated with the "up" or "down" band. However, as soon as we have made a choice for one solute element the convention is fixed for all solutes since all sets of ternary alloys are interrelated (fig. 3.3). Our convention is explained in the next sec. (4.3).

For a number of elements dissolved in iron we did not determine the sub-band resistivities from an analysis of the residual resistivity of ternary alloys. For these solute elements, the elements asterisked in table 2-III, we estimated the sub-band resistivities by analysing the temperature dependence of the resistivity of binary alloys. In a sense binary alloys at higher temperatures can be considered as ternary alloys in which one of the solute elements is replaced by phonons and spin waves. At higher temperatures in a scattering process the

spin direction is no longer rigorously conserved and scattering processes in which the spin of the current carriers flips from the one direction to the other have to be taken into account. For the simplest model of two sub-bands with equal numbers of electrons, each having the same effective mass Campbell et al.[10]) and Fert [68,81]) showed that the resistivity can be described by

$$\varrho = \frac{\varrho^{\uparrow}\varrho^{\downarrow} + \varrho^{\uparrow\downarrow}(\varrho^{\uparrow} + \varrho^{\downarrow})}{\varrho^{\uparrow} + \varrho^{\downarrow} + 4\varrho^{\uparrow\downarrow}}, \tag{4.1}$$

where $\varrho^{\uparrow}$ and $\varrho^{\downarrow}$ are the sums of the impurity resistivity and the temperature-related resistivity in the two sub-bands. The spin flip scattering is characterized by $\varrho^{\uparrow\downarrow}$. When $\varrho^{\uparrow\downarrow} = 0$ we have a rigorous two-current model. When $\varrho^{\uparrow\downarrow} \gg \varrho^{\uparrow}, \varrho^{\downarrow}$ we have

$$\varrho = \tfrac{1}{4}(\varrho^{\uparrow} + \varrho^{\downarrow}), \tag{4.2}$$

since both bands have the average resistivity $\frac{1}{2}(\varrho^{\uparrow} + \varrho^{\downarrow})$ and the total resistivity is half of this. In a later publication Fert and Campbell [69]) claimed that the simple formula (4.1) is quite general and that the resistivity in a two-current model with interband scattering can always be described by a formula like (4.1).

For the solutes in iron, which are not marked with an asterisk in table 2-III, we determined $(i^{\downarrow}/i_{\text{total}})_{||}$ at low temperature from ternary alloys in the way described before. For the corresponding binary alloys we also measured the deviations from Matthiessen's rule at room temperature. By interpolation we obtained for each solute in iron the deviations from Matthiessen's rule which would correspond to alloys with a residual resistivity (at 4.2 K) of 3 and 6 μΩcm. It is clear from relation (4.1) that when the residual resistivity of a particular solute in iron is given the deviation from Matthiessen's rule only depends on $(i^{\downarrow}/i_{\text{total}})_{||}$ for that particular solute since all other parameters occurring in

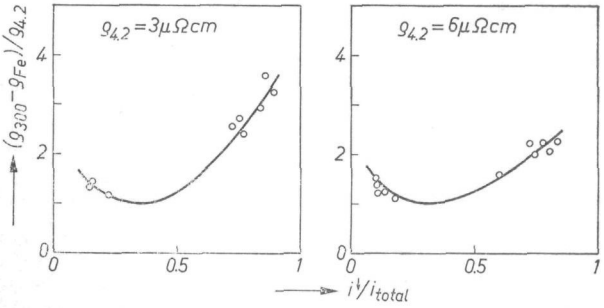

Fig. 4.6. Deviations from Matthiessen's rule in iron-based alloys as a function of the solute parameter at 4.2 K: $i^{\downarrow}/i_{\text{total}}$. In the vertical direction we have plotted $(\varrho_{300} - \varrho_{Fe})/\varrho_{4.2}$ where ϱ_{300} is the room-temperature resistivity of a particular alloy, ϱ_{Fe} is the resistivity of pure iron at room temperature (about 10 μΩcm) and $\varrho_{4.2}$ is the residual resistivity of the iron-based alloy.

(4.1) are determined by the temperature dependent scattering in the iron matrix. For these alloys we plotted as open circles in fig. 4.6 the deviations from Matthiessen's rule at room temperature versus $(i^{\downarrow}/i_{\text{total}})_{\text{II}}$ at 4.2 K, derived from ternary alloys. The curve drawn through the points shows a minimum at $(i^{\downarrow}/i_{\text{total}})_{\text{II}} = 0.35$ which suggests that for the temperature-dependent part of the resistivity in iron at room temperature $(i^{\downarrow}/i_{\text{total}})_{\text{II}}$ is near that value. When the deviations from Matthiessens' rule at 300 K for additional solutes (marked with an asterisk in table 2-III) are measured, there is a choice between two values of $(i^{\downarrow}/i_{\text{total}})_{\text{II}}$. The choice to be made, however, is quite obvious. It is based on the general correlation we found between the solute parameter $(i^{\downarrow}/i_{\text{total}})_{\text{II}}$ and the anisotropy effect (see chapter 5) where $(i^{\downarrow}/i_{\text{total}})_{\text{II}}$ was determined from ternary alloys. Once this solute parameter is known $\varrho_{\text{A}}{}^{\uparrow}$ and $\varrho_{\text{A}}{}^{\downarrow}$ can be calculated separately from $\varrho_{4.2}$.

Earlier an extensive study of the deviations from Matthiessen's rule at room temperature in binary iron-based alloys was carried out by Arajs et al.[48]). Though they do not analyse their results in terms of a two-current model, they observe an apparent subdivision of all solute elements. One group of elements (Mn, Mo, Re, Cr, V, Ti, W and possibly Pd) is associated with large deviations from Matthiessen's rule at room temperature. The other group (formed by non-transition elements such as Si, Ge, Al and the transition elements Co and Ni) is associated with small deviations, in agreement with our results.

4.3. Interpretation and discussion of the resistivities

In this section we shall deal with the problem of the convention as to which are the "up" and which the "down" carriers. We will simultaneously demonstrate that the sub-band residual resistivities correlate in a simple way with experimental data from neutron diffraction, magnetization and heat-capacity experiments. This correlation can be considered as a strong support for the validity of the two-current model, which is independent of transport properties.

Our up–down convention for nickel is based on the fact that $\varrho^{\uparrow}$ and $\varrho^{\downarrow}$ have also been found to be different for phonon scattering at room temperature. Since the densities of states for the two nickel sub-bands differ considerably it is a straightforward matter to identify the spin band with the high density of states, i.e. the minority one, as the one having the high resistivity. An alternative way to arrive at this result is to use existing information about the magnetic moments of Co, Fe and Mn in nickel, as found in Collins and Low [82]) and Low [83]). The magnetic moment of Co as a solute in nickel is about 1.5 μ_{B}, i.e. 1 μ_{B} larger than that of nickel, and Co has 1 valence electron less than nickel. The fact that the magnetic moment is 1 μ_{B} larger must mean *) that the missing valence electron is one with the minority-spin direction. But since

*) We ignore here the amount by which g differs from 2.

Co and Ni are nearly indistinguishable for the majority-spin direction while the number of minority-spin electrons is different, we would expect $\varrho^{\downarrow} > \varrho^{\uparrow}$, which is the case.

In this example, as in the following ones, we assume that the impurity resistivity is correlated with the difference in valence between the solute and the solvent atoms. Such a correlation is known to exist in non-ferromagnetic metals (Linde's rule [86])). Here we extend this rule to the case of ferromagnetic alloys.

Similar considerations can be applied to other solutes in nickel. Iron has two valence electrons less than nickel and its magnetic moment in nickel exceeds 2 μ_B; for Mn the magnetic moment is about 3 μ_B and $\Delta Z = -3$; α for Mn and Fe in nickel is therefore expected to be similar to Co in nickel, as is indeed the case; see table 2-III. A contrasting example is Cr, for which $\Delta Z = -4$, but the magnetic moment is smaller than that of nickel. Consequently, $\varrho^{\uparrow} > \varrho^{\downarrow}$ for Cr in nickel *).

For solute metals in iron the experimental information on impurity magnetic moments is much more accurate than in nickel because the spatial extent of the magnetic disturbances is smaller and the magnetic moment of iron is larger. Furthermore, extensive NMR experiments have been providing accurate values for μ_{solute} for a number of solutes. From this information the up and down convention for iron is obvious. Mn, which has one valence electron less than iron, has a magnetic moment which is about 1.2 μ_B smaller, indicating that this valence electron is taken from the up band: $\varrho^{\uparrow} > \varrho^{\downarrow}$ is expected for Mn in iron. Similarly, V in iron has $\Delta Z = -3$ and the magnetic moment of V is 2.4 μ_B smaller than that of iron (−0.2 as compared to +2.2). Clearly, the reduction in number of valence electrons in particular affects the up band and thus V will resemble Mn as a solute in iron. For Pt in iron, on the other hand, we have $\Delta Z = +2$ while $\Delta\mu = -2\ \mu_B$, since the magnetic moment of Pt in iron is near 0. Thus the two additional electrons are added to the down band and we expect $\varrho^{\downarrow} > \varrho^{\uparrow}$.

In table 4-II we give the results of this type of analysis for all the solute metals investigated. We estimated $\Delta Z^{\uparrow}$ and $\Delta Z^{\downarrow}$ from

$$\mu_{\text{solute}} - \mu_{\text{Fe}} = \Delta Z^{\uparrow} - \Delta Z^{\downarrow} \tag{4.3a}$$

and

$$\Delta Z = \Delta Z^{\uparrow} + \Delta Z^{\downarrow}, \tag{4.3b}$$

where ΔZ is the valence difference between solute and solvent, and μ_{solute} and μ_{Fe} are expressed in Bohr magnetons μ_B. In cases where data from both neutron and NMR experiments were available, we preferred the NMR values. The expected correlation between $\varrho^{\uparrow}$ and $\varrho^{\downarrow}$ on the one hand and $\Delta Z^{\uparrow}$ and $\Delta Z^{\downarrow}$ on the other

*) A more sophisticated treatment of this problem, involving self-consistent energy-band calculation, can be found, among others, in Demangeat [84]) and Campbell and Gomès [85]).

is clearly seen in table 4-II. When $\Delta Z^{\uparrow}$ is large compared to $\Delta Z^{\downarrow}$, $\varrho^{\uparrow}$ is large compared to $\varrho^{\downarrow}$. This is also shown in fig. 4.7, where $i^{\downarrow}/i_{\text{total}}$ is plotted versus $|\Delta Z^{\uparrow}|/(|\Delta Z^{\uparrow}| + |\Delta Z^{\downarrow}|)$. In view of the drastic simplifications involved in the calculations (e.g. charge neutrality for impurities) and experimental uncertainties in μ_{solute}, the agreement is surprisingly good.

In addition to the comparison of the ratio of the resistivities to that of the changes in the numbers of valence electrons, one can also compare resistivities for a given sub-band with values of ΔZ in that band. If a kind of Linde's rule [86]) would apply to each sub-band individually it makes sense to plot $\varrho^{\uparrow}$ vs $|\Delta Z^{\uparrow}|$ and $\varrho^{\downarrow}$ vs $|\Delta Z^{\downarrow}|$. This plot is shown in fig. 4.8. Values for $\varrho^{\uparrow}$ and $\varrho^{\downarrow}$ are taken from table 2-III; $\Delta Z^{\uparrow}$ and $\Delta Z^{\downarrow}$ are from table 4-II. The curves suggest that the resistivity becomes very small if ΔZ for the sub-band considered is small, independent of ΔZ for the other sub-band.

TABLE 4-II

A correlation between impurity sub-band resistivities and their magnetic moment in iron-based alloys. Residual resistivities are characterized by $i^{\downarrow}/i_{\text{total}}$, while the magnetic moment offers a value for $|\Delta Z^{\uparrow}|/(|\Delta Z^{\uparrow}| + |\Delta Z^{\downarrow}|)$, where ΔZ is the difference in the number of valence electrons between solute and solvent.

solute	data on μ_{sol} in Bohr magnetons μ_B				$\Delta\mu/\mu_B$	ΔZ	$\Delta Z^{\downarrow}$	$\Delta Z^{\uparrow}$	$\frac{\lvert\Delta Z^{\uparrow}\rvert}{\lvert\Delta Z^{\uparrow}\rvert+\lvert\Delta Z^{\downarrow}\rvert}$	$\frac{i^{\downarrow}}{i_{\text{total}}}$
	1	2	3	4						
Ti	−0.7	−1.2		−1.2	−3.4	−4	−0.3	−3.7	0.93	0.60
V	−0.4	−0.9	−0.2	−0.2	−2.4	−3	−0.3	−2.7	0.90	0.88
Cr	−0.7	−0.9		−0.9	−3.1	−2	+0.55	−2.55	0.82	0.73
Mn	0	0	+1.0	+1.0	−1.2	−1	+0.1	−1.1	0.92	0.85
Co	+2.1	+2.1	+1.9	+1.9	−0.3	+1	+0.65	+0.35	0.35	0.21
Ni	+0.9	+1.2	+1.4	+1.4	−0.8	+2	+1.4	+0.6	0.30	0.13
Mo	−0.1	−0.7	+0.2	+0.2	−2.0	−2	0	−2.0	1.00	0.83
Ru	+0.9	+0.7	+1.0	+1.0	−1.2	0	+0.6	−0.6	0.50	0.72
Rh	+0.5	+0.5	+1.1	+1.1	−1.1	+1	+1.05	−0.05	0.04	0.15
W	−0.7	−0.5		−0.5	−2.7	−2	+0.35	−2.35	0.87	0.81
Re	−0.3	−0.5		−0.5	−2.7	−1	+0.85	−1.85	0.69	0.77
Os	0	+0.1		+0.1	−2.1	0	+1.05	−1.05	0.50	0.75
Ir	0	+0.2		+0.2	−2.0	+1	+1.5	−0.5	0.25	0.10
Pt	0	+0.1		+0.1	−2.1	+2	+2.05	−0.05	0.02	0.11

sol-ute	data on μ_{sol} in Bohr magnetons μ_B				$\Delta\mu/\mu_B$	ΔZ	$\Delta Z^{\downarrow}$	$\Delta Z^{\uparrow}$	$\frac{\lvert\Delta Z^{\uparrow}\rvert}{\lvert\Delta Z^{\uparrow}\rvert+\lvert\Delta Z^{\downarrow}\rvert}$	$\frac{i^{\downarrow}}{i_{total}}$
	1	2	3	4						
Zn	(0)			0	(−2.2)	+4	+3.1	+0.9	0.23	0.35
Be	(0)			0						0.14
Ga	0			0	−2.2	+5	+3.6	+1.4	0.28	0.11
Al	0			0						0.11
Ge	0			0	−2.2	+6	+4.1	+1.9	0.32	0.14
Si	0			0						0.15
Pd	+0.4		+1.0	+1.0	−1.2	+2	+1.6	+0.4	0.20	?
Cu	0			0	−2.2	+3	+2.6	+0.4	0.13	?

Experimental data on μ_{sol} in the first column are from neutron diffraction experiments: Holden et al.[91]), Comly et al.[92]) and Collins and Low [82]). Data in the second column are from a reanalysis by Campbell [93]) of data from Collins and Low. In the third column we give results from NMR experiments by Stearns [94,101]). Our preferred values are collected in the fourth column. $\Delta\mu$ is the difference between the magnetic moments of solute atoms and iron atoms (as solvent). Estimated values are between brackets.

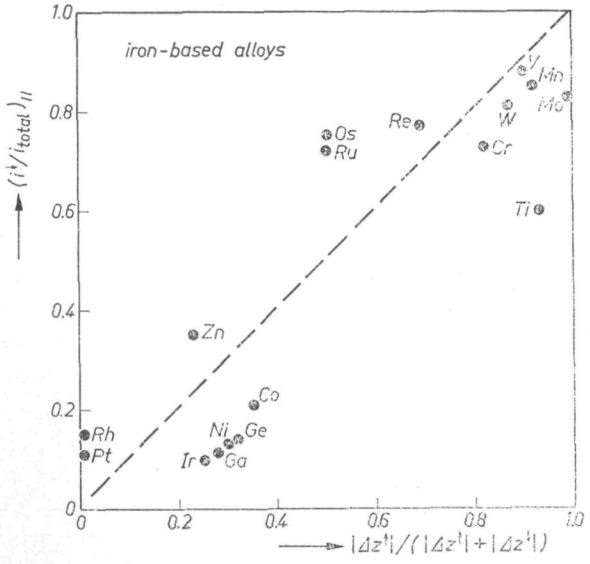

Fig. 4.7. A plot of the two-current parameter at 4.2 K: $(i^{\downarrow}/i_{total})_{II}$ as a function of $|\Delta Z^{\uparrow}|/(|\Delta Z^{\uparrow}| + |\Delta Z^{\downarrow}|)$. Data points are also recorded in table 4-II.

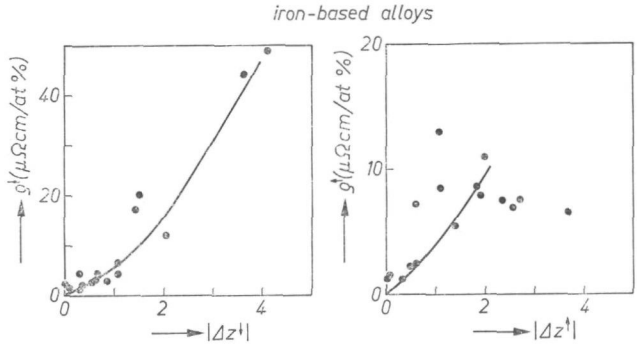

Fig. 4.8. Plots of the specific residual resistivities $\varrho^{\uparrow}$ and $\varrho^{\downarrow}$ of different solute elements in iron as a function of $|\Delta Z^{\uparrow}|$ and $|\Delta Z^{\downarrow}|$, respectively.

As has been extensively demonstrated by Caudron et al.[87]), there is a close resemblance between the variation of γ with solute concentration for a given solute element in nickel and the value of $\varrho^{\uparrow}$ for that solute. Here γ is the coefficient of the linear term in the electronic heat capacity and its variation is expressed as $(1/\gamma_0)\,(\partial\gamma/\partial c)$, where γ_0 is the electronic heat-capacity coefficient for pure nickel (7.02 mJ/K^2 mol). In principle γ may be taken as a measure for the total density of states at the Fermi surface, which in pure nickel is predominantly due to the minority-spin band. If the densities of states $n^{\uparrow}(\varepsilon_F)$ and $n^{\downarrow}(\varepsilon_F)$ in nickel would be of a comparable order of magnitude we would expect that dissolving foreign atoms might increase as well as decrease the total density of states, depending on the solute involved. Since in pure nickel $n^{\uparrow}(\varepsilon_F)$ is very small it is expected that $n^{\uparrow}(\varepsilon_F)$ can only increase by dissolving foreign atoms. Then considering different solutes we expect that on the average the total density of states will increase when adding impurities to pure nickel. The large positive change in γ which can occur $(1/\gamma_0)\,(\partial\gamma/\partial c)$ up to 10% per at%, is therefore mainly due to effects in the up band. We demonstrate this by plotting $(1/\gamma)\,(\partial\gamma/\partial c)$ versus $\varrho^{\uparrow}$ in fig. 4.9. The heat-capacity information is taken from Caudron et al.[87,88]) and from Gregory and Moody [89]). Values for $\varrho^{\uparrow}$ are either from table 2-III or from table 4-III in the next section. The correlation is convincing.

In the case of iron alloys the situation of a low density of states in one of the bands does not exist and consequently changes in γ upon alloying are smaller, viz. -2% per at% $< (1/\gamma)\,(\partial\gamma/\partial c) < +2\%$ per at%. In this case γ will be related to comparable effects in both bands, which may have either sign.

4.4. Discussion of temperature-dependent resistivities

In this section we compare our values for $\varrho^{\uparrow}$ and $\varrho^{\downarrow}$ for nickel-based alloys as derived from ternary alloys at low temperatures, with data from other authors. As far as the latter data have been obtained from ternary alloys at

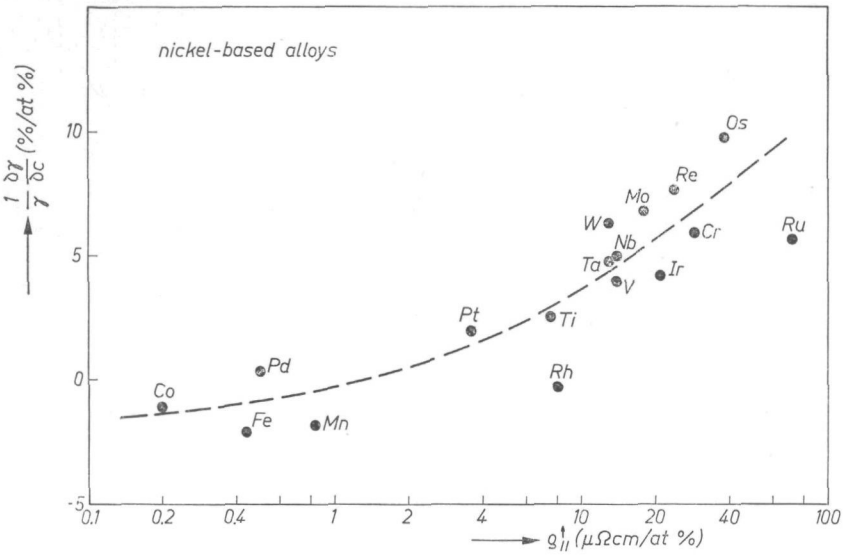

Fig. 4.9. The variation of the electronic heat capacity $(1/\gamma_0)\,(\partial\gamma/\partial c)$ in % per at % solute versus the specific residual resistivity in the spin-up band for different solute elements in nickel.

TABLE 4-III

The residual sub-band resistivities in μΩcm/at% of nickel-based alloys, analysed in terms of a two-current model

solute element		present work	data from literature				
Ti	↑	7.6	4.5 [17])	4.1 [8])	4.4 [16])		
	↓	7.2	12.3	9.9	13.1		
V	↑	14	6.0 [17])	11.6 [8])			
	↓	6.4	14.1	7.5			
Cr	↑	29	17.6 [20])	30 [65])	28 [17])	16.4 [8])	18.3 [16])
	↓	6.1	7	6.0	5.8	7.3	5.9
Mn	↑	0.83	0.94 [17])	0.68 [8])	0.6 [16])		
	↓	5.2	5.1	9.9	9.7		
Fe	↑	0.44	0.45 [17])	0.34 [8])			
	↓	4.8	3.3	7.3			
Co	↑	0.20	0.21 [20])	0.15 [65])	0.15 [17])	0.13 [8])	0.2 [16])
	↓	2.6	4.3	3.2	2.0	4.4	6.0

TABLE 4-III (continued)

Zr	↑		4 [13])
	↓		30
Nb	↑		16 [13])
	↓		7
Mo	↑		29 [13])
	↓		8
Ru	↑	72	40 [13])
	↓	5.4	6
Rh	↑	8.0	12 [13])
	↓	2.3	2
Pd	↑		0.3 [17])
	↓		0.3
Hf	↑		3.5 [13])
	↓		30
Ta	↑		16 [13])
	↓		7.6
W	↑		17.4 [13])
	↓		7.0
Re	↑	24	29 [13])
	↓	7.5	7.6
Os	↑		50 [13])
	↓		6.4
Ir	↑	21	35 [13])
	↓	5.0	4.7
Pt	↑	3.6	6.9 [13])
	↓	0.85	1.2
Cu	↑	1.3	0.98 [17])
	↓	3.8	3.6
Au	↑	0.44	
	↓	2.6	
Zn	↑	1.3	
	↓	2.9	
Al	↑	3.4	
	↓	5.8	
Si	↑	5.0	
	↓	6.4	
Sn	↑	4.4	7.1 [15])
	↓	7.2	7.1

4.2 K, direct comparison is possible (e.g. Co and Cr by Leonard et al.[20])). We prefer our own values because they were obtained by fitting a large number of data simultaneously.

However, most values were derived from the temperature dependence of the resistivity and merit further discussion. According to formula (4.1), ϱ is a function of three parameters: $\varrho^{\uparrow}$, $\varrho^{\downarrow}$ and $\varrho^{\uparrow\downarrow}$. For a binary alloy $Ni_{100-x}A_x$ we have $\varrho^{\uparrow} = x\,\varrho_A{}^{\uparrow} + \varrho_T{}^{\uparrow}$ and $\varrho^{\downarrow} = x\,\varrho_A{}^{\downarrow} + \varrho_T{}^{\downarrow}$. The three parameters which characterize the temperature-dependent part of the resistivity viz. $\varrho_T{}^{\uparrow}$, $\varrho_T{}^{\downarrow}$ and $\varrho^{\uparrow\downarrow}$, are assumed to be independent of the alloy and hence to be parameters of the pure nickel. Furthermore, $\varrho_A{}^{\uparrow}$ and $\varrho_A{}^{\downarrow}$ are assumed to be independent of T. By measuring the deviations from Matthiessen's rule either as a function of x or as a function of temperature for a given alloy, it is possible in principle to determine the parameters involved. For the analysis the resistivity of pure nickel as a function of T and the residual resistivity of the alloy are also needed. In practice the number of parameters proves too large to enable variations in $\varrho^{\uparrow\downarrow}$ to be distinguished from complimentary variations in $\alpha_T = \varrho_T{}^{\downarrow}/\varrho_T{}^{\uparrow}$. This has led different investigators to arrive at somewhat different conclusions.

Fert and Campbell [16]) suggest that for nickel $\alpha_T = 2.3$ at temperatures below 50 K and that the spin-flip resistivity varies as $\varrho^{\uparrow\downarrow} = A\,T^2$, with $A = 5 \cdot 10^{-5}$ μΩcm K^{-2}. Farrell and Greig [17]) assume that the spin-mixing resistivity at room temperature is very large, so that the current carriers have an equal probability of having up spin or down spin. The resistivity is then given by expression (4.2) and the residual sub-band resistivities for different solute elements are easily obtained. Durand [90]) and Durand and Gautier [13]) found $\alpha_T = 2.6$ and $\varrho^{\uparrow\downarrow} = 0.3$ μΩcm at 77 K, in fair agreement with the above result of Fert and Campbell. At 297 K Durand finds $\varrho^{\uparrow\downarrow} = 0$ and a α_T value between 1.60 and 1.86. Fert [68]), however, proposes $\varrho^{\uparrow\downarrow} = 11$ μΩcm and $\alpha_T = 4$ at room temperature; Fert's values for the thermal resistivities are reproduced as table 4-IV. Price and Williams [15]) fitted data for NiSn alloys

TABLE 4-IV

Values of $\varrho^{\uparrow\downarrow}(T)$, $\varrho^{\uparrow}(T)$ and $\varrho^{\downarrow}(T)$ for nickel at 77, 200 and 300 K, taken from Fert [68]) and Fert and Campbell [69])

T	77 K	200 K	300 K
$\varrho^{\uparrow\downarrow}(T)$	0.9 ± 0.3 μΩcm	5 ± 2 μΩcm	11 ± 4 μΩcm
α_T	5 ± 1	5 ± 2	4 ± 2
$\varrho^{\uparrow}(T)$	0.38 μΩcm	3 μΩcm	6.7 μΩcm
$\varrho^{\downarrow}(T)$	1.9 μΩcm	15 μΩcm	26.8 μΩcm

over the entire temperature range (up to 300 K) with $\alpha_T = 3.6$ and $A = 2 \cdot 10^{-5}$ $\mu\Omega$cm K^{-2} but the fit was not very satisfactory. In experiments on a few nickel-based alloys with non-transition metals Hugel [14]) corroborated the above-mentioned results of Durand and Gautier [13]). Greig and Rowlands [70]) denied the need to introduce a spin-mixing term at temperatures below 273 K provided α_T is taken as < 1. These results have been criticized by Fert and Campbell [69]).

In conclusion, values for α_T and $\varrho^{\uparrow\downarrow}$ remain uncertain since experimental results are not very sensitive to simultaneous changes in $\varrho_T{}^{\uparrow}$, $\varrho_T{}^{\downarrow}$ and $\varrho^{\uparrow\downarrow}$ such that they leave the resistivity of Ni at room temperature unchanged. For practical purpose, e.g. predicting the resistivity anisotropy at room temperature, $\varrho^{\uparrow\downarrow} \approx 0$ can be taken as a good approximation.

The determination of $\varrho_A{}^{\uparrow}$ and $\varrho_A{}^{\downarrow}$ from temperature-dependent investigations is less ambiguous than that of the other three parameters. The agreement between the ternary alloy data and the temperature-dependent data is quite reasonable; see table 4-III. This shows that the temperature dependence of the impurity resistivity cannot be large since otherwise $\varrho_A{}^{\uparrow}$ and $\varrho_A{}^{\downarrow}$ determined from room-temperature measurements would not agree with our low-temperature results. A similar conclusion was reached by Durand and Gautier [13,90]).

5. THE RESISTIVITY ANISOTROPY OF DILUTE ALLOYS AT 4.2 K

5.1. Determination of the resistivity anisotropy

For polycrystalline alloys we define the resistivity anisotropy as the rate of decrease of the resistivity when, at zero induction, the magnetization is tilted from parallel to perpendicular to the current:

$$\Delta\varrho/\varrho_{\parallel} = (\varrho_{\parallel} - \varrho_{\perp})/\varrho_{\parallel}. \tag{5.1}$$

Our reasons for choosing $B = 0$ and $\varrho_{\parallel}$ as the reference situation have already been explained in chapter 4. The definition is at variance with that of most other authors who put $\bar{\varrho} = (\varrho_{\parallel} + 2\,\varrho_{\perp})/3$ in the denominator of (5.1). In some cases $\bar{\varrho}$ is defined more pragmatically at $H = 0$ instead of at $B = 0$ (e.g. McGuire [95]).

The way in which we determined $\varrho_{\parallel}$ and $\varrho_{\perp}$, and hence the anisotropy effect $\Delta\varrho/\varrho_{\parallel}$ expressed in %, is illustrated in fig. 1.1. For reasons already discussed in chapter 4, the resistivities of nickel-based alloys were extrapolated quadratically to zero induction, while for the iron-based alloys this extrapolation was done linearly.

Since the resistivity anisotropy is a relative effect the main source of error which is present in a measurement of the resistivity, i.e. the form factor, is absent in the anisotropy effect. Taking this into account we estimate the absolute error in our data for the resistivity anisotropy to be of the order of about 0.3% for nickel-based alloys and about 0.7% for iron-based alloys. The difference in inaccuracy between nickel and iron alloys is due to the difference in the range of extrapolation ($4\pi M_s = 6.4$ kG for nickel and 21.9 kG for iron).

It might be thought that the accuracy of $\Delta\varrho/\varrho_{\parallel}$ could be improved by constructing a detailed Kohler plot for $\varrho_{\perp}$ and $\varrho_{\parallel}$ and extrapolating according to $\varrho(B)/\varrho_0 = f(B/\varrho_0)$. Since at least two different Kohler functions are involved, one for each spin-current, the resulting Kohler function will be different for each solute metal; see fig. 4.2*a*. For the alloys with the lowest resistivity ϱ_0, and a large transverse magnetoresistivity, e.g. Co, Fe, Mn and Au in nickel, we verified that using the proper Kohler function results in values for $\Delta\varrho/\varrho_{\parallel}$ which are not significantly different from those obtained from a nearly quadratic low-field extrapolation. In addition, we note that there is no reason why Kohler's rule should be rigorously valid since the normal Hall coefficient for nickel alloys, for instance, varies with solute concentration; see chapter 2. Moreover, the side-displacement contribution to the anomalous Hall effect will interfere with the magnetoresistance, Berger [96]) and Majumdar and Berger [44]).

In table 5-I we compare our results with data from the literature on the anisotropy effect in nickel-based alloys. As a rule all results to which we refer were obtained at 4.2 K except those reported by Van Elst and Gorter [22]) and

TABLE 5-I

Survey of literature data on the anisotropy effect of nickel alloys. We selected values with concentrations as near as possible to 3 at %. In general $T = 4.2$ K and $B = 0$. Effects have been recalculated in accordance with expression (5.1) used as the definition of the effect. The upper value for each element represents anisotropy effect in % and the lower the solute concentration in at %

solute element	anisotropy effect in % from literature solute concentration in at % between brackets				present results in %
Ti					+0.55
V	+0.6 [a] (3.5)				+0.15
Cr	−0.6 [a] (1.1)	−0.3 [f] (0.9)			−0.35
Mn	+9.5 [a] (2.4)	+8.7 [c] (2.0)	+8.9 [f] (2.0)		+7.8
Fe	+14 [b] (1)	+11.8 [c] (3)	+9.9 [d] (2.3)	+12.1 [f,g] (3)	+12.5
Co	+14.2 [c] (3)	+8.2 [e] (2.5)	+14.9 [f] (3)	+14 [g] (2.8)	+13.5
Nb	+0.1 [f] (1.6)				
Mo	+0.1 [a] (3.1)	0 [f] (3.4)			
Ru	−0.8 [f] (3.8)				−0.6
Rh	+0.1 [f] (2.3)				+0.05
W	+0.4 [a] (3.2)				
Re	−0.4 [f] (0.9)				−0.5
Os	+0.2 [f] (1.6)				
Ir	−1.5 [f] (3)				−1.5
Pt	+0.4 [f] (4)				+0.4

TABLE 5-I (continued)

solute element	anisotropy effect in % from literature solute concentration in at % between brackets	present results in %
Cu	+6.8 [f]) (2.9)	+6.8
Au	+5.5 [f]) (1.0)	+7.5
Zn	+5.6 [a]) (4.5)	+4.6
Al	+4.6 [a]) (2.2)	+3.8
C	+1.8 [b]) (0.4)	
Si	+2.5 [a]) (1.7)	+2.1
Sn	+3.3 [a]) (3.0)	+2.9
phonons	+3.5 [b])	
dislocations	+3.3 [b])	

[a]) Van Elst and Gorter [22]) and Van Elst [1]); $H = 0$, $T = 14$ K.
[b]) Schwerer and Silcox [102]).
[c]) Fert [68]) and Campbell et al.[25]).
[d]) McGuire and Potter [30]); $H = 0$.
[e]) McGuire [95]) and McGuire and Potter [30]); $H = 0$.
[f]) Jaoul [31]).
[g]) Jaoul et al.[103]).

Van Elst [1]), which are for 14 K, and by Smit [21]), which are for 20 K. Data from Vasilyev [26]) on binary alloys at 77 K are not included. Unless otherwise indicated, the anisotropy effect is defined at $B = 0$. It will be seen that there is generally good agreement between our values and those reported by other authors. Only in the case of NiCo and NiFe is there a rather large scatter between results from different authors but in view of the relatively small resistivity this is not too surprising. It will also be observed that of the solute metals not considered in our work Nb is similar to V, while Mo and W, as was to be expected, do not differ greatly from Cr.

For iron-based alloys there are no literature data with which to make comparisons. The only information available, with solute concentrations near 3 at% concerns FeV, for which Sueda and Fujiwara [33]), quoted by McGuire and Potter [30]), report an effect of 6%.

5.2. Concentration dependence of the anisotropy effect

For isolated solute atoms in an otherwise ideally pure matrix, the anisotropy effect is expected to be concentration independent, as we have in fact demonstrated for a number of nickel- and iron-based alloys in table 2-IV. Solute atoms clearly cannot be considered isolated if the concentration becomes too high. For f.c.c. nickel an atomic concentration of 8% must be considered high since each solute atom will have on the average one other solute atom as its neighbour. In this region of concentration the effect may be expected to become dependent on the concentration. The effect will also change for concentrations for which the resistivity becomes comparable to the residual resistivity due to non-deliberate impurities or lattice defects. This is because the unwanted scattering centres will generally have a different value of $\Delta\varrho/\varrho_{11}$ and because for low values of ϱ the procedure of extrapolation may introduce ambiguities into the determination of the effect. The effect should therefore be determined at concentrations between 1 and 5 at%.

In fig. 5.1 we have plotted the concentration dependence of $\Delta\varrho/\varrho_{11}$ for NiCo, NiFe and FeV alloys, combining experimental information from different sources. The concentration dependence of $\Delta\varrho/\varrho_{11}$ for FeV may represent the general behaviour that interaction of impurities reduces the effect. This holds for many

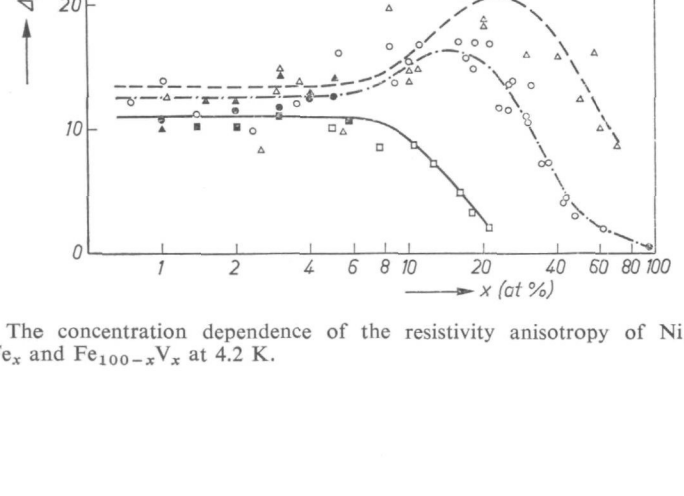

Fig. 5.1. The concentration dependence of the resistivity anisotropy of $Ni_{100-x}Co_x$, $Ni_{100-x}Fe_x$ and $Fe_{100-x}V_x$ at 4.2 K.

nickel alloys as well, because ferromagnetism is gradually lost upon alloying. Favourable exceptions in the sense that interaction between solute atoms tends to increase the effect are NiCo and NiFe. This "accidental" increase is quite important for applications of the anisotropy effect in recording devices. Here it is desirable to have a large effect at room temperature so that the impurity producing the effect should also produce a resistivity comparable to the room temperature resistivity of the pure matrix.

5.3. Analysis of the resistivity anisotropy

In our analysis of the data for the resistivity anisotropy we assume that the model of two independent currents is valid not only in the parallel but also in the transverse configuration. In the first section of chapter 4 we argued that owing to a coupling between the two currents by means of the (anomalous) Hall electric field the two-current model cannot be rigorously valid in the perpendicular configuration. However, maximum anomalous Hall angles observed are only a few % so that we expect this coupling to be unimportant.

When the magnetization is tilted from the parallel to the perpendicular orientation we generally observe a decrease $\Delta\varrho$ of the resistivity. In terms of the two-current model this results from the decrease of the sub-band resistivities: $\Delta\varrho^{\uparrow}$ and $\Delta\varrho^{\downarrow}$. For small variations we differentiated the resistivity in the two-current model and obtained expression (2.9) which is repeated here:

$$\Delta\varrho/\varrho_{\text{II}} = (i^{\uparrow}/i_{\text{total}})_{\text{II}}\,(\Delta\varrho/\varrho_{\text{II}})^{\uparrow} + (i^{\downarrow}/i_{\text{total}})_{\text{II}}\,(\Delta\varrho/\varrho_{\text{II}})^{\downarrow}. \tag{5.2}$$

Since in a ternary alloy $M_{99}A_{1-x}B_x$

$$\varrho^{\uparrow} = (1-x)\,\varrho_{\text{A}}{}^{\uparrow} + x\,\varrho_{\text{B}}{}^{\uparrow}$$

and (5.2*a*)

$$\varrho^{\downarrow} = (1-x)\,\varrho_{\text{A}}{}^{\downarrow} + x\,\varrho_{\text{B}}{}^{\downarrow}$$

we write

$$\Delta\varrho^{\uparrow} = (1-x)\,\Delta\varrho_{\text{A}}{}^{\uparrow} + x\,\Delta\varrho_{\text{B}}{}^{\uparrow}$$

and (5.2*b*)

$$\Delta\varrho^{\downarrow} = (1-x)\,\Delta\varrho_{\text{A}}{}^{\downarrow} + x\,\Delta\varrho_{\text{B}}{}^{\downarrow}.$$

In (5.2), of course, we have

$$(i^{\uparrow}/i_{\text{total}})_{\text{II}} = \varrho_{\text{II}}{}^{\downarrow}/(\varrho_{\text{II}}{}^{\uparrow} + \varrho_{\text{II}}{}^{\downarrow})$$

and (5.2*c*)

$$(i^{\downarrow}/i_{\text{total}})_{\text{II}} = \varrho_{\text{II}}{}^{\uparrow}/(\varrho_{\text{II}}{}^{\uparrow} + \varrho_{\text{II}}{}^{\downarrow}).$$

For each binary or ternary alloy of known composition the resistivities of the spin-up and the spin-down band can be calculated with expression 5.2*a* and the specific sub-band resistivities given in table 2-III. We determined the change $\Delta\varrho$ of the resistivities for different solute elements within each sub-band by fitting all our data points, plotted in the appendix, simultaneously to the theoretical curve (5.2). The adjustable parameters were $\Delta\varrho_A{}^{\uparrow}$ and $\Delta\varrho_A{}^{\downarrow}$. For each solute element A in a particular matrix only one value $\Delta\varrho_A{}^{\uparrow}$ and one value $\Delta\varrho_A{}^{\downarrow}$ were allowed. The fitting was effected by minimizing the sum of

TABLE 5-II

The resistivity anisotropy for iron-based alloys. The effects for the two spin directions were determined separately. Since the effect is positive in the down band and about zero in the up band, the total effect correlates with $(i^{\downarrow}/i_{\text{total}})_{||}$. Elements marked * were not investigated in sets of ternary alloys. The total effect has therefore not been broken down into contributions from the separate spin currents.

solute element	$(i^{\downarrow}/i_{\text{total}})_{||}$	$\Delta\varrho/\varrho_{||}$ (%)	$(\Delta\varrho/\varrho_{||})^{\downarrow}$ (%)	$(\Delta\varrho/\varrho_{||})^{\uparrow}$ (%)
V	0.88	+11.0	+12.3	+3.1
Mn	0.85	+ 8.0	+ 9.4	−1.8
Mo	0.83	+ 8.4	+ 9.8	+2.1
W*	0.81	+ 8.0		
Re	0.77	+ 8.3	+ 9.1	+2.7
Os	0.75	+ 6.8	+ 8.7	+1.5
Cr*	0.73	+ 5.6		
Ru	0.72	+ 4.7	+ 6.7	−0.4
Ti*	0.60	+ 3.0		
Zn*	0.35	+ 3.6		
Co	0.21	+ 0.40	+ 3.7	−0.5
Rh	0.15	+ 1.0	+ 2.4	+0.7
Si	0.15	− 0.20	+ 2.7	−0.8
Be*	0.14	+ 0.45		
Ge*	0.14	0.0		
Ni	0.13	+ 1.6	+ 0.9	+2.1
Pt*	0.11	+ 0.60		
Al	0.11	− 0.30	− 2.5	−0.1
Ga*	0.11	+ 0.15		
Ir*	0.10	+ 0.30		

the squares of differences between the experimental value and the theoretical value of the resistivity anisotropy. We used the numerical Direct Search procedure referred to in sec. 4.2. The results of this fitting procedure have already been given in table 2-V for nickel-based alloys. For iron alloys the results are given in table 5-II, where we tabulate the resistivity anisotropy for individual solute elements within each spin band.

With these values for the anisotropy the r.m.s. deviation between the data points and the calculated curves (see the figures in the appendix) was 0.65% for iron-based alloys and 0.37% for nickel-based alloys. Note that this is an absolute, not a relative, deviation, since the resistivity anisotropy is expressed in %; we minimized the absolute deviations. The accuracy of the fit may be assessed from the figures in the appendix where we plotted the experimental points together with the best fitting curves calculated in the two-current model with the optimum parameters. The remaining deviations can safely be attributed to experimental uncertainties. For nickel-based alloys we determined 34 parameters, corresponding to the values $\Delta\varrho_A{}^{\uparrow}$ and $\Delta\varrho_A{}^{\downarrow}$ for 17 solute elements A, from 108 data points. For iron-based alloys we determined 22 parameters, corresponding to 11 solute elements, from 66 data points. The black data points (●) for the resistivity anisotropy given in the appendix represent data which were obtained from two or more (in most cases three) alloys with different total solute concentration. The ratio of the solute element concentrations was kept the same for these data points. The white points (○) represent measurements on a single alloy, in most cases with a total solute concentration of 3 at%. All points plotted in the figures in the appendix were given equal weight in the fitting procedure. However, data points for binary alloys were given extra weight proportional to the number of sets of alloys in which the solute concerned did occur.

The results given in tables 2-V and 5-II reveal a pattern of striking simplicity. For the nickel alloys it appears that, with Ir as a single exception, the anisotropy effects for all solute elements in the spin-up band are positive. In the spin-down band the anisotropy effects for all solute elements investigated are found to be negative, without a single exception. In other words this means that in the spin-up band the resistivity always decreases, except in the case of Ir, by a certain ratio when the magnetization is tilted from the parallel to the perpendicular orientation. In the spin-down band the resistivity always increases when the magnetization is tilted. It can also be seen that the effect in the spin-up band is on the average significantly larger than in the spin-down band. In the spin-up band the effect is of the order of +10% while in the spin-down band it is of the order of −2%; see also fig. 2.8.

A similar pattern can be observed for iron-based alloys, although less pronounced than in nickel. In the spin-down band the resistivity anisotropy is positive for all solute elements investigated, except Al. It is roughly of the

order of +8%. In the spin-up band the effect varies around zero, depending on the solute element; see also fig. 2.9.

5.4. Interpretation of the resistivity anisotropy effect

Our results on the resolution of the resistivity anisotropy data in a two-current model can be summarized in a straightforward manner. The cross-section for scattering by solute elements depends systematically on the orientation of the magnetization. For the ↑ band in nickel and the ↓ band in iron the cross-section is largest for $M_s \parallel i$. The reverse situation applies to the other band of nickel and iron. An anisotropic scattering cross-section fits naturally into a picture of impurities which are non-transparent for electrons, as we proposed at the end of sec. 2.3. Other reasoning, however, may also produce an effective cross-section which is anisotropic.

For nickel alloys in particular Smit related the resistivity anisotropy with the typical band filling of ferromagnetic nickel. For one spin direction the d band is practically full, so that scattering of electrons is predominantly of the s–s type, whereas for the other spin direction s–d-type scattering is dominant. According to Smit, there is some mixing of $d^{\downarrow}$ states into the ↑ band due to spin–orbit interaction. This interaction is also seen in the deviation of the g factor from 2. The introduction of $d^{\downarrow}$ states into the ↑ band is anisotropic with respect to the direction of the magnetization which leads to an anisotropic resistivity. Campbell et al.[8,24,25]) formulated Smit's suggestion as follows:

$$\begin{aligned} \varrho_{\parallel}{}^{\uparrow} &= \varrho_{\perp}{}^{\uparrow} + \zeta\, \varrho_{\perp}{}^{\downarrow}, \\ \varrho_{\parallel}{}^{\downarrow} &= \varrho_{\perp}{}^{\downarrow} - \zeta\, \varrho_{\perp}{}^{\downarrow}. \end{aligned} \tag{5.3}$$

The extra resistivity in the ↑ band is higher according as the density of states in the ↓ band is higher, the down resistivity being taken as the measure. The mixing coefficient is $\zeta \approx \frac{3}{4}(A/H_e)^2$, where A is the coefficient of the L–S coupling and H_e the exchange field. It would follow from the above that Smit's theory applies to solutes in nickel that do not affect the full d band of nickel; in other words, this model applies specifically to Mn, Fe, Co, Cu and Au in nickel. For Zn, Al, Si and Sn, also, it is reasonable to expect the s–d scattering in the ↑ band to be relatively small compared to s–s scattering. In the case of Ti, V, Cr, Re, Ru, Rh, Ir and Pt, however, there is a large local density of states in the ↑ band so that Smit's assumption of dominant s–s scattering no longer applies.

We compare our experimental results with Smit's model in table 5-III. The values for $\varrho_{\parallel}{}^{\uparrow} - \varrho_{\perp}{}^{\uparrow}$ and $\varrho_{\parallel}{}^{\downarrow} - \varrho_{\perp}{}^{\downarrow}$ are directly obtained from our analysis using the computer fit described above. If formula (5.3) were valid $(\varrho_{\parallel}{}^{\uparrow} - \varrho_{\perp}{}^{\uparrow})/\varrho_{\perp}{}^{\downarrow}$ would give the value of $+\zeta$ while $(\varrho_{\parallel}{}^{\downarrow} - \varrho_{\perp}{}^{\downarrow})/\varrho_{\perp}{}^{\downarrow}$ would

TABLE 5-III

Test of the Smit–Campbell description of the resistivity anisotropy in nickel-based alloys

solute element	$\varrho_{\parallel}^{\uparrow} - \varrho_{\perp}^{\uparrow}$ ($\mu\Omega$cm/at%)	$\varrho_{\parallel}^{\downarrow} - \varrho_{\perp}^{\downarrow}$ ($\mu\Omega$cm/at%)	$(\varrho_{\parallel}^{\uparrow} - \varrho_{\perp}^{\uparrow})/\varrho_{\perp}^{\downarrow}$ (%)	$(\varrho_{\parallel}^{\downarrow} - \varrho_{\perp}^{\downarrow})/\varrho_{\perp}^{\downarrow}$ (%)
little s–d scattering in the spin-up band				
Mn	+0.08	−0.17	+1.5	−3.2
Fe	+0.06	−0.11	+1.2	−2.2
Co	+0.03	−0.04	+1.1	−1.5
Cu	+0.13	−0.08	+3.3	−2.0
Au	+0.04	−0.06	+1.3	−2.1
relatively weak s–d scattering in the spin-up band				
Zn	+0.10	−0.08	+3.3	−2.8
Al	+0.25	−0.13	+4.2	−2.2
Si	+0.31	−0.20	+4.7	−3.1
Sn	+0.28	−0.19	+3.8	−2.6
large local density of states in the spin-up band				
Ti	+0.32	−0.23	+4.3	−3.1
V	+1.11	−0.20	+17	−3.0
Cr	+1.7	−0.10	+27	−1.7
Re	+1.6	−0.18	+20	−2.3
Ru	+5.4	−0.06	+99	−1.1
Rh	+0.62	−0.05	+26	−2.3
Ir	−0.52	−0.07	−10	−1.4
Pt	+0.20	−0.01	+24	−0.8

yield $-\zeta$. For the solute metals for which Smit's theory is most likely to be valid, the results are quite satisfactory with ζ about 0.02. For non-transition solutes, the results combine favourably with those above, although they indicate a slightly higher ζ value. As expected, the remaining impurities behave differently, but only for the $\uparrow$ band. For the $\downarrow$ band $(\varrho_{\parallel}^{\downarrow} - \varrho_{\perp}^{\downarrow})/\varrho_{\perp}^{\downarrow}$ remains about −2%.

In the case of iron-based alloys, too, the mechanism of mixing of d-up and d-down bands might be expected to lead to a formula (5.3) for the band with the low density of states, carrying the main fraction of the current. This would mean that for solute metals with large $(i^{\downarrow}/i_{\text{total}})_{\parallel}$, $(\varrho_{\parallel}^{\downarrow} - \varrho_{\perp}^{\downarrow})/\varrho_{\perp}^{\uparrow}$ would be

TABLE 5-IV

Smit's model applied to iron-based alloys for which $(i^{\downarrow}/i_{\text{total}})_{\parallel}$ differs considerably from 0.5

solute element	$(i^{\downarrow}/i_{\text{total}})_{\parallel}$	$\varrho_{\parallel}{}^{\downarrow} - \varrho_{\perp}{}^{\downarrow}$ ($\mu\Omega$cm/at%)	$(\varrho_{\parallel}{}^{\downarrow} - \varrho_{\perp}{}^{\downarrow})/\varrho_{\perp}{}^{\uparrow}$ (%)
V	0.88	+0.13	+1.7
Mo	0.83	+0.22	+2.1
Mn	0.85	+0.14	+1.6
Re	0.77	+0.24	+2.9
Ru	0.72	+0.19	+2.6
Os	0.75	+0.37	+3.0

solute element	$(i^{\downarrow}/i_{\text{total}})_{\parallel}$	$\varrho_{\parallel}{}^{\uparrow} - \varrho_{\perp}{}^{\uparrow}$ ($\mu\Omega$cm/at%)	$(\varrho_{\parallel}{}^{\uparrow} - \varrho_{\perp}{}^{\uparrow})/\varrho_{\perp}{}^{\downarrow}$ (%)
Co	0.21	−0.01	−0.1
Rh	0.15	+0.01	+0.1
Ni	0.13	+0.05	+0.3
Al	0.11	−0.01	−0.0
Si	0.15	−0.05	−0.1

an approximate constant: for solute metals with small $(i^{\downarrow}/i_{\text{total}})_{\parallel}$ the reverse situation would apply, i.e. $(\varrho_{\parallel}{}^{\uparrow} - \varrho_{\perp}{}^{\uparrow})/\varrho_{\perp}{}^{\downarrow}$ would be an approximate constant. The expectation is well borne out, as we demonstrate in table 5-IV.

Although there is a fair agreement between the experimental results and the predictions from Smit's model a firm conclusion about its validity cannot be drawn. It has been demonstrated in tables 5-III and 5-IV that for the solute elements for which agreement is expected, it is indeed obtained. For those remaining — Ti, V, Cr, Re, Ru, Rh, Ir and Pt — the experimental result is quite simple with respect to the sign of $\Delta\varrho/\varrho_{\parallel}$ (see table 2-V) but it is not predicted by this model.

Smit's model has recently been criticized by Potter [97]) who performed more detailed calculations to derive an anisotropic conductivity. Surprisingly enough, Potter finds that within the formalism proposed by Smit it is the charge carriers of the minority-spin direction that produce the large anisotropy effect.

A difficulty we have with both Smit's paper and Potter's is the rigorous separation of all energy states into s and d states. A number of 0.3 s electron per atom and per spin band would lead to a value for the normal Hall effect of about $-2.5\ 10^{-12}$ Ωcm/G, a value which is much higher than that derived

from experiment; see fig. 2.20. Another objection we have is that the theoretical calculations are made within the Born approximation and that perturbation theory is used, which, in the case of residual resistivities of, say, 2 $\mu\Omega$cm/at%, cannot be justified. For this value of the specific residual resistivity the mean free path is smaller than 100 atomic distances at a solute concentration of 1 at%.

Leaving the Born approximation, and considering impurities as non-transparent for current carriers, we naturally arrive at a picture in which the shape of the scattering centre determines the anisotropy effect. In the picture presented in fig. 2.16 the shape will correspond with the region where the transmission coefficient is near 0.5. In this picture the resistivity anisotropy might reflect the lack of spherical symmetry of 3d wave functions.

It is not unreasonable that the band properties of the matrix metal should be determinant. Combining our data on the ↑ and the ↓ band of nickel and iron alloys we observe that the anisotropy effect is large and positive when the numbers of carriers of one spin direction is either 5.3 (Ni up band) or 3.0 electrons per atom (Fe down band). It is about zero for a band containing 5.0 carriers (Fe up band) and small and negative for a spin band with 4.7 carriers per atom (Ni down band). A relation between cross-section and band filling might reflect the symmetry of 3d wave functions. At this moment there is no serious theoretical support for this simple picture. The fact that b.c.c. and f.c.c. are treated similarly is open to criticism.

A unique sign for the anisotropy effect for carriers with a given spin direction could also be accounted for if the Fermi surface properties depended closely on the direction, i.e. if the effective mass, the Fermi velocity or the number of carriers were anisotropic with respect to the magnetization. Effects of this type have indeed been found for nickel, both experimentally and in theoretical calculations. In nickel some pockets increase in size as the field is rotated from parallel to transverse (Hodges et al.[98]), Gold [99]) and Stark and Tsui [100]). However, these pockets are assumed to be part of the minority band. In addition, it is difficult to imagine that they carry a major fraction of the current. In any case Fermi-surface anisotropies must be considered as a possible mechanism.

It is disappointing that in the above explanation of the anisotropy effect in terms of anisotropic mixing of up-spin and down-spin densities of states, or other anisotropic Fermi-surface properties, there is no straightforward connection to be seen between the resistivity anisotropy and the anomalous Hall effect. A priori one would expect that the two effects have a similar origin. For strongly scattering solute atoms (effective cross section for scattering of the order of the cross-section of the atom) a mechanism that leads to a large side displacement would also be expected to influence the resistivity. The side displacements involved are of the order of Å units! See also chapter 7. The

side-displacement contribution to the Hall effect is only observed in the Hall geometry. However, its effect on the resistivity will be present in the parallel configuration as well. Without a detailed theoretical insight into the mechanism of side displacement, it is not even possible to conclude whether $\varrho_{\parallel} > \varrho_{\perp}$ or vice versa is obtained from this.

6. NORMAL GALVANOMAGNETIC EFFECTS IN NICKEL AND IRON

6.1. The normal Hall effect

In chapter 2 we discussed the normal galvanomagnetic properties of nickel- and iron-based alloys in terms of a simple two-current model. The normal Hall effect is a sensitive means of detecting the limitations of this model. As a matter of fact, metals with complicated Fermi surfaces such as iron and nickel may have several distinguishable groups of carriers with different relaxation times. A division according to spin is only one of many possibilities. It is only meaningful if the largest differences in relaxation times occur for carriers with opposite spin. If the two-current model were rigorously valid, the two spin bands would each be characterized by a single Hall coefficient $R_0{}^{\uparrow}$ and $R_0{}^{\downarrow}$. The total Hall coefficient would then be determined by

$$R_0 = (i^{\uparrow}/i_{\text{total}})_{\perp}{}^2 \, R_0{}^{\uparrow} + (i^{\downarrow}/i_{\text{total}})_{\perp}{}^2 \, R_0{}^{\downarrow}. \tag{6.1}$$

In chapter 2 we showed that for nickel-based alloys a relation (6.1) holds, although $R_0{}^{\downarrow}$ varies around $(-0.7 \pm 0.3)\ 10^{-12}$ Ωcm/G for different impurities, while $R_0{}^{\uparrow}$ also varies systematically with the resistivity for the spin-up current. For $\varrho_{\perp}{}^{\uparrow} = 0.5$ μΩcm it is about $(-0.3 \pm 0.1)\ 10^{-12}$ Ωcm/G while for $\varrho_{\perp}{}^{\uparrow} = 10$ μΩcm it equals $(-2.5 \pm 1)\ 10^{-12}$ Ωcm/G (see figs 2.20 and 2.21). The negative sign corresponds to conduction by electrons, as expected. We note, however, that these small values for the Hall effect imply that the simple picture of conduction by free s electrons, namely 0.3 per spin band, is unrealistic. For 0.3 electron per atom both $R_0{}^{\uparrow}$ and $R_0{}^{\downarrow}$ would have had a value of about $-2.5\ 10^{-12}$ Ωcm/G.

The curves in figs 2.20 and 2.21 were derived as follows. From eq. (6.1) it appears that for $i^{\uparrow}/i_{\text{total}} > 0.75$ the contribution of the down band to R_0 is less than 11% of that of the up band. Hence, knowing $i^{\uparrow}/i_{\text{total}}$ for all our binary and ternary alloys and estimating $R_0{}^{\downarrow}$, we can easily obtain $R_0{}^{\uparrow}$ from the experimental value of R_0. We can then derive $R_0{}^{\downarrow}$ in the range $i^{\uparrow}/i_{\text{total}} < 0.25$ from experimental values of R_0 and the $R_0{}^{\uparrow}$ values derived above. There is no need to repeat the procedure to obtain self-consistency. Since, as follows from fig. 2.20, $R_0{}^{\downarrow}$ is a real constant, and quite small, alloys for which $0.5 < i^{\uparrow}/i_{\text{total}} < 0.75$, comprising most of the ternary alloys, can also be included to derive $R_0{}^{\uparrow}$ (see fig. 2.21).

The values of $R_0{}^{\uparrow}$ and $R_0{}^{\downarrow}$ derived here represent the Hall effect in the low-field approximation. Since there exists a lower limit for B: $B_{\text{sat}} = 4\pi M_s$, the low-field Hall coefficient can only be studied for alloys with a sufficiently high resistivity. For this reason binary alloys of the low specific residual resistivity solutes, e.g. Fe, Co, Mn, Cu and Au, should have concentrations of at least 1 at%. From fig. 2.10 it can be seen that if the current is dominated by spin-up

carriers, the Hall coefficient becomes field-dependent at $B/\varrho_\perp = 2 \cdot 10^4$ G/μΩcm. Measurements by Huguenin and Rivier [41]) of the Hall effect of NiFe, NiCo and NiCu alloys in the concentration range below 1 at % therefore cannot be expected to represent the true low-field value. The same difficulty holds for Jaoul's [31]) results for NiMn alloys.

This additional difficulty of a field-dependent Hall coefficient applies specifically to the spin-up carriers. For nickel alloys in which spin-down carriers carry the main fraction of the current the field dependence of R_0 can be neglected up to field values of at least $B/\varrho_\perp = 5 \cdot 10^4$ G/μΩcm.

The actual experimental data on the Hall effect can be found in the appendix, where the Hall coefficient is given for all sets of ternary alloys as a function of the relative solute concentration for alloys with a total concentration of 3 at.% For nickel-based alloys the curves are calculated from formula (6.1), using $R_0{}^{\downarrow} = -0.65 \cdot 10^{-12}$ Ωcm/G and the average dependence of $R_0{}^{\uparrow}$ on the resistivity as displayed by fig. 2.21. The fit obtained gives an indication of the variation of $R_0{}^{\uparrow}$ and $R_0{}^{\downarrow}$ with the type of impurity. For many alloy systems deviations remain within the experimental uncertainties.

As we have already suggested in chapter 2, the variation of the Hall effect with resistivity, as observed for the spin-up band, can be easily explained. Increasing the resistivity means reducing the mean free path of the carriers involved. This introduces an uncertainty in all electron wave numbers (k values) and a corresponding uncertainty in the electron energy. For example, the mean free path in a metal with 1 electron per atom is about 100 atomic distances at a resistivity of a few μΩcm, so that the uncertainty in k is about 1%. Details of the Fermi surface corresponding to variations in k of the order of 1% are consequently devoid of meaning.

In the case of pure nickel small pockets have been observed with De Haas–Van Alphen experiments. These details are, however, considered to be part of the minority-carrier surface, but the possibility that similar small pockets also exist for the majority-spin band cannot be excluded. Franse et al.[57,58]) have ascribed the loss, upon alloying, of detailed structure in the magneto-crystalline anisotropy with respect to the crystallographic direction (fig. 2.19) to mean free path effects in the spin-down band. In view of our observations on the normal Hall effect it seems likely, however, that the higher-order terms of the magneto-crystalline anisotropy are a property of the majority-spin band in nickel.

It is interesting to compare the present information about the normal Hall effect in nickel-based alloys with information about the type of carriers — electrons and holes — that one can obtain from band-structure calculations or high-field galvanomagnetic effects in nickel. A rough sketch, due to Reed and Fawcett [59]), of the band structure that would agree with the high-field galvanomagnetic effects is reproduced as fig. 6.1. All but one of the d sub-bands is entirely full and the exchange splitting is such that spin-down d states become

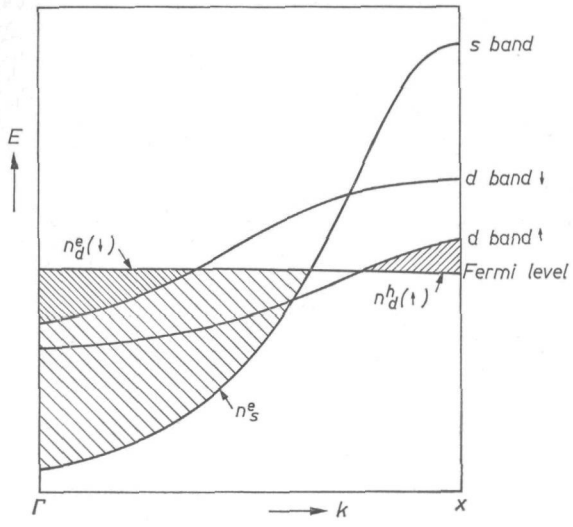

Fig. 6.1. Schematic band structure of nickel. From Reed and Fawcett [59]).

electron-like at the Fermi surface. For the majority-spin band, which is nearly full, the d states are hole-like. The splitting of the s band is assumed to be negligible in comparison. The s band has an electron-like character. The picture of Reed and Fawcett clearly leads to a normal Hall effect of the electron sign for spin-down carriers. Since the density of states is very high one expects $R_0{}^{\downarrow}$ to be negative and small. There is no reason that a change in mean free path of carriers should influence $R_0{}^{\downarrow}$ drastically. In the spin-up band, however, we have electron-like s carriers and a relatively small number of d type holes. Our results for R_0 suggest that these holes contribute to the current in low resistivity alloys but are lost when the spin-up part of the Fermi surface is blurred. In the literature there has been much discussion on whether the $d^{\uparrow}$ band really crosses the Fermi surface or not. Our experiments strongly support the idea that small hole pockets are present.

The existence of a relation between the mean free path of current carriers and band structure, can be expected to be quite general for complicated metals. Systematic experimental information on this type of effect is lacking.

In the case where the Hall coefficient becomes field-dependent Majumdar and Berger [44]) proposed a procedure to derive both contributions to the anomalous Hall effect and the normal Hall effect. It is assumed that the skew-scattering term and the normal Hall effect are jointly described by a Kohler-type function *). Treating the side-displacement term as an additive field-independent

*) The theoretical proof that in the absence of side displacement, the Hall effect for a given band is described by a Kohler-type curve, has been given by Berger [96]).

contribution we have

$$\varrho_H/\varrho_0 = \varphi_{sk} + \frac{R_0 B}{\varrho_0}\left[1 + f\left(\frac{B}{\varrho_0}\right)\right] + b\,\varrho_0 . \qquad (6.2)$$

If this expression applied, data for a number of alloys with different concentrations of the same solute could be combined, thus varying ϱ_0, so as to construct the Kohler curve for the Hall effect. However, this procedure does not work for nickel-based alloys with dominant spin-up conduction since R_0 also depends on ϱ_0 in a complicated way.

Campbell [24]) has already derived $R_0{}^{\uparrow}$ and $R_0{}^{\downarrow}$ in an analysis of data published by Huguenin and Rivier [41]), on the temperature dependence of the ordinary Hall coefficient of NiFe alloys. In this analysis $R_0{}^{\downarrow}$ is estimated at $-2.4 \cdot 10^{-12}$ Ωcm/G, which is a factor of 3 too high. Huguenin and Rivier's results indicate that $R_0{}^{\uparrow}$ varies with the iron concentration in the way described above.

For iron-based alloys the complications in the derivation of the normal Hall coefficient that were already present in nickel alloys are increased in principle by the fact that $B_{sat} = 4\pi M_s$ is three times higher. It is therefore difficult to derive R_0 straightforwardly as it is not desirable to have to rely on data from alloys with solute concentrations of more than 3 at %. An alternative is to use formula (6.2), which turns out to be an acceptable approximation for resistivities that are not too large. However, the field regions, expressed as B/ϱ_0, in which data with different concentrations of the same solute have been studied, show little overlap. Data on nickel alloys were obtained in a field range from 7 to 50 kG but for iron the field range was only a factor of two, i.e. 25 to 50 kG. In conclusion we must say that if a Kohler-type curve is assumed to exist, it can be constructed from the data. The merits of this procedure remain somewhat uncertain.

The derivation of the Kohler plot for the Hall effect is illustrated in fig. 6.2 where fig. 6.2*a* present the resuls of FeOs, which apparently has no side displacement. A single curve can be drawn through the data points corresponding to alloys with different Os concentrations. In the iron-based alloys with Ir, Ni or Re b can also be taken as zero. In fig. 6.2*b* we recorded the Kohler plot of FeCo which exemplifies a significant side-displacement contribution to the Hall effect. It is assumed that expression (6.2) may describe the total Hall effect. By shifting the observed values of the Hall angle ϱ_H/ϱ_0 (white symbols) by an amount proportional to ϱ_0, a common curve can be obtained (indicated by black symbols). This procedure provides values of φ_{sk}, b and R_0. If, however, it is accepted that the Hall effect can vary somewhat with concentration, it is equally possible to arrive at $b = 0$. The three straight lines through the data points intersect the vertical axis in the same point. Similar results are obtained when Ru, Rh or Pt are dissolved in iron.

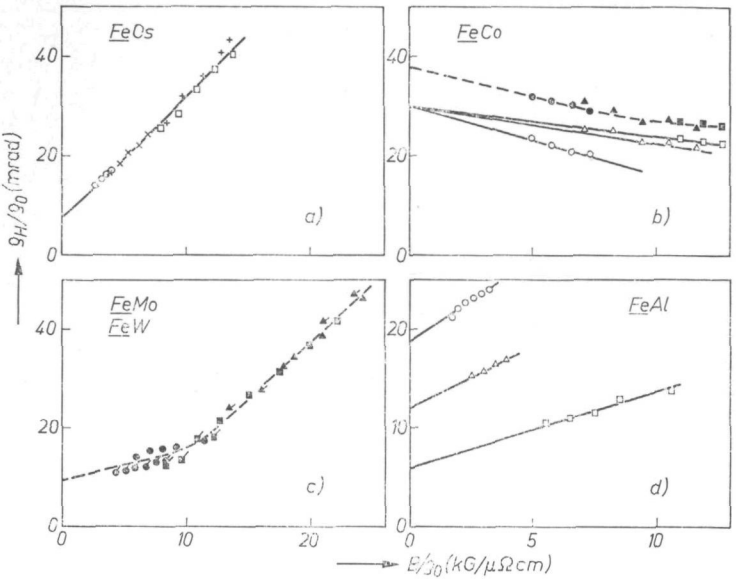

Fig. 6.2. Normal and anomalous Hall effects for some iron-based alloys. Experimental Hall angles are plotted in a type of Kohler plot (versus B/ϱ_0).
(*a*) A Kohler plot for FeOs which is an example of no side displacement where experimental data for different concentrations of a given solute fall on a single curve. Values of ϱ_0 in μΩcm are: ○ 8.98, × 5.88, + 2.79, □ 2.94. The last sample was annealed at 1000 °C, see chapter 3.
(*b*) Kohler plots for FeCo which exemplify a significant side displacement. A common curve is obtained by shifting curves of different Co concentrations (white symbols) by an amount of $\Delta\varrho_H/\varrho_0 = b\,\varrho_0$. Values of ϱ_0 in μΩcm are: ○ and ● 2.7, △ and ▲ 1.9, □ and ■ 1.2.
(*c*) An example of a markedly field-dependent Hall effect, found in all binary alloys with large $i^{\downarrow}/i_{\text{total}}$. The correction for side displacement has already been applied. Included are FeW with 1, 2 and 3 at % W (▲, ■ and ●, respectively) and FeMo with 1, 2 and 3 at % Mo (dashed ▲, ■ and ●, respectively).
(*d*) An example of FeAl alloys with relatively high resistivity where the normal Hall effect varies with the resistivity; the side-displacement contribution is very clear. The resistivities are ○ = 14, △ = 9, □ = 4 μΩcm.

The results for FeMo and FeW after a small correction is applied for side displacement are shown in fig. 6.2*c*. It will be seen that a sharp change in slope occurs around $B/\varrho_0 = 10$ kG/μΩcm. This behaviour is also shown by FeV. Finally, we have recorded in fig. 6.2*d* the Kohler plot for the Hall angle of some FeAl alloys, in which the specific resistivity is much higher and the differences between the three curves corresponding to solute concentrations of 1, 2 and 3 3 at % Al are dominated by the side-displacement contribution. The slopes of the three curves are different, which indicates that either R_0 depends on the resistivity when ϱ_0 is around 10 μΩcm or formula (6.2) does not apply when the third term is large.

The resulting R_0 values for binary iron-based alloys are given in table 6-I. In all cases, except Co dissolved in iron, the normal Hall coefficient has the

TABLE 6-I

The normal Hall effect in binary iron-based alloys, Where the low-field Hall coefficient depends on the resistivity, the value of R_0 at $\varrho_0 \approx 5$ $\mu\Omega$cm is quoted. For comparison we also give the magnetoresistivity at a fixed value of the reduced field

solute element	$(i^{\downarrow}/i_{\text{total}})_{\text{II}}$	R_0 (10^{-12} Ωcm/G)	$(\varrho(B) - \varrho_0)/\varrho_0$ (%) at $B/\varrho_0 = 20$ kG/$\mu\Omega$cm
Al	0.11	+0.6	3.0
Ga	0.11	+1.0	1.8
Si	0.15	+0.7	2.5
Ge	0.14	+0.5	1.0
Rh	0.15	+0.8	2.0
Ir	0.10	+1.1	2.7
Co	0.21	−0.6	7.0
Ni	0.13	+1.4	8.0
Pt	0.11	+0.1	2.2
Cr	0.73	+0.3	12
Re	0.77	+2.3	9
Ru	0.72	+1.8	5.5
Os	0.75	+2.3	5
V	0.88	(+1)	18
Mo	0.83	+0.7	11
W	0.81	+0.6	11
Mn	0.85	(2.5)	(16)

sign of conduction by holes. If the solute elements are distinguished into those with small $i^{\downarrow}/i_{\text{total}}$ and those with large $i^{\downarrow}/i_{\text{total}}$, the average values are +0.6 and $+1.4 \cdot 10^{-12}$ Ωcm/G, respectively. The scatter, however, is much too large for there to be any point in analysing the Hall effect in terms of $R_0{}^{\uparrow}$ and $R_0{}^{\downarrow}$, as we did for nickel-based alloys.

In table 6-I Co is a clear exception in the sense that the normal Hall coefficient of FeCo has the electron-like sign. Since $i^{\downarrow}/i_{\text{total}}$ is small when Co is dissolved in iron, this negative sign is connected with the spin-up current. The fact that for some of the solute metals with large $i^{\downarrow}/i_{\text{total}}$ the Hall effect in the spin-up band has the electron-like sign clearly cannot be excluded from the data in this table. Information on this point can be obtained from the Hall effect of

ternary alloys. For example, if we replace some of the Co in iron by Mn the Hall effect keeps the electron-like sign, even when ϱ_{Co} and ϱ_{Mn} become about equal. This indicates that the scattering of spin-up carriers by Mn produces a Hall effect of the same sign as scattering by Co. On the other hand, if some of the Co is replaced by Re, the measured Hall effect changes sign immediately (see fig. 6.3), indicating that when spin-up carriers are scattered by Re a positive Hall effect is produced. From the experimental data on the ternary alloys (see appendix) we concluded that Mo, Ru and Os behave like Re. The information on $R_0{}^{\uparrow}$ for other impurities is insufficient. Inversely, it can also be deduced that Al and Si in iron produce a positive Hall effect in the spin-down band.

A number of authors (for a review see Hurd [35])) have indicated that both spin bands in iron contain electron-like as well as hole-like states. According to Kondorskii [107]) the volume enclosed by the electron surface dominates in the spin-up band while in the spin-down band the volume enclosed by the hole surface is largest. This agrees qualitatively with our results. In the spin-down band the normal Hall effect always has the hole-like sign indeed. In the spin-up band we find both signs depending on the scattering centre.

6.2. The Kohler magnetoresistivity

Another transport property which tests the applicability of a simple two-current model is the Kohler magnetoresistivity. If we had to deal with two currents, each with a single type of carrier, the magnetoresistivity would be correlated with $i^{\uparrow}/i_{total}$. It would be small when $i^{\uparrow}/i_{total}$ is near 0 or near 1. A significant effect occurs for $i^{\uparrow}/i_{total}$ near 0.5. In fig. 4.2 we have recorded the Kohler magnetoresistivity of a number of nickel-based binary alloys. Alloys with Co, Fe, Mn, Cu and Au have a large magnetoresistivity in a reduced field scale, while Ru, Cr and Pt produce a much smaller magnetoresistivity. If the spin-up band would be uniform we would expect the first group of solutes to produce a small magnetoresistivity. We note that the large value of the Kohler magnetoresistivity correlates with a field-dependent Hall effect.

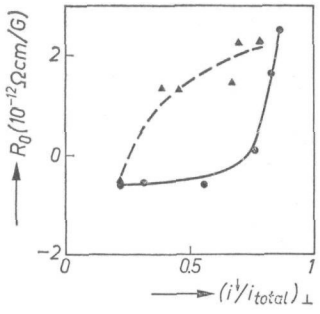

Fig. 6.3. The normal Hall effect of some ternary FeCoMn (●) and FeCoRe (▲) alloys as a function of $i^{\downarrow}/i_{total}$ at 4.2 K. The curves are drawn to guide the eye.

The Kohler plots of nickel-based alloys in figs 4.2 and 4.3 agree reasonably well with those reported by Fert et al.[104]) and Schwerer and Silcox [75,102]). Our results refer to somewhat higher resistivities and consequently lower values of B/ϱ_0. Schwerer and Silcox have developed an elegant method for constructing a Kohler curve. The zero-field resistivity ϱ_0 is treated as an unknown parameter. In their procedure both the Kohler curve and the ϱ_0 values involved are obtained with much care. Nevertheless it is questionable whether the procedure gives accurate results as the Kohler curve is obtained only by assuming first of all that the Kohler curve is unique. If the normal Hall effect varies with ϱ_0, such an assumption is questionable. It is for this reason that in the derivation of resistivities and corresponding resistivity anisotropies we decided to use a simple quadratic extrapolation rather than the procedure proposed by Schwerer and Silcox.

We did not resolve the observed magnetoresistivity into contributions by two currents. Clearly, in order to reproduce the high effects of, for example, NiCo alloys, it is necessary to introduce different types of carriers, e.g. holes and electrons, within the up band.

As far as the Kohler magnetoresistivity is concerned, iron- and nickel-based alloys are comparable, as can be learned from a comparison of figs 4.2 with table 6-I. In table 6-I we included the resistivity increment $[\varrho(B) - \varrho_0]/\varrho_0$ at a fixed value of the reduced field $B/\varrho_0 = 20$ kG/$\mu\Omega$cm. It will be seen that the effect is quite large when $i^{\downarrow}/i_{\text{total}}$ is near unity and much smaller when $i^{\downarrow}/i_{\text{total}}$ is only 10%.

To summarize we have found that in nickel- and iron-based alloys the spin current which produces the large resistivity anisotropy also has a large Kohler magnetoresistivity and a markedly field-dependent Hall effect.

Although the two-current model proved very successful in describing residual resistivities, resistivity anisotropies and anomalous Hall effects, the present chapter indicates that the two-current model should not be "pushed" to far. Conduction by holes and conduction by electrons clearly takes place simultaneously within a single (spin-) band. The positive Hall effect of most iron alloys also indicates that a picture of conduction in transition metals by s electrons which are scattered predominantly into d states, without significant conductivity by d-like carriers, is too simple.

7. THE ANOMALOUS HALL EFFECT

7.1. Determination of the anomalous Hall effect in nickel-based alloys

The anomalous Hall effect as it is observed experimentally is displayed in fig. 7.1, where the data for three NiAl alloys are given. It will be noted that in addition to the normal Hall effect, linear in B, there is a large contribution which is attributed to the ferromagnetism. This contribution is present when the sample is magnetized. Thus the Hall effect of nickel alloys increases steeply between $B = 0$ and $B = 4\pi M_s = 6.4$ kG. In fig. 7.1 the anomalous Hall effect is obtained by extrapolating the experimental data obtained at $B > 4\pi M_s$ by means of

$$\varrho_H = R_0 B + \varrho_{aH}. \tag{7.1}$$

The linear extrapolation may be criticized in the case of low resistivities which are small enough to correspond to a field-dependent normal Hall effect; see fig. 2.10. For nickel alloys this is not a serious drawback since it only interferes in alloys of nickel with Co, Fe, Mn and Au at low concentrations.

In the literature the parameter R_s defined by

$$\varrho_H = R_0 B + R_s 4\pi M_s$$

is often introduced to characterize the anomalous Hall effect. The use of this expression suggests a proportionality between ϱ_{aH} and the magnetization M_s. In our opinion it is misleading. There is no reason why the anomalous Hall effect should be a linear function of the magnetization or the band-splitting, except in the range of very small splittings, e.g. M_s corresponding to about 0.1 μ_B.

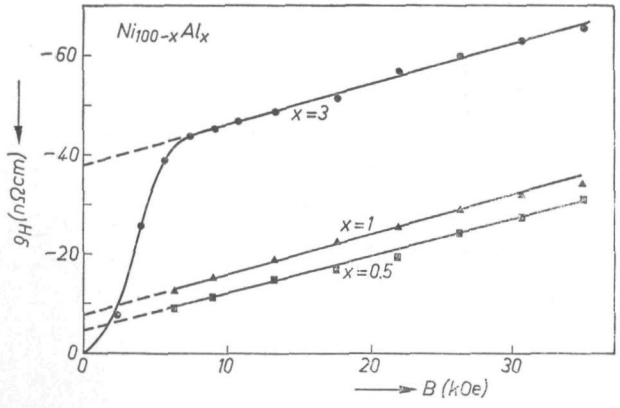

Fig. 7.1. The Hall resistivity of some NiAl alloys as a function of the magnetic induction B. The parameter x indicates the nominal concentration of Al. The resistivities measured in the transverse configuration are 6.3, 1.7 and 1.1 μΩcm for $x = 3$, 1 and 0.5, respectively.

In fig. 7.1 it will be observed that ϱ_{aH} for Al in nickel depends on the concentration. The anomalous Hall effect increases with increasing resistivity. Also, the anomalous Hall angle $\varphi_{aH} = \varrho_{aH}/\varrho_{\perp}$ increases with concentration. This behaviour can be described by

$$\varphi_{aH} = \varphi_{sk} + b\,\varrho_{\perp}. \tag{7.2}$$

The relation implies that the anomalous Hall angle converges to some finite value φ_{sk}, which is determined by the solute element involved, when the resistivity is decreased by decreasing the solute concentration. Thus the anomalous Hall resistivity disappears when the resistivity decreases. For pure nickel this has been verified (Jan [105]) and Smit and Volger [52])). Relation (7.2) might be introduced formally by arguing that a function of the resistivity which is zero at $\varrho = 0$ can always be expanded in a Taylor series in terms of increasing powers of ϱ. Relation (7.2) then includes only the first two terms. A physical picture, reproducing these two terms, was given by Berger [54]); see fig. 2.12. In this picture φ_{sk}, termed skew-scattering angle, represents the average angle between electron trajectories before and after scattering, while b represents the displacement sidewards of the trajectories.

For nickel-based alloys experiments on the resistivity dependence of φ_{aH} for a particular impurity or a particular combination of impurities are in good agreement with formula (7.2) as may be seen from figs 2.11 and 7.2. This formula may be expected to break down at sufficiently high concentrations since solute atoms will interact, or since the band structure will be seriously affected. An

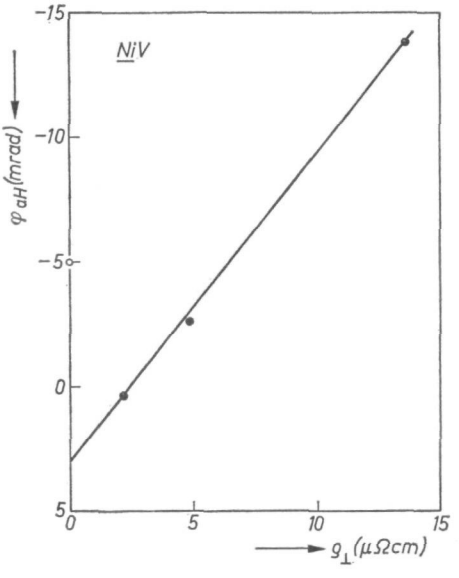

Fig. 7.2. The anomalous Hall angle in some NiV alloys as a function of the resistivity; ○: value of φ_{sk} given by Jaoul [31]), ●: present work.

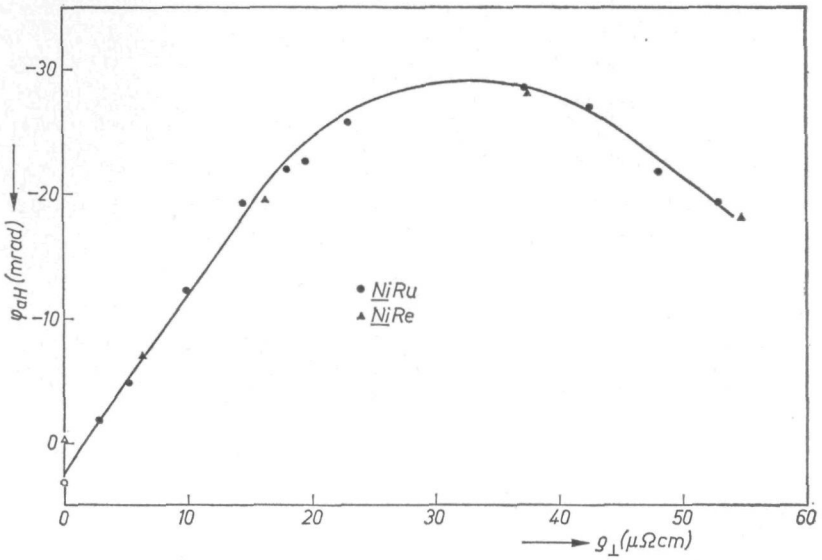

Fig. 7.3. The anomalous Hall angle in some NiRu and NiRe alloys as a function of the resistivity. Black symbols: present work; white symbols: values given by Jaoul [31]) for the skew-scattering angle. At small resistivities the solid line corresponds to values of φ_{sk} and b given for NiRu in table 2-VI.

impression of the upper concentration required for relation (7.2) to be valid can be obtained from fig. 7.3 for NiRu and NiRe alloys. The linear dependence of φ_{aH} on the resistivity breaks down at resistivities around 20 $\mu\Omega$cm, corresponding to concentrations of about 4 at %. Ru and Re may be expected to represent less favourable cases: both solute elements produce a large specific resistivity and considerably reduce the Curie temperature (Crangle and Parsons [106])).

In table 7-I we compare our measurements on the anomalous Hall angle at solute concentrations of 3 at % and the derived values of φ_{sk} with results reported in the literature. To permit comparison with literature data relating to different concentrations we calculated the anomalous Hall angle at the resistivity reported by means of relation (7.2), using our values of φ_{sk} and b. This calculated Hall angle is given between brackets. The present values for NiAl, NiSn and NiSi are in good agreement with those reported by Smit and Volger [52]). For NiV there is a large difference. However, since the alloys studied by Smit and Volger contain 7 at % of V and our parameters refer to alloys with concentrations below 3 at %, this is not surprising. Similarly, the differences between values observed by Smit [63]) for NiCo, NiFe and NiCu and our calculated values, based on low concentrations, cannot be considered as a serious discrepancy. That relation (7.2) becomes invalid for concentrations near 10 at % is clear from the fact that the same anomalous Hall angle is reported for $Ni_{91}Cu_9$ as for $Ni_{82}Cu_{18}$.

TABLE 7-I

A comparison between data from literature on the anomalous Hall effect in nickel-based alloys and the present work. The numerical subscript to φ denotes the solute concentration of the alloy involved. The anomalous Hall angles between brackets were calculated with the parameters φ_{sk} and b from the present work and the resistivity cited in literature.

solute element	present work			data from literature	
	φ_3 (mrad)	φ_{sk} (mrad)	b (mrad/$\mu\Omega$cm)	φ_{sk} (mrad)	other information
Al	− 6.0	− 3.7	−0.42		φ_8 = − 9.3 [a]) (−8.9)
Co	− 4.0	− 6.2	+4.2	−10 [b,c])	φ_{10} = − 1.8 [a]) (+3)
Cu	− 4.2	−10	+2.0	−23 [b,c])	φ_9 = − 4.5 [a]) (+6.6)
Fe	− 3.7	− 6.2	+2.25	−10 [b,c])	$\varphi_{10.7}$ = − 3.4 [a]) (+2.3)
					φ_3 = − 5 [c])
Mo				− 0 [b])	φ_3 = −19 [a]), ϱ = 21 $\mu\Omega$cm
Si	− 6.5	+ 1.1	−0.93		φ_3 = − 9.2 [a]) (−7.7)
Sn	−10	− 2.7	−0.90		φ_3 = − 8.3 [a]) (−12.4)
V	−13.8	+ 3	−1.26	− 5 [b])	φ_7 = −22 [a]) (−39)
W				− 4 [b])	$\varphi_{1.6}$ = −10.7 [a]), ϱ = 11 $\mu\Omega$cm

[a]) Smit and Volger [52]) at T = 20 K and Smit [63]).
[b]) Jaoul [31]).
[c]) Huguenin and Rivier [41]).

For nickel with Co, Fe or Cu Jaoul [31]) reports values for φ_{sk} obtained by analysing experimental data published by Huguenin and Rivier [41]). Table 7-I clearly shows that Jaoul's values of φ_{sk} are higher than the present ones. The difference can be attributed to the field dependence of the normal Hall effect; see fig. 2.10. The values derived by Jaoul for the skew scattering are based on alloys in which the impurity resistivity becomes as low as 0.3 $\mu\Omega$cm, which is much too low in view of our fig. 2.10.

Jaoul's data on the skew scattering due to solute elements with $i^{\uparrow}/i_{total} < 0.5$ can in principle be compared with the present results in spite of the much lower concentration used in Jaoul's work. If $i^{\uparrow}/i_{total} < 0.5$, the Kohler magneto-resistivity and the curvature of the normal Hall effect remain unimportant, even at solute concentrations of a few tenths of a percent. The comparison with Jaoul's work is given in tables 7-I and 7-II.

For the solute metals Cr, Re, Rh and Ru there is reasonable agreement between Jaoul's results and ours. For Mn and Au the difference is small. This difference may be due to the low solute concentration considered by Jaoul,

TABLE 7-II

A comparison between data reported by Jaoul [31]) and results from the present work

solute in nickel	φ_{sk} (mrad) (Jaoul)	φ_{sk} (mrad) (present work)	b (mrad/$\mu\Omega$cm) (present work)	φ_3 (mrad) (present work)
Ti	−4.5	+1.5	−1.0[5]	−10.9
Cr	+2	+2.8	−1.3	−17
Mn	−9.5	−6.5	+1.6	− 3.6
Nb	−0			
Ru	+3	+2.5	−1.4	−19.3
Rh	−0.4	0	−1.1	− 5.6
Re	−0.2	+1	−1.2[5]	−19.6
Os	+1.8			
Ir	+3.2		−1.1[7]	−10.6
Pt	−2.5	+1.7	−2.2[5]	− 3.5
Au	−3	−4.8	+1.1	− 3.4

which may have led to complications due to the low-field range. There is a large difference between his results and our values for the skew scattering in nickel alloys with Ti, V and Pt. This difference is difficult to explain. Our result for NiV was derived by measuring the anomalous Hall effect at three different solute concentrations. From the data in fig. 7.2 it is clear that they do not extrapolate to a negative φ_{sk}.

We note that the values for φ_{sk} reported by Jaoul were derived from experimental data (partly on temperature-dependent quantities) assuming relation (7.2) to be valid and treating b as a single constant, irrespective of the solute element. As Jaoul's resistivities are rather low, the use of constant b is not expected to lead to poor results.

A few solute elements which we did not consider were studied by Jaoul, viz. Nb, Mo, W, Os and Ir. The large negative value of W as compared to Mo and Cr may be somewhat surprising.

A comparison with earlier work such as we make here for the skew scattering cannot be made for the side-displacement coefficient b. Data in the literature on the anomalous Hall effect of alloys with a reasonably high resistivity have been predominantly obtained at high temperatures, where it was possible to describe all data assuming a single value of b (which was taken about −0.6 mrad/$\mu\Omega$cm). This value of b is about the linear average for a large number of solutes we observed in the present work.

7.2. Analysis of the anomalous Hall effect in nickel-based alloys

In terms of the two-current model it is not sufficient to characterize the anomalous Hall effect due to a solute element in nickel by single values for φ_{sk} and b. Instead, these values should be resolved into contributions from the separate spin bands. For each impurity A this leads to: $\varphi_A{}^{\uparrow}$, $\varphi_A{}^{\downarrow}$, $b_A{}^{\uparrow}$ and $b_A{}^{\downarrow}$. In the same way as we determined sub-band resistivity anisotropies (see chapter 5) we can derive $\varphi_A{}^{\uparrow}$ and $\varphi_A{}^{\downarrow}$ once φ_{sk} has been determined for a number of alloys with different compositions. In fact, the formulae describing the skew scattering and the resistivity anisotropy are completely identical

$$\varphi_{sk} = (i^{\uparrow}/i_{total})_{\perp}\, \varphi_{sk}{}^{\uparrow} + (i^{\downarrow}/i_{total})_{\perp}\, \varphi_{sk}{}^{\downarrow} \tag{7.3}$$

with

$$\varphi_{sk}{}^{\uparrow} = (c_A\, \varrho_{A\perp}{}^{\uparrow}\, \varphi_A{}^{\uparrow} + c_B\, \varrho_{B\perp}{}^{\uparrow}\, \varphi_B{}^{\uparrow})/\varrho_{\perp}{}^{\uparrow}$$

and

$$\varphi_{sk}{}^{\downarrow} = (c_A\, \varrho_{A\perp}{}^{\downarrow}\, \varphi_A{}^{\downarrow} + c_B\, \varrho_{B\perp}{}^{\downarrow}\, \varphi_B{}^{\downarrow})/\varrho_{\perp}{}^{\downarrow}.$$

Having measured φ_{sk} at a number of ternary alloys in a system NiAB, where the concentrations of A and B in at% are c_A and c_B, and using the values of $\varrho_{A\perp}{}^{\uparrow}$, $\varrho_{A\perp}{}^{\downarrow}$, $\varrho_{B\perp}{}^{\uparrow}$ and $\varrho_{B\perp}{}^{\downarrow}$ as derived from tables 2-III and 2-V, we can find $\varphi_A{}^{\uparrow}$, $\varphi_A{}^{\downarrow}$, $\varphi_B{}^{\uparrow}$ and $\varphi_B{}^{\downarrow}$. The experimental data on binary and ternary alloys from which we derived $\varphi_{sk}{}^{\uparrow}$ and $\varphi_{sk}{}^{\downarrow}$ for Al, Co, Cr, Cu, Fe, Pt, Rh, Ru, Sn, Ti and V dissolved in nickel are given in table 7-IIIA. Each data point is obtained from a linear relation between the experimental total anomalous Hall angle and the solute concentration.

The theoretical relation (7.3) was fitted to the experimental points by minimizing the sum of the squared deviations between the experimental and the theoretical value of the skew-scattering angle, giving binary alloys some extra weight. We used the numerical Direct Search procedure mentioned in sec. 4.2. The results of the fitting procedure were given in table 2-VII. After this fitting procedure the r.m.s. deviation between the data points in table 7-IIIA and the calculated curves, which are given in the appendix, was 0.4 mrad. We determined 22 parameters $\varphi_{sk}{}^{\uparrow}$ and $\varphi_{sk}{}^{\downarrow}$ from 42 data points. The accuracy of the sub-band angles determined is estimated at about 0.5 mrad. By way of example we show the result for the NiCuV system in fig. 7.4. Other systems are given in the appendix.

The main result of this analysis is that for a given spin direction φ_{sk} always has one sign, namely $\varphi_{sk}{}^{\uparrow} < 0$ and $\varphi_{sk}{}^{\downarrow} > 0$, independent of the particular solute element, which seems quite significant. Jaoul, too, has resolved φ_{sk} into the contributions by the two separate spin currents. However, his analysis heavily relies on experimental information on the temperature dependence of the anomalous Hall angle, in which b is considered to be a constant. In spite

TABLE 7-IIIA

Experimental data on the skew-scattering angle and the side-displacement coefficient of nickel-based alloys. The data were obtained by varying the total concentration of the solute elements, keeping the ratio of the solute elements, indicated in the left hand column, the same for each composition. The data in this table were used to determine the values of $\varphi_{sk}{}^{\uparrow}$, $\varphi_{sk}{}^{\downarrow}$, $b^{\uparrow}$ and $b^{\downarrow}$ for the elements Al, Co, Cr, Cu, Fe, Pt, Rh, Ru, Sn, Ti and V dissolved in nickel.

alloy	φ_{sk} (mrad)	b (mrad/ $\mu\Omega$cm)
$Al_{1.00}$	— 3.7	—0.42
$Al_{0.976}Cr_{0.024}$	— 2.6	—0.34
$Al_{0.91}Cr_{0.09}$	— 1.2	—0.93
$Al_{0.72}Cr_{0.28}$	— 0	—0.98
$Cr_{1.00}$	+ 2.8	—1.30
$Co_{1.00}$	— 6.2	+4.20
$Co_{0.80}Rh_{0.20}$	— 0.4	—0.96
$Co_{0.50}Rh_{0.50}$	+ 0.3	—0.98
$Co_{0.33}Rh_{0.67}$	+ 1.1	—1.38
$Rh_{1.00}$	— 0	—1.10
$Cr_{1.00}$	+ 2.8	—1.30
$Cr_{0.073}Fe_{0.927}$	— 0.4	—1.14
$Fe_{1.00}$	— 6.25	+2.25
$Cr_{1.00}$	+ 2.8	—1.30
$Cr_{0.61}Sn_{0.39}$	+ 1.5	—0.96
$Cr_{0.28}Sn_{0.72}$	— 1.0	—0.84
$Cr_{0.09}Sn_{0.91}$	— 2.2	—0.65
$Cr_{0.023}Sn_{0.977}$	— 1.6	—1.00
$Sn_{1.00}$	— 2.7	—0.90
$Cu_{1.00}$	—10.0	+2.00
$Cu_{0.607}Rh_{0.393}$	+ 0.4	—0.94
$Rh_{1.00}$	— 0	—1.10
$Cu_{1.00}$	—10.0	+2.0
$Cu_{0.927}Ru_{0.073}$	— 0.9	—0.76
$Cu_{0.76}Ru_{0.24}$	+ 1.5	—1.19
$Ru_{1.00}$	+ 2.5	—1.43

alloy	φ_{sk} (mrad)	b (mrad/ $\mu\Omega$cm)
$Cu_{1.00}$	—10.0	+2.00
$Cu_{0.78}V_{0.22}$	— 1.5	—0.56
$Cu_{0.72}V_{0.28}$	— 0.5	—1.00
$Cu_{0.56}V_{0.44}$	+ 0.55	—0.95
$Cu_{0.39}V_{0.61}$	+ 1.4	—0.96
$V_{1.00}$	+ 3.0	—1.26
$Fe_{1.00}$	— 6.25	+2.25
$Fe_{0.76}Pt_{0.24}$	— 2.25	+0.77
$Fe_{0.61}Pt_{0.39}$	+ 0.1	—0.34
$Fe_{0.25}Pt_{0.75}$	+ 1.3	—0.87
$Pt_{1.00}$	+ 1.7	—2.25
$Rh_{1.00}$	— 0	—1.10
$Rh_{0.95}Ru_{0.05}$	+ 1.2	—1.32
$Rh_{0.90}Ru_{0.10}$	+ 1.7	—1.49
$Rh_{0.87}Ru_{0.13}$	+ 1.4	—1.33
$Ru_{1.00}$	+ 2.5	—1.43
$Ru_{1.00}$	+ 2.5	—1.43
$Ru_{0.967}Ti_{0.033}$	+ 1.8	—1.18
$Ru_{0.90}Ti_{0.10}$	+ 3.2	—1.42
$Ru_{0.10}Ti_{0.90}$	+ 2.4	—1.36
$Ru_{0.033}Ti_{0.967}$	+ 0.5	—1.04
$Ti_{1.00}$	+ 1.5	—1.05
$Al_{0.726}Ru_{0.274}$	+ 1.8	—1.30
$Fe_{0.74}Ru_{0.26}$	+ 2.7	—1.45
$Ru_{0.306}Sn_{0.694}$	— 0.5	—0.99

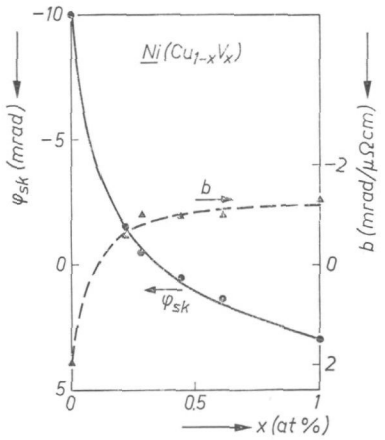

Fig. 7.4. A comparison between the values of the skew-scattering angle φ_{sk} (●, left-hand scale) and the side-displacement coefficient b (▲, right-hand scale) experimentally observed in a set of ternary Ni($Cu_{1-x}V_x$) alloys and a best fitting curve calculated in a two-current model with the parameters given in chapter 2. The solid line indicates the skew-scattering angle, the broken line the side-displacement coefficient.

of this, he reports the same sign as we do for $\varphi_{sk}{}^{\uparrow}$ and $\varphi_{sk}{}^{\downarrow}$ for most solutes, viz. Au, Co, Cr, Cu, Fe, Mn and Re. Jaoul reports a different sign for $\varphi_{Ir}{}^{\uparrow}$, $\varphi_{Ru}{}^{\uparrow}$ and $\varphi_{V}{}^{\uparrow}$, while for Nb and Mo, impurities that we did not study, both signs are found to be different from the general pattern observed by us. In view of the fact that our results were obtained from more straightforward experiments on ternary alloys, these differences should not be considered too seriously.

Having also derived b for a number of ternary alloys (see table 7-IIIA), we can resolve the total side-displacement coefficient of a solute element A into the contributions from the two spin bands $b_A{}^{\uparrow}$ and $b_A{}^{\downarrow}$. The relevant formula was given in (2.15) where we showed that b values can only be obtained apart from an arbitrary constant b_0 which is to be added to all $b^{\uparrow}$ values and to be subtracted from all $b^{\downarrow}$ values. In fact, therefore a fit of a separate ternary system NiAB, with adjustable parameters $b_A{}^{\uparrow}$, $b_A{}^{\downarrow}$, $b_B{}^{\uparrow}$ and $b_B{}^{\downarrow}$, involves only three parameters since one side-displacement coefficient can be taken as zero.

In the same way as described for the skew scattering we fitted the relation (2.15) to the experimental points for b, recorded in table 7-IIIA, by minimizing the sum of the squared deviations between the experimental and the theoretical value of the side displacement-coefficient b, giving binary alloys some extra weight. The resulting $b_A{}^{\uparrow}$ and $b_A{}^{\downarrow}$, where A stands for Al, Co, Cr, Cu, Fe, Pt, Rh, Ru, Sn, Ti or V, are given in table 2-VIII. The r.m.s. deviation between the data points and the calculated values of b is found to be 0.12 mrad/μΩcm. We determined 21 parameters, corresponding to 11 elements dissolved in nickel, from 42 data points. An example of a fit is given for the NiCuV system in fig. 7.4. Clearly, it is now important that impurities should be studied in dif-

ferent ternary systems so that once we have chosen, for example, $b^{\uparrow}$ for one impurity, all other b values are connected. For this reference we chose $b_{Co}{}^{\uparrow} = 0$. The reason for this is found in Berger's phenomenological picture (see fig. 2.12) from which it may be expected that if the spatial extension of an impurity is small, the side displacement Δy and correspondingly b will also be small. The resistivity of Co for up electrons is the smallest of all specific resistivity values, so $b_{Co}{}^{\uparrow}$ may be expected to be the smallest that occurs. In our system it is defined as to be zero.

The resulting values of $b^{\uparrow}$ and $b^{\downarrow}$ are also recorded as black symbols in fig. 7.5. It is striking that by defining $b_{Co}{}^{\uparrow} = 0$ all other $b^{\uparrow}$ values become negative and all $b^{\downarrow}$ values become positive. In other words, skew scattering

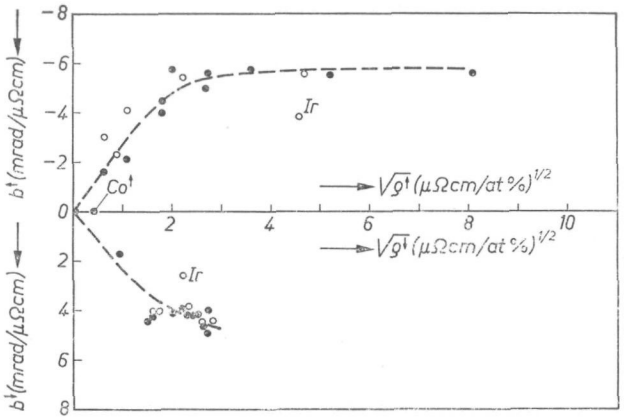

Fig. 7.5. The side-displacement coefficient b per sub-band as a function of the square root of the specific residual resistivity within that sub-band. The circles represent various impurity elements. Black circles represent impurity elements that were investigated in detail in sets of ternary alloys with various total impurity concentration, as in fig. 7.4. White circles represent impurity elements for which the side-displacement contribution was analysed after applying a correction φ_{sk} to φ_3, which was estimated from fig. 2.13; see text. Significant deviations from the general pattern are observed in NiIr.

and side displacement are to the left for one spin direction and to the right for the other. Fig. 7.5 also displays a correlation between the numerical value of b and the corresponding sub-band resistivity. Relating the side-displacement coefficient to the spatial extension of the scattering centre involved, it seems natural to connect the side-displacement coefficient with the cross section for scattering of the solute element, which is proportional to the square root of the specific residual sub-band resistivity. From fig. 7.5 it can be seen that such a correlation is in fact found.

Only 11 solute elements have been included in table 7-IIIA. We decided to derive $b^{\uparrow}$ and $b^{\downarrow}$ for 6 other impurities from the experimental value of φ_3, the anomalous Hall angle of the alloy with a total solute concentration of 3 at %,

thus avoiding the elaborate experimental work involved in studying the concentration dependence of the anomalous Hall angle of a large number of alloys. The b values of the ternary alloys given in table 7-IIIB were determined from $b = (\varphi_3 - \varphi_{sk})/\varrho_3$, where φ_3 and ϱ_3 are the anomalous Hall angle and the resistivity of alloys with total solute concentrations of 3 at %. φ_{sk} is usually much smaller than φ_3. We therefore decided to estimate φ_{sk} from the straight line in fig. 2.13, calculating $(i^{\uparrow}/i_{total})_{\perp}$ from the known sub-band resistivities.

TABLE 7-IIIB

Experimental data on the side-displacement coefficient of nickel-based alloys. The data were obtained from the difference between the anomalous Hall angle of the corresponding alloy with a total solute concentration of 3 at % and the skew-scattering angle which was estimated from the correlation between φ_{sk} and $(i^{\uparrow}/i_{total})_{\perp}$ as given in fig. 2.13. The values of the binary alloys of nickel with Au, Ir, Mn, Re, and Si were determined in the usual way by studying alloys with different solute concentrations.

alloy	b (mrad/μΩcm)
$Au_{1.00}$	+1.10
$Au_{0.50}Co_{0.50}$	+1.80
$Au_{1.00}$	+1.10
$Au_{0.93}Ir_{0.07}$	+0.45
$Au_{0.87}Ir_{0.13}$	−0.13
$Au_{0.73}Ir_{0.27}$	−0.51
$Au_{0.60}Ir_{0.40}$	−0.84
$Au_{0.40}Ir_{0.60}$	−0.97
$Ir_{1.00}$	−1.17
$Au_{1.00}$	+1.10
$Au_{0.91}Rh_{0.09}$	−0.60
$Au_{0.76}Rh_{0.24}$	−1.50
$Au_{0.44}Rh_{0.56}$	−1.14
$Au_{0.09}Rh_{0.91}$	−1.20
$Cr_{0.44}Mn_{0.56}$	−1.34
$Cr_{0.39}Mn_{0.61}$	−1.51
$Cr_{0.24}Mn_{0.76}$	−1.35
$Cr_{0.14}Mn_{0.86}$	−1.26
$Mn_{1.00}$	+1.60

alloy	b (mrad/μΩcm)
$Fe_{0.95}Re_{0.05}$	−0.82
$Fe_{0.84}Re_{0.16}$	−1.27
$Fe_{0.72}Re_{0.28}$	−1.34
$Re_{1.00}$	−1.25
$Rh_{0.91}Zn_{0.09}$	−1.26
$Rh_{0.71}Zn_{0.29}$	−1.22
$Rh_{0.24}Zn_{0.76}$	−1.08
$Rh_{0.09}Zn_{0.91}$	−0.65
$Rh_{0.67}Si_{0.33}$	−1.15
$Rh_{0.50}Si_{0.50}$	−1.05
$Rh_{0.33}Si_{0.67}$	−0.96
$Si_{1.00}$	−0.93
$Au_{0.85}Ru_{0.15}$	−1.10
$Mn_{0.73}Ru_{0.27}$	−1.25

The fitting was then extended to these new data to find $b^{\uparrow}$ and $b^{\downarrow}$ for Au, Ir, Mn, Re, Si and Zn. In this fitting procedure the values of $b^{\uparrow}$ and $b^{\downarrow}$, which had already been determined from the data in table 7-IIIA, were kept constant (this concerns the side-displacement coefficients of Co, Cr, Fe and Rh). The fitting procedure was effected in the same way as described before. We determined 12 adjustable parameters, corresponding to 6 solute elements, from 33 data points. After the fitting procedure the r.m.s. value was 0.14 mrad/$\mu\Omega$cm. The results, plotted as white circles in fig. 7.5, combine nicely with the other data.

A complete survey of the experimental values of the anomalous Hall angles of the alloys with a total solute concentration of three at % is given in the appendix. There we compare these values with the calculated ones using the values of $b^{\uparrow}$ and $b^{\downarrow}$ from table 2-VIII and the values of $\varphi_{sk}{}^{\uparrow}$ and $\varphi_{sk}{}^{\downarrow}$ from table 2-VII, together with a few estimated values of the skew-scattering angles.

Above and in chapter 2 we have already stressed the simple result for the two contributions to the anomalous Hall effect in nickel alloys, viz. that carriers of the majority-spin direction have negative φ_{sk} and b values, while carriers of the minority-spin direction have positive φ_{sk} and b values. The negative sign means that the anomalous Hall voltage has the same polarity as the normal Hall voltage due to free electrons. A phenomenological explanation assuming that impurities are at least partly non-transparent for electrons which can only bypass the impurities sideways was introduced in chapter 2. In this explanation the sign of $\varphi_{sk}{}^{\uparrow}$ and $b^{\uparrow}$ is determined by the orbital moment of the current carriers with respect to the impurity. This orbital moment, the sign of which is known when the spin direction is known, leads to a preference to bypass the impurity at a given side. In fact, it follows from this consideration that the anomalous Hall effect of electrons with the majority-spin direction should have the negative sign and electrons with the minority-spin direction a positive anomalous Hall effect (see table 7-IV).

A similar reversal of sign both with spin direction or with a change from electrons to holes was proposed by Kondorskii [107]). His sign convention, however, is just the reverse.

TABLE 7-IV

direction of the magnetic moment	type of carriers	sign of ϱ_{aH}
"up" (majority)	electrons	—
"up" (majority)	holes	+
"down" (minority)	electrons	+
"down" (minority)	holes	—

As explained in chapter 6, there is reason to believe that the conduction in nickel is predominantly by electron-like current carriers in both spin bands, i.e. the largest contribution to $n(\varepsilon_F)^{\uparrow}$ and $n(\varepsilon_F)^{\downarrow}$ is due to electron-like states, so that in the spin-down band, too, the anomalous Hall effect should have the sign of electrons. In iron the situation may be different, a point which will be discussed below.

Finally it may be wondered whether the values of the side-displacement coefficient b displayed in table 2-VIII correspond to side displacements Δy of the order of atomic dimensions. b values may be associated with Δy under certain assumptions as to the number of carriers and their properties. For an order-of-magnitude calculation we may take 1 electron/atom, with the mass of a free electron for the effective mass. Then $b = 1$ mrad/$\mu\Omega$cm corresponds to side displacements Δy of about 0.4 Å which is of the right order of magnitude in terms of Berger's phenomenological picture.

7.3. The anomalous Hall effect in iron-based alloys

For experimental purposes iron-based alloys are less accessible than the corresponding nickel-based alloys, the main reason being the large value of the saturation magnetization which is $4\pi M_s = 21.9$ kG in iron compared to 6.4 kG in nickel and makes it difficult to study the low-field region. In order to have B/ϱ_0 sufficiently small, resistivities of a few $\mu\Omega$cm are needed which for many impurities would result in solute concentrations of about 3 at % or more. An additional difficulty is that the field range over which the Hall effect can be measured in our experimental situation is only a factor of two. The upper field limit, which is determined by the instrument, is about 55 kOe. The lower limit is due to the magnetization and is about 22 kOe. Consequently, the uncertainties in R_0 have quite a considerable influence on the anomalous Hall effect.

For the experimental determination of φ_{sk} and b it is necessary to study φ_{aH} as a function of the total impurity concentration. Since concentrations larger than about 3 at % are not suitable and linear extrapolation of the normal Hall effect is not permissible in alloys with impurity concentrations of about 1 at %, the only possibility is to assume that a Kohler type of relation, i.e. relation (6.2), holds for the normal Hall effect. The procedure for deriving φ_{sk} and b has been described in fig. 6.2. We would like to emphasize that φ_{sk} and b values derived here only have a meaning if a single Kohler curve is thought to exist. If, as we found for nickel, the normal Hall coefficient varies with the resistivity, apart from being a function of B/ϱ_0, the Kohler procedure is invalid. In view of the restricted field range over which Hall angles are measured at various concentrations of a given impurity, it is impossible to investigate the limitations of this procedure in detail.

In table 7-V we collate information about φ_{sk} and b for iron alloys with impurities of relatively large specific resistivity, i.e. alloys in which at impurity

TABLE 7-V

The anomalous Hall effect of solutes in iron with a relatively high specific resistivity. Included are φ_3, the Hall angle at 3 at % solute concentration, and two sets of values for φ_{sk} and b. The first set was obtained in a Kohler-type analysis, the second by correcting linearly for the normal Hall effect.

solute	φ_3 (mrad)	Kohler		linear	
		φ_{sk} (mrad)	b (mrad/μΩcm)	φ_{sk} (mrad)	b (mrad/μΩcm)
Al	+18.5	+ 1	+1.3	+ 1	+1.1
Ga	+22	− 2	+1.5	− 2	+1.6
Si	+15	− 3	+1.1	0	+0.85
Ge	+23	− 1	+0.9	− 3	+0.9
Rh	+ 6	+ 2	+2	− 2	+2.6
Ir	+10	+10	0	+10	0
Pt	+ 4.5	+ 1	+0.9	+ 3	+0.4
Ru	+ 5	+ 3.5	+1.5	+ 2	+1.2
Os	+ 8	+ 8	0	+ 1	+0.8

concentrations of 1 at % the Kohler magneto*resistivity* remains below 5%. Both the values derived from the Kohler-type analysis and those obtained by linear extrapolation, assuming a field-independent normal Hall effect, are given. The differences between the two values reflect the uncertainties involved. Note that the anomalous Hall angle at a solute concentration of 3 at % does not include these uncertainties. In table 7-V there are 7 solute elements which have $i^{\downarrow}/i_{total}$ near 0 and two which have $i^{\downarrow}/i_{total}$ above 0.5. Within the uncertainties of the determination it is clear that the systematics observed earlier in nickel-based alloys are not found in iron-based alloys. As a rule we find b to be positive. However, φ_{sk} is found to have different signs even in alloys in which the same spin current dominates.

The values of φ_3, φ_{sk} and b for the remaining impurities are given in table 7-VI. Since the Kohler magnetoresistivity here exceeds 5% in the 1 at % alloys, only the Kohler-type analysis has been used to derive φ_{sk} and b. The difference relative to the systematics found in nickel-based alloys becomes even more clear, if, for example FeV and FeMn, which have about the same value of $i^{\downarrow}/i_{total}$ are compared. This difference can not be accounted for by experimental uncertainties only since the Hall angles in the 3 at % alloys are also very different. Independently of the analysis, it can be concluded that Co, Cr, Mn and V as impurity metals in Fe behave differently from the impurities recorded in

TABLE 7-VI

The anomalous Hall angle of impurity metals in iron which have a low resistivity and a Kohler magnetoresistivity larger than 5% in the 1 at % alloy. φ_{sk} and b were derived by a Kohler-type analysis. Values between brackets are less certain than the others.

solute	φ_3 (mrad)	φ_{sk} (mrad)	b (mrad/$\mu\Omega$cm)
Ni	+12	+12	0
Co	+34	(+38)	(−2)
Re	+ 8	+ 5	0
Cr	+53	+28	+4.5
Mo	+ 3	+ 7	−1
W	+ 3	+11	−2
Mn	+38	(+21)	(+3)
V	−10	(0)	(−3)

table 7-V. The small values of φ_{sk} and b found in table 7-V can never lead to the large Hall angles observed in iron alloys with 3 at % of Co, Cr, Mn or V.

Earlier information about the anomalous Hall effect in iron alloys was given for FeCo and FeCr by Majumdar and Berger [44]) and Carter and Pugh [108]). Majumdar and Berger studied FeCo alloys with concentrations between 0.25 and 1 at % Co from which they concluded that φ_{sk} is 14 mrad and b about zero. The difference in relation to our value can be easily accounted for by the fact that even at the highest concentration of Co in the experiment by Majumdar and Berger the Hall coefficient is still field-dependent in the lowest field of measurement. Nevertheless, the large difference between the two values stresses the difficulties encountered in these investigations. Majumdar and Berger observed φ_{aH} in iron with 0.25 to 0.7% Cr; Carter and Pugh studied iron alloys

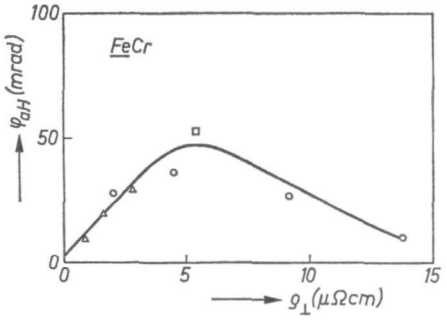

Fig. 7.6. The anomalous Hall angle in FeCr alloys as a function of the resistivity. φ_{aH} is obtained by treating R_0 as a constant, which will be doubtfull for resistivities below 2 $\mu\Omega$cm. △: Majumdar and Berger [44]), ○: Carter and Pugh [108]), □: present work.

with 0.7, 2 and 5 at % Cr. The data are compared in fig. 7.6. The anomalous Hall angles were obtained by linear extrapolation. The agreement between different experiments is quite good and one tends to the conclusion that φ_{sk} is small and b is unusually large. The maximum in φ_{aH} of 50 mrad is reached at a Cr concentration of 5 at %, suggesting that at higher concentrations impurities start to interact.

An important question is whether or not the picture for $\varphi_{sk}{}^{\uparrow}$, $\varphi_{sk}{}^{\downarrow}$, $b^{\uparrow}$ and $b^{\downarrow}$ may be a simple one, as in the case of nickel, taking into account the possibility that additional sign changes in iron occur when holes and electrons are interchanged. For iron alloys the two-current model might then be better replaced by a four-current model, viz. ↑ electrons, ↑ holes, ↓ electrons and ↓ holes. Taking for granted that φ_{sk} and b have opposite signs for electrons as compared to holes, the resulting sign for a given spin sub-band is difficult to predict. It is possible to construct a four-current model so that the trends of tables 7-V and 7-VI and the observed normal Hall effect are reproduced. It should be borne in mind that such a model is very speculative. It serves to show that the anomalous Hall effect may be basically simple, even in iron.

We assume that the conduction in iron takes place through 4 currents, i.e. the two spin currents are each subdivided into equal numbers of electrons and holes having the same $n(\varepsilon_F)$, v_F, m etc. If the four currents are scattered differently, their contributions are weighted differently. The contributions are weighted according to $1/\varrho^2$ in the normal Hall effect and according to $1/\varrho$ in the skew-scattering angle. In a four-current model the side-displacement coefficient in a binary alloy is given by $b = b_e{}^{\uparrow} + b_h{}^{\uparrow} + b_e{}^{\downarrow} + b_h{}^{\downarrow}$. If, as we derived for nickel alloys, the value of b is larger according as the resistivity is larger, we have a reversed weighting factor for the side-displacement contribution. The group of carriers that contributes least to the current, and has a large resistivity, contributes most to the side displacement. For simplicity we suppose additionally that φ_{sk} is small, as observed in table 7-V, so that φ_3 is mainly due to side displacement. We now investigate whether the sign convention adopted in table 7-IV applies to iron.

In the spin-down current we found that the normal Hall effect of all impurities has the hole sign and consequently b is expected to have the sign of ↓ electrons, which is the positive sign. If we now take as an example Co in iron, the Hall effect in the ↑ band has the electron sign. Hence in this band $b^{\uparrow}$ has the hole sign, which is also positive. The resulting b of Co in iron now has the same sign for both spin directions so that a large positive value of φ_3 is to be expected. Mn and Cr are similar to Co in the sense that here, too, the normal Hall effect has the electron sign in the down band. These two impurities likewise produce very large positive φ_3 values.

The impurities Al, Ga, Si, Ge, Ir, Rh, Ni and Pt, which have $\varrho^{\downarrow} > \varrho^{\uparrow}$ and a normal Hall effect with the hole sign in both spin bands, are expected to have a side-displacement coefficient whose sign is determined by the band with the higher resistivity. Hence φ_3 will be positive, but not as large as for Co and Mn in iron.

The reverse holds for V in iron where the normal Hall effect again has the hole sign in both spin bands and $\varrho^{\downarrow} < \varrho^{\uparrow}$. b is then expected to be negative. In fact, φ_3 is negative in $Fe_{97}V_3$.

We conclude that the anomalous Hall effects observed in iron alloys are not inconsistent with the scheme shown in table 7-IV.

If a distinction has to be made between electrons and holes in a two-spin-current model, calculation of the anomalous Hall effect would necessitate knowing four specific residual resistivities associated with each impurity element. Since this is beyond our possibilities we studied only φ_3 in ternary alloys. The results are given without further analysis in the appendix.

7.4. Some remarks on the theory of the anomalous Hall effect

Since the paper of Karplus and Luttinger [109]) the anomalous Hall effect in ferromagnetic metals has been the subject of many theoretical studies. A review of this literature up to 1972 is given by Hurd [35]). All the theories have one common feature: they are too complicated to be accessible for experimental physicists. Furthermore, the various authors disagree with each other on major points. For example, one discrepancy which has never been settled completely is whether an anomalous effect can exist in a fully periodic lattice (Karplus and Luttinger versus Smit [63])). More recently Smit [110]) and Berger [111]) have argued about the possible existence of a side-displacement contribution.

Several requirements for a reliable theoretical description of the anomalous Hall effect due to dissolved elements may be inferred from the present work.

(i) Conduction by parallel non-interacting currents of carriers with opposite spin direction should be taken into account.

(ii) The use of perturbation theory and the calculation of resistivities by integrating a scattering probability over a volume occupied by the impurity are not allowed.

(iii) A model in which conduction is assumed to be exclusively by s carriers which are scattered into d states is not acceptable.

Furthermore, impurities have, from our point of view, to be considered as large compared to the electron wavelength and non-transparent. There is no need for the anomalous Hall effect due to phonons and magnons (Ryshanova and Voloshinskiy [112])) to be treated on the same footing as that due to impurity scattering. In all theories in which the anomalous Hall effect disappears in the pure metal the effect can be expected to be a function of the resistivity that may well contain a linear and a quadratic term. It is therefore dangerous to consider the side displacement due to phonons as additive to that due to impurities. The quadratic term in the anomalous Hall effect due to phonons can only be added to the quadratic term in the anomalous Hall effect due to impurities if the physical mechanism that causes these terms is known, e.g. if both terms are known to originate in real displacements sidewards.

In view of criticisms (i), (ii) and (iii), all that remains is a phenomenological model combining skew scattering, proposed by Smit, and side displacement as proposed by Berger. The change of sign of the anomalous effects upon reversal of the spin direction was suggested by Kondorskii [107]). No quantitative comparison with theory can be made since Lyo and Holstein [113]) found that the side displacement coefficient b is a constant which depends not on the impurity but only on the matrix.

8. CONCLUSIONS

We reported experimental data on the electrical-transport properties of ferromagnetic iron- and nickel-based alloys. Binary and ternary alloys, representing all metals that can be dissolved in nickel and iron at a concentration of at least 3 at % have been investigated at 4.2 K. A main conclusion from this work is that in a description of electrical conduction properties of ferromagnetic metals one should take into account that conduction takes place by two mutually independent currents associated with the two possible spin orientations.

For 17 solute metals in nickel and 20 solute metals in iron we have derived two specific residual resistivities, one for each spin current. The identification of the two resistivities with the majority- and the minority-spin direction is made by correlating quantitatively resistivities with the magnetic-moment disturbance observed in nickel- and iron-based alloys with neutron diffraction and nuclear magnetic resonance techniques. That this correlation can be made strongly supports the validity of the two-spin-current model for nickel as well as iron.

For all alloys we determined the resistivity anisotropy (i.e. the dependence of the resistivity on the angle between the current and the magnetization). It was found that in iron alloys, too, large effects can occur, which makes iron- and nickel-based alloys very similar. The resistivity anisotropy is characteristic for the solute metal, being different for different solutes. These differences find a simple interpretation in terms of the two-current model. Within a given spin band the anisotropy effect depends only little on the solute. It is positive in the majority-spin band of nickel and the minority-spin band of iron, it is negative in the minority-spin band of nickel and around zero in the majority-spin band of iron. Thus the observed resistivity anisotropy is determined by the distribution of the total current over the two spin currents.

The present experiments on the anomalous Hall effect in nickel-based alloys show that for a given solute (or a combination of solutes) the Hall voltage is well described by a sum of two terms, one of which is linear in the resistivity and the other which varies quadratically with the resistivity. The linear term is associated with the mechanism of skew scattering, the quadratic term with that of a displacement sidewards during the scattering process. We found that both terms depend on the solute metal. As regards the skew scattering this result is in agreement with data from the literature, for the side displacement it is unexpected.

Within the two-current model the picture that emerges is simple. For the majority-spin band in nickel both terms have a negative sign, while for the minority-spin direction both terms are positive. From experiments on iron-based alloys there are indications that besides the above described change of

sign upon spin reversal, the anomalous Hall effects also change their sign when going from electron conduction to hole conduction.

Information about the limits of validity of the two-current model has been obtained from an extensive study of the normal Hall effect and the Kohler magnetoresistivity. In nickel we deduced that in the majority-spin band the Hall coefficient is not a constant but a parameter which varies systematically with the resistivity in that band, i.e. the mean free path of current carriers.

Acknowledgement

The present investigation was done in close cooperation with Dr A. R. Miedema of the Philips Research Laboratories. His contributions to both the experimental work and the physical interpretations are substantial. I am not sure whether he would have done this work without me, but I am certain that, without him, the investigation would have been much more restricted.

APPENDIX

In this appendix we give the experimental data on the electrical transport properties of nickel- and iron-based alloys at 4.2 K. The data for nickel-based alloys are given in figs A.1 up to A.19 inclusive. For iron-based alloys the data are given in figs A.20 up to and including A.35. White circles represent data which were determined for only one alloy. Black circles were determined by measuring more than one alloy with different total solute concentration.

In the top left-hand figures of figs A.1 to A.19 we recorded the resistivity in $\mu\Omega$cm in the parallel configuration ($M_s \parallel i$) at $B = 0$ for ternary nickel-based alloys as a function of the relative solute concentration. The resistivities are recalculated to a total solute concentration of 1 at %. In the top right-hand figures we give the resistivity anisotropy in %. In the bottom left-hand figures the anomalous Hall angle in mrad at a total solute concentration of 3 at % is plotted as white circles. The black circles represent the skew-scattering angle in mrad. The bottom right-hand figures give the normal Hall coefficient in 10^{-12} Ωcm/G for alloys with a total solute concentration of 3 at %. In table A-I we give some data on nickel-based alloys which were not included in the figures.

In figs A.20 up to and including A.35 we give the resistivity in $\mu\Omega$cm, left-hand figures, and the resistivity anisotropy in %, right-hand figures, for iron-based alloys. The data for the resistivity are recalculated to a total solute concentration of 1 at %. In table A-II we give experimental data on the Hall effects in ternary iron-based alloys.

The solid curves (for the skew scattering of nickel-based alloys the broken curve) are best fitting curves calculated in the two-current model. In the bottom left-hand figures of A.1 up to and including A.19 the solid curve is the best fitting curve, calculated in the two-current model, for the total anomalous Hall

TABLE A-I

Experimental data for some nickel-based alloys

alloy	$\varrho_{\parallel}$ ($\mu\Omega$cm)	$\Delta\varrho/\varrho_{\parallel}$ (%)	φ_{sk} (mrad)	b (mrad/$\mu\Omega$cm)
$Al_{0.726}Ru_{0.274}$	4.51	0.0	+1.8	—1.3
$Au_{0.854}Ru_{0.146}$	2.54	—0.2	0.0	—1.1
$Fe_{0.90}Rh_{0.10}$	1.01	+7.2		
$Fe_{0.985}Ru_{0.015}$	1.20	+6.6		
$Fe_{0.74}Ru_{0.26}$	4.17	+0.2	+2.7	—1.4
$Fe_{0.93}V_{0.07}$	4.3	+6.6		
$Mn_{0.733}Ru_{0.267}$	4.36	—0.4	+0.5	—1.25
$Ru_{0.306}Sn_{0.694}$	5.12	—0.2	—0.5	—1.0

angle in alloys with a total solute concentration of 3 at %. The broken line represents the calculated value of the skew-scattering angle. The difference between the two curves represents the Hall angle due to the side-displacement mechanism in alloys with solute concentrations of 3 at %.

TABLE A-II

Experimental data for the anomalous Hall angle and the normal Hall coefficient in iron-based alloys

alloy	φ_{aH} (mrad)	R_0 (10^{-12} Ωcm/G)
$Al_{3.0}$	+18.5	+2.0
$Al_{2.5}Co_{0.5}$	+16.4	+1.5
$Al_{2.0}Co_{1.0}$	+13.5	+0.9
$Al_{1.0}Co_{2.0}$	+ 9.5	+0.3
$Al_{0.5}Co_{2.5}$	+ 6.7	+0.4
$Co_{3.0}$	+34	−0.6
$Al_{3.0}$	+18.5	+2.0
$Al_{2.5}V_{0.5}$	+21.9	+1.1
$Al_{1.54}V_{1.0}$	+18.0	+2.0
$Al_{1.0}V_{2.0}$	+12.2	+3.2
$Al_{0.5}V_{2.5}$	+ 9.0	+2.7
$V_{3.0}$	−10	+1.0
$Co_{3.0}$	+34	−0.6
$Co_{2.73}Mn_{0.27}$	+34.3	−0.6
$Co_{1.82}Mn_{1.18}$	+36.4	−0.6
$Co_{0.86}Mn_{2.14}$	+36.2	+0.1
$Co_{0.27}Mn_{2.73}$	+36.2	+1.6
$Mn_{3.0}$	+38	+2.5
$Co_{3.0}$	+34	−0.6
$Co_{2.5}Re_{0.5}$	+13.1	+1.3
$Co_{1.96}Re_{0.69}$	+13.0	+1.3
$Co_{1.0}Re_{2.0}$	+ 5.8	+1.4
$Co_{0.59}Re_{1.89}$	+ 3.3	+2.3
$Re_{3.0}$	+ 8	+2.3

alloy	φ_{aH} (mrad)	R_0 (10^{-12} Ωcm/G)
$Mn_{3.0}$	+38	+2.5
$Mn_{2.5}Si_{0.5}$	+ 5.4	+0.9
$Mn_{2.0}Si_{1.0}$	+10.7	+1.2
$Mn_{1.0}Si_{2.0}$	+12.3	+0.5
$Mn_{0.5}Si_{2.5}$	+21.2	−0.4
$Si_{3.0}$	+15	+0.7
$Mo_{3.0}$	+ 3.0	+0.7
$Mo_{2.5}Rh_{0.5}$	+ 5.1	+0.6
$Mo_{2.0}Rh_{1.0}$	+ 4.1	+0.7
$Mo_{0.5}Rh_{2.5}$	+ 6.5	+1.8
$Rh_{3.0}$	+ 6.0	+0.8
$Os_{3.0}$	+ 8	+2.3
$Os_{2.5}Si_{0.5}$	+ 7.1	+3.3
$Os_{2.0}Si_{1.0}$	+ 7.8	+0.9
$Os_{1.0}Si_{2.0}$	+10.1	+1.0
$Os_{0.5}Si_{2.5}$	+11.8	+1.1
$Si_{3.0}$	+15	+0.7
$Rh_{3.0}$	+ 6.0	+0.8
$Rh_{4.06}Ru_{1.23}$	+ 7.9	+1.8
$Rh_{2.10}Ru_{1.15}$	+ 2.5	+1.5
$Rh_{1.13}Ru_{3.58}$	+ 5.5	+2.0
$Rh_{0.58}Ru_{2.50}$	+ 2.8	+1.8
$Ru_{3.0}$	+ 5.0	+1.8
$Ru_{3.0}$	+ 5	+1.8
$Ru_{2.41}V_{0.5}$	0	+2.3
$Ru_{1.74}V_{1.0}$	+ 0.8	+2.0
$Ru_{0.94}V_{2.0}$	+ 3.6	+1.7
$Ru_{0.54}V_{2.5}$	− 5.0	+2.0
$V_{3.0}$	−10	+1.0

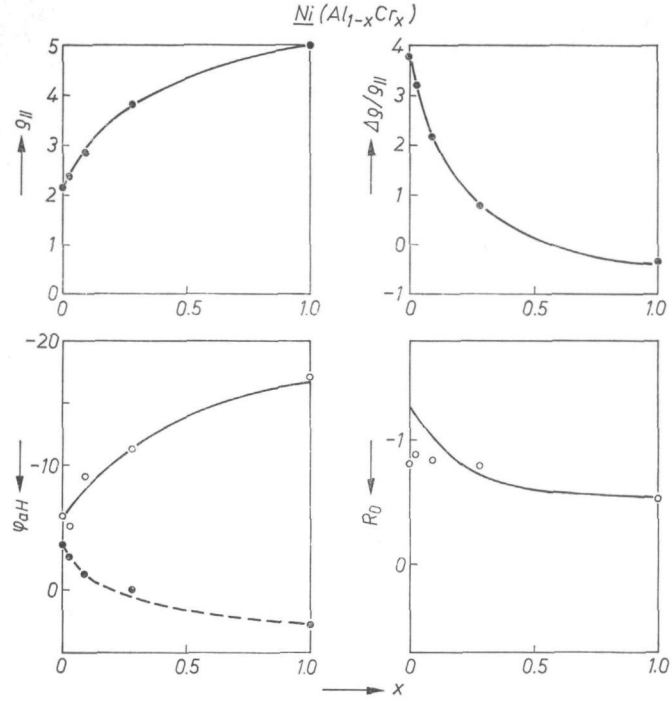

Fig. A.1

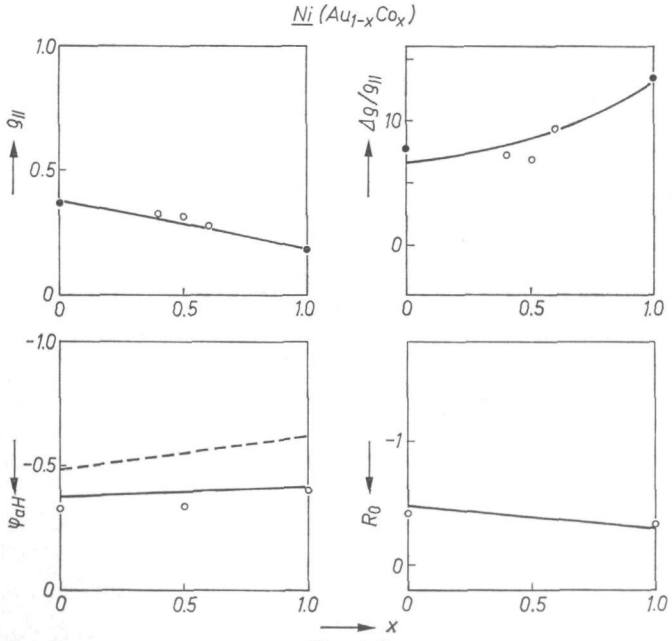

Fig. A.2

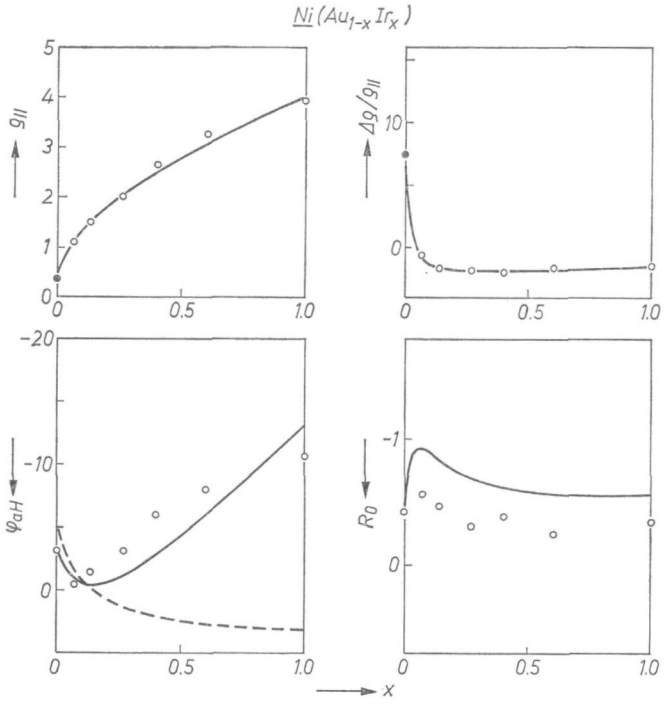

Fig. A.3

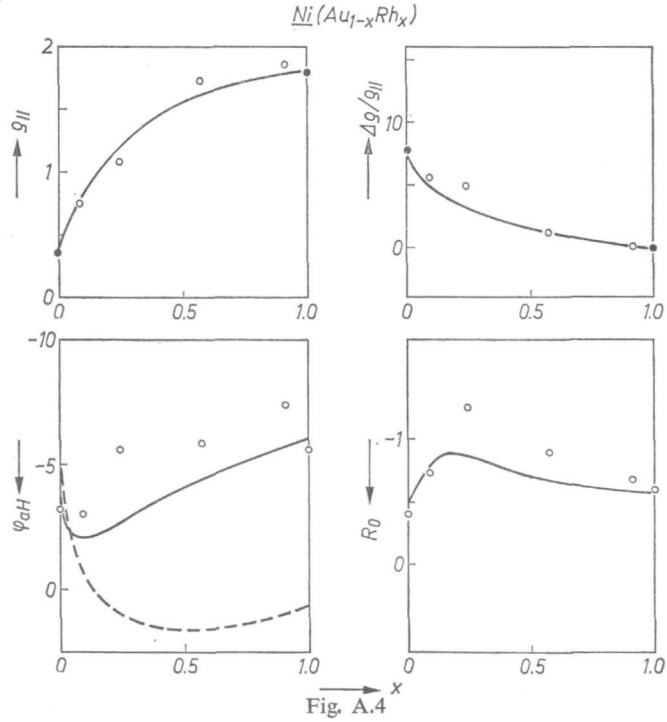

Fig. A.4

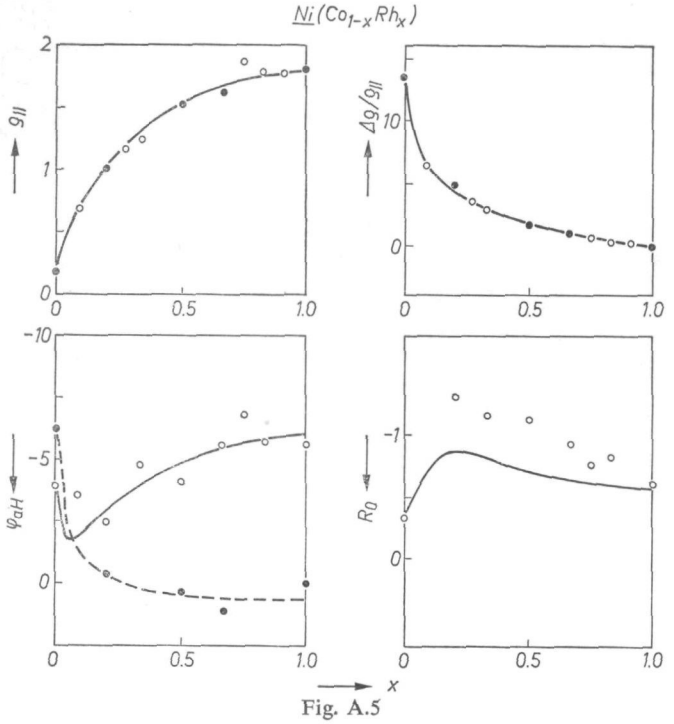
Ni(Co1-xRhx)
ρII
Δρ/ρII
ρaH
R0
x
0
0.5
1.0
2
1
-10
-5
10
-1

Fig. A.5

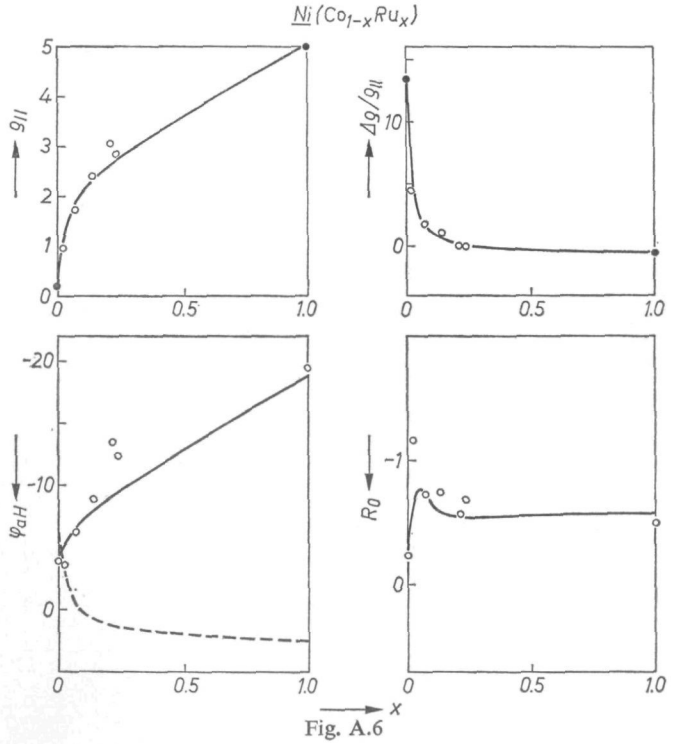
Ni(Co1-xRux)
ρII
Δρ/ρII
ρaH
R0
x
0
0.5
1.0
5
4
3
2
1
-20
-10
10
-1

Fig. A.6

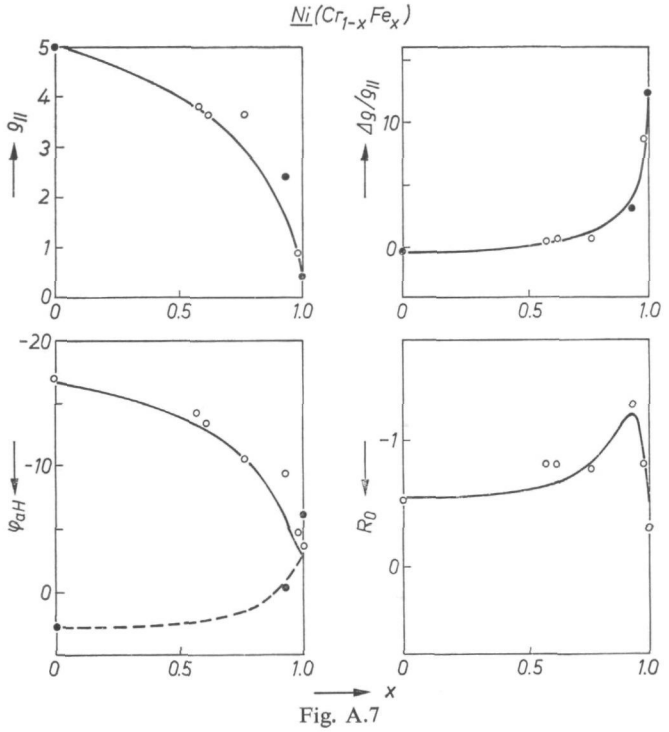

Fig. A.7

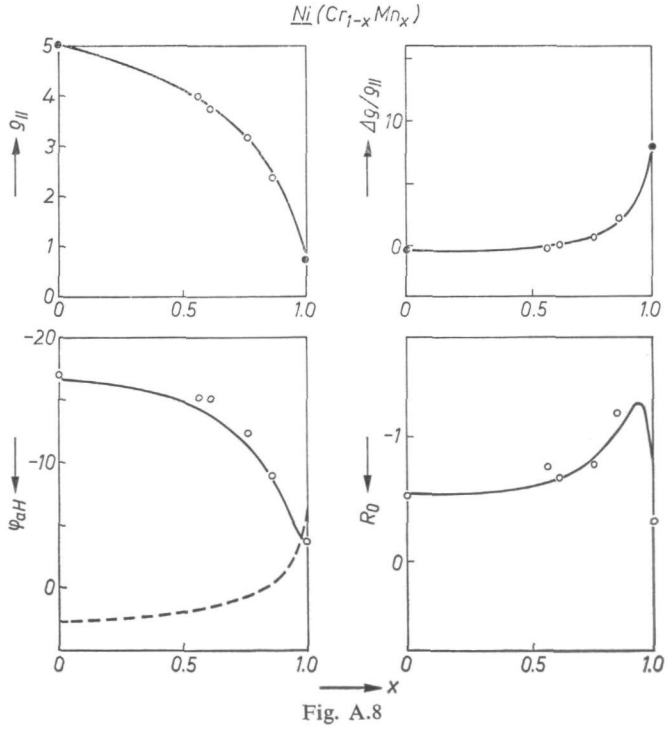

Fig. A.8

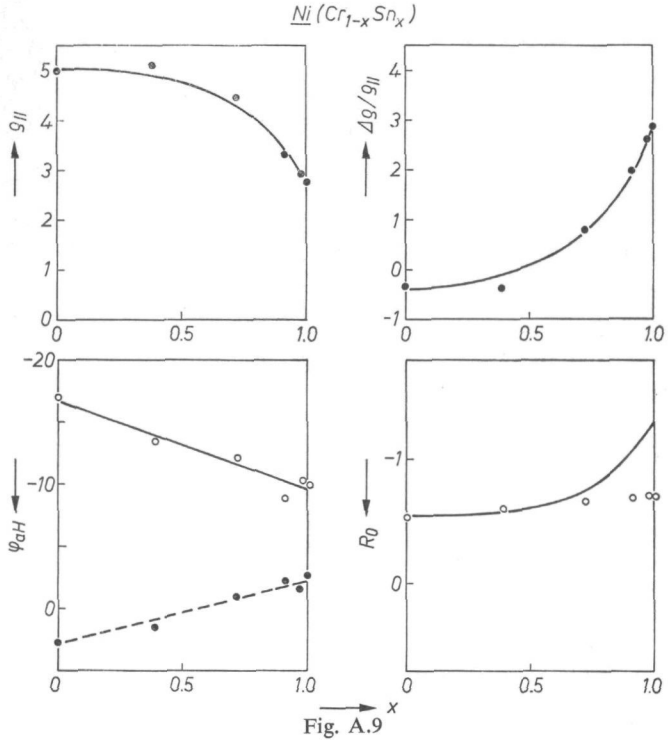

Fig. A.9

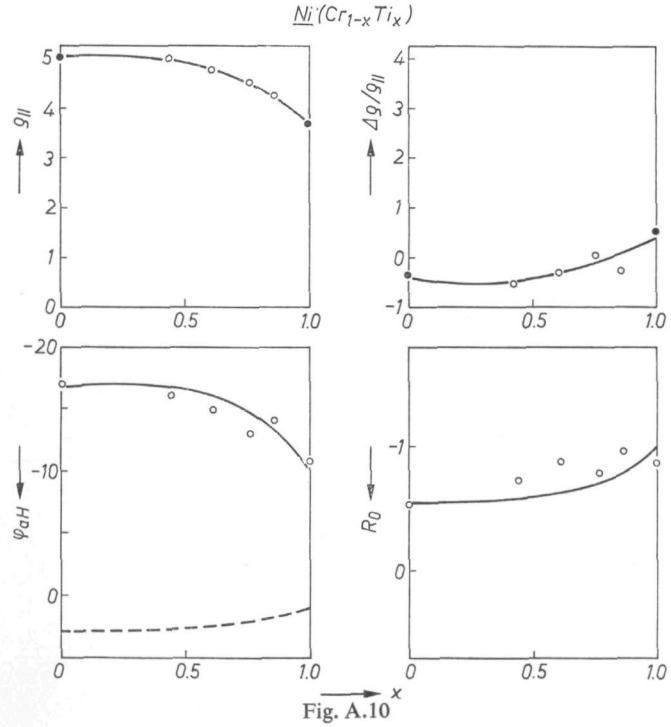

Fig. A.10

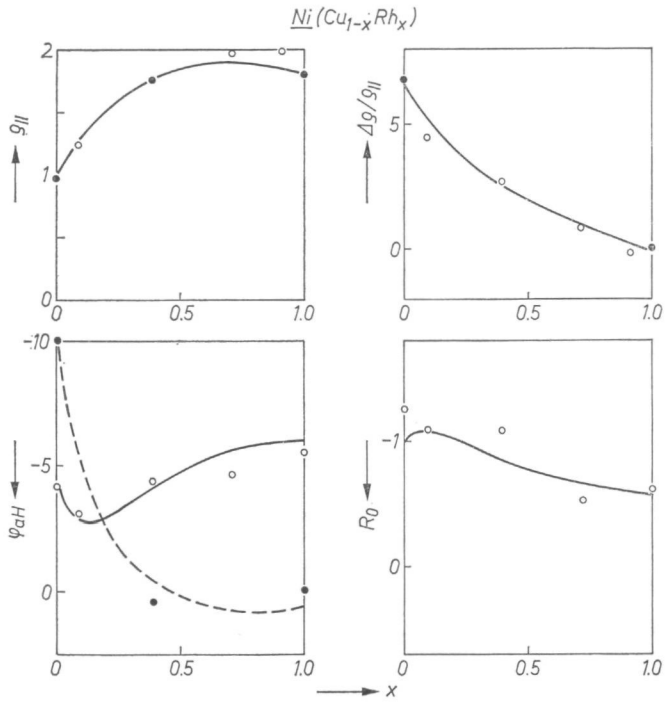

Fig. A.11

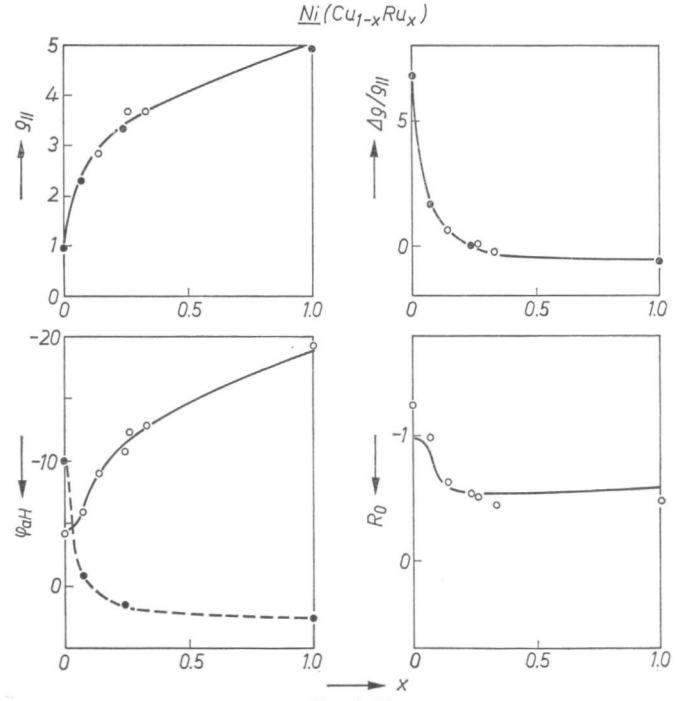

Fig. A.12

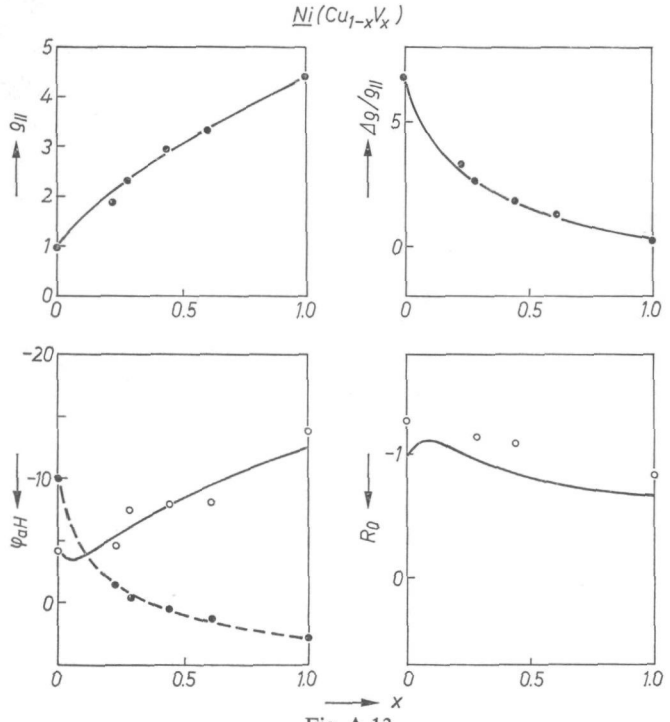

Fig. A.13

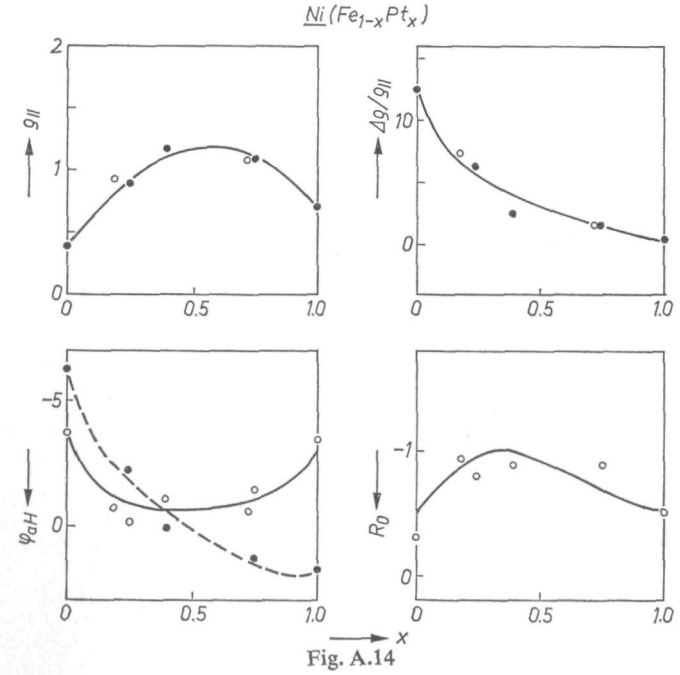

Fig. A.14

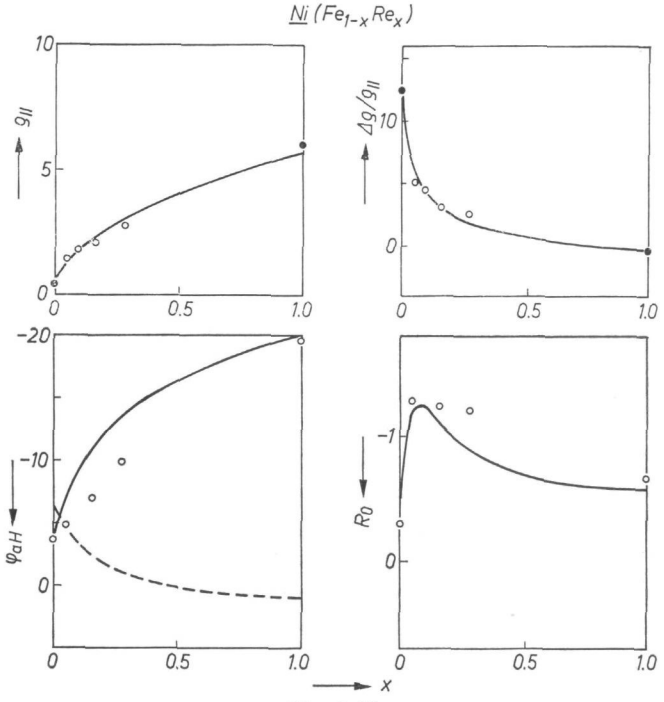

Fig. A.15

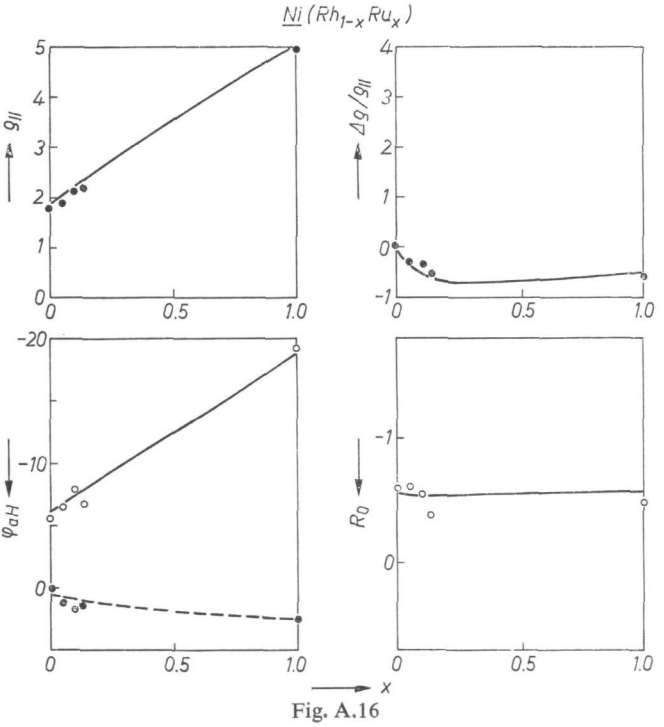

Fig. A.16

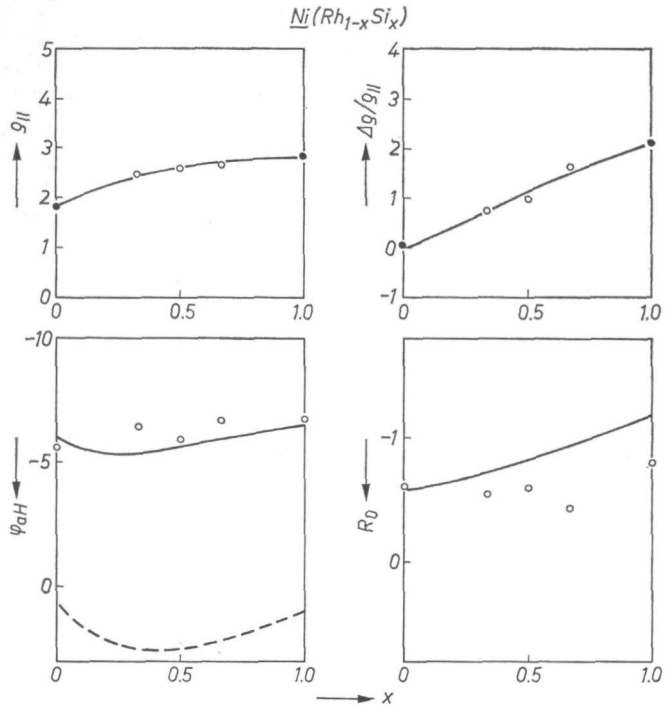

Fig. A.17

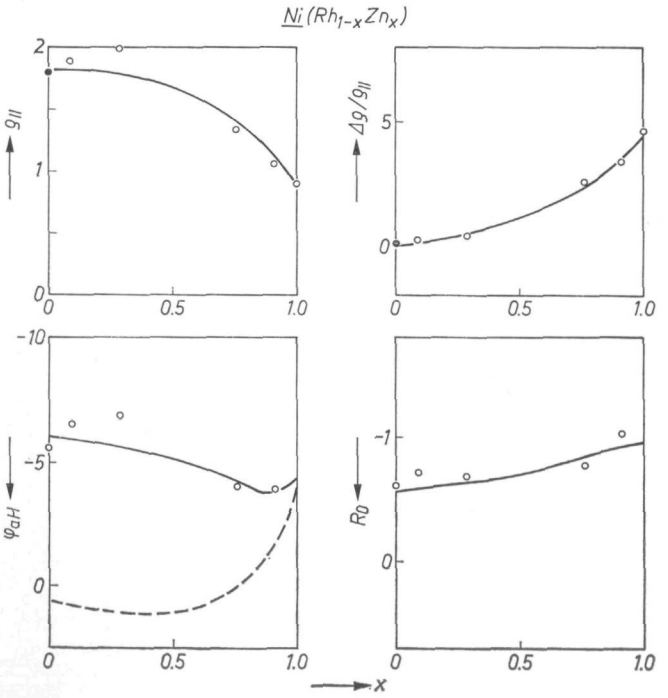

Fig. A.18

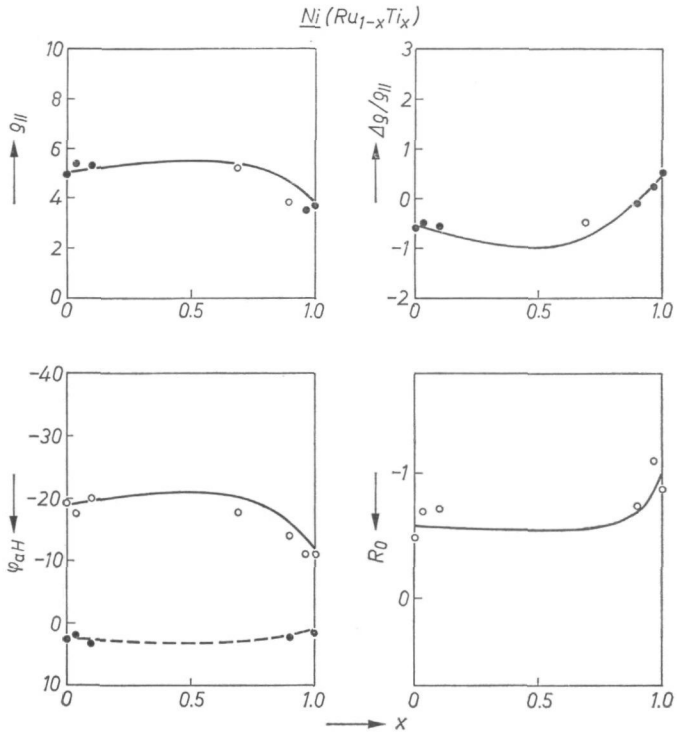

Fig. A.19

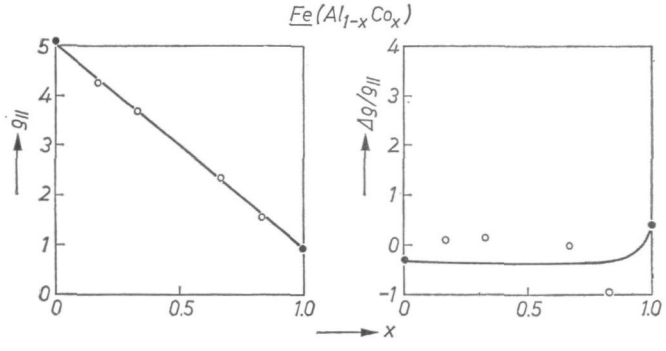

Fig. A.20

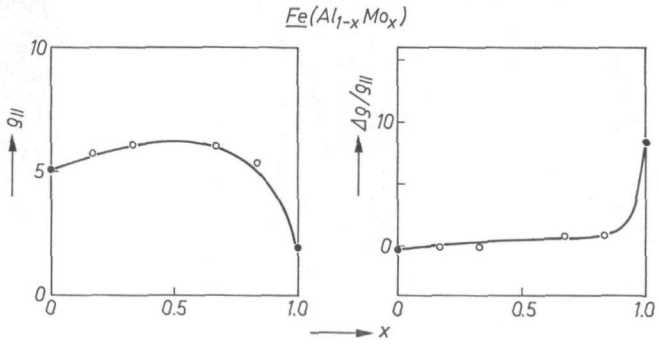

Fig. A.21

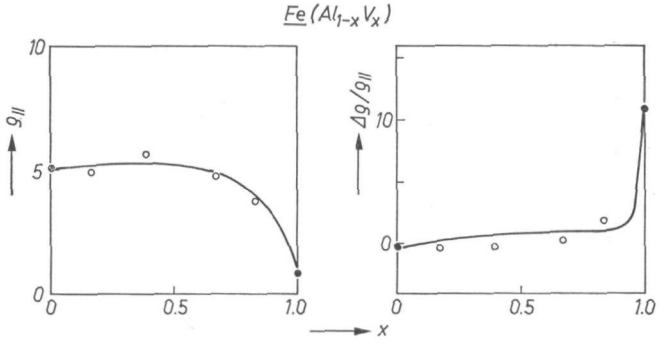

Fig. A.22

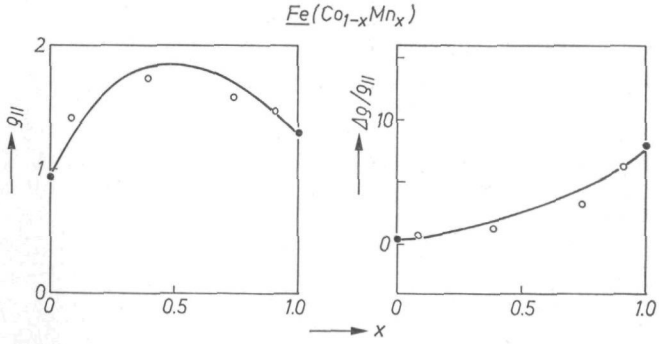

Fig. A.23

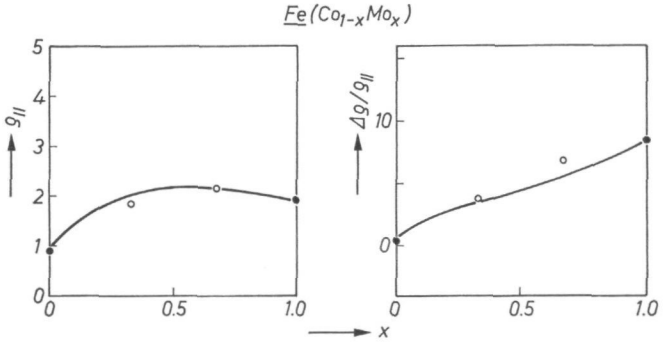

Fig. A.24

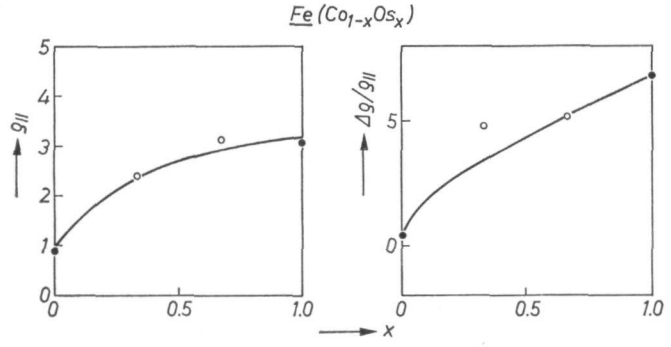

Fig. A.25

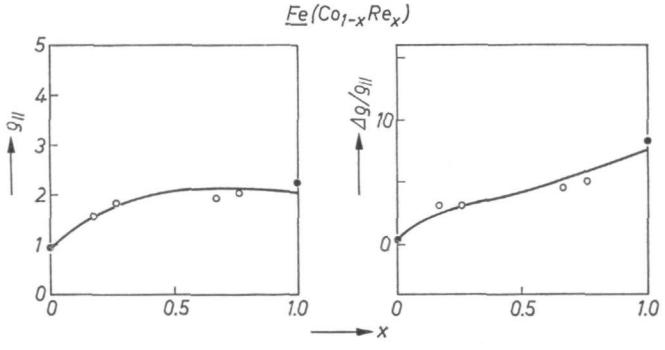

Fig. A.26

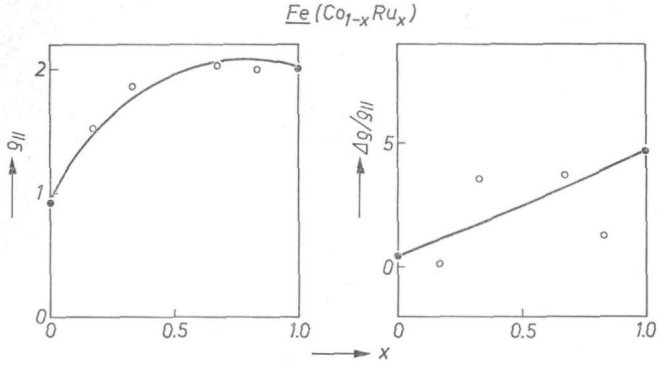

Fig. A.27

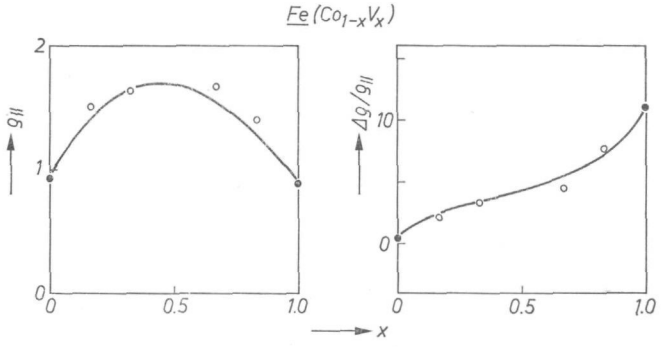

Fig. A.28

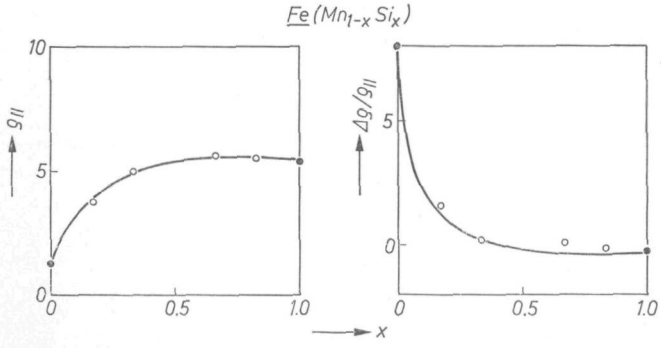

Fig. A.29

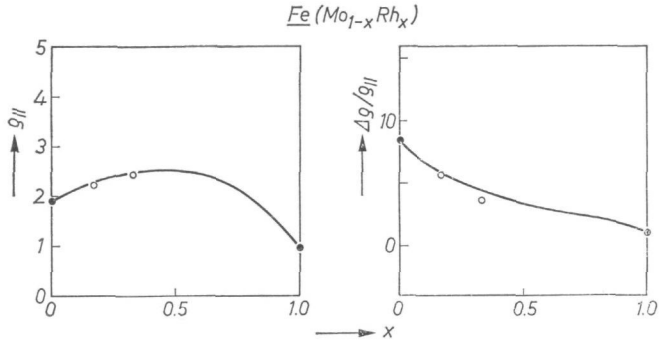

Fig. A.30

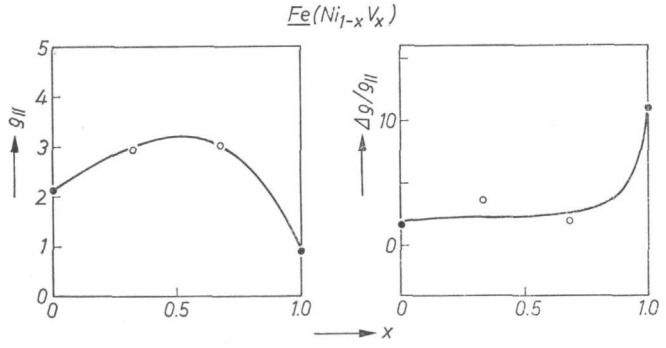

Fig. A.31

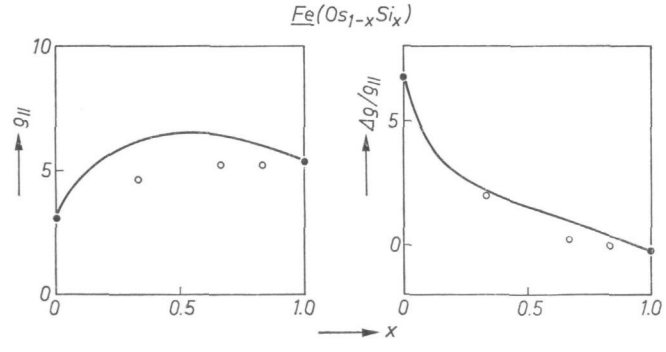

Fig. A.32

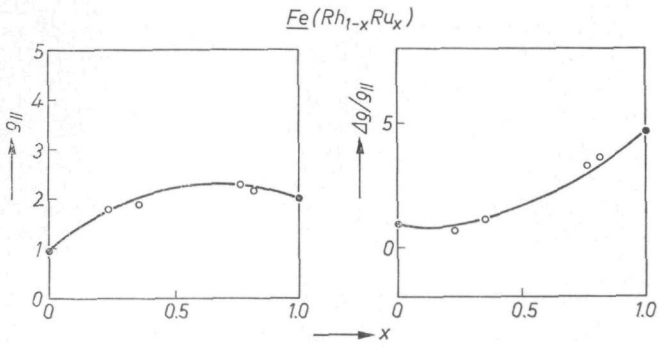

Fig. A.33

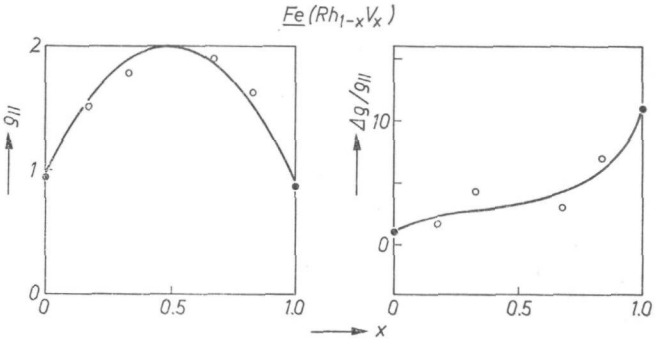

Fig. A.34

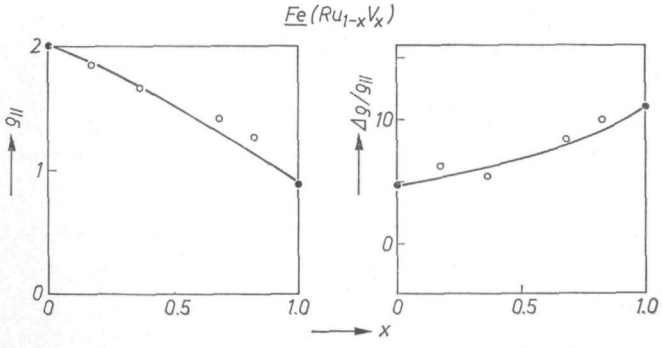

Fig. A.35

REFERENCES

1) H. C. van Elst, Physica **25**, 708, 1959.
2) R. P. Hunt, IEEE Trans. **Mag.-7**, 150, 1971.
3) F. W. Gorter, J. A. L. Potgiesser and D. L. A. Tjaden, IEEE Trans. **Mag.-10**, 899, 1974.
4) D. A. Thompson, L. T. Romankiw and A. F. Mayadas, IEEE Trans. **Mag.-11**, 1039, 1975.
5) N. F. Mott, Proc. Royal Soc. (London) **A 153**, 699, 1936.
6) N. F. Mott, Proc. Royal Soc. (London) **A 156**, 368, 1936.
7) N. F. Mott, Adv. Phys. **13**, 325, 1964.
8) A. Fert and I. A. Campbell, J. de Physique, Colloque C1, **32**, C1-46, 1971.
9) M. C. Cadeville and J. Roussel, J. Phys. F: Metal Phys. **1**, 686, 1971.
10) I. A. Campbell, A. Fert and A. R. Pomeroy, Phil. Mag. **15**, 977, 1967.
11) F. C. Schwerer, J. W. Conroy and S. Arajs, J. Phys. Chem. Solids **30**, 1513, 1969.
12) B. Loegel and F. Gautier, J. Phys. Chem. Solids **32**, 2723, 1971.
13) J. Durand and F. Gautier, J. Phys. Chem. Solids **31**, 2773, 1970.
14) J. Hugel, J. Phys. F: Metal Phys. **3**, 1723, 1973.
15) D. C. Price and G. Williams, J. Phys. F: Metal Phys. **3**, 810, 1973.
16) A. Fert and I. A. Campbell, Phys. Rev. Letters **21**, 1190, 1968.
17) T. Farrell and D. Greig, J. Phys. C (Proc. Phys. Soc.) **1**, Ser. 2, 1359, 1968.
18) F. Gautier and B. Loegel, Solid State Comm. **11**, 1205, 1972.
19) F. C. Schwerer and J. W. Conroy, J. Phys. F: Metal Phys. **1**, 877, 1971.
20) P. Leonard, M. C. Cadeville, J. Durand and F. Gautier, J. Phys. Chem. Solids **30**, 2169, 1969.
21) J. Smit, Physica **17**, 612, 1951.
22) H. C. van Elst and C. J. Gorter, Appl. sci. Res. **B4**, 87, 1954-55.
23) L. Berger, Physica **30**, 1141, 1964.
24) I. A. Campbell, Phys. Rev. Letters **24**, 269, 1970.
25) I. A. Campbell, A. Fert and O. Jaoul, J. Phys. C: Solid State Phys. **3**, Metal Phys., Suppl. 1, S95, 1970.
26) Yu. V. Vasilyev, Phys. Stat. sol. **38**, 479, 1970.
27) I. A. Campbell, J. Phys. F: Metal Phys. **4**, L181, 1974.
28) G. Dedié, J. Phys. F: Metal Phys. **5**, 706, 1975.
29) O. Jaoul and I. A. Campbell, J. Phys. F: Metal Phys. **5**, L69, 1975.
30) T. R. McGuire and R. I. Potter, IEEE Trans. **Mag.-11**, 1018, 1975.
31) O. Jaoul, Thesis, Université de Paris-Sud, Centre d'Orsay, France 1974.
32) Y. Gondo and Z. Funatogawa, J. Phys. Soc. Japan **7**, 41, 1952.
33) N. Sueda and H. Fujiwara, J. Sci. Hiroshima Univ., Ser. A, **35**, 59, 1971.
34) A. Kundt, Annalen der Physik und Chemie **49**, 257, 1893.
35) C. M. Hurd, The Hall effect in metals and alloys, Plenum Press, N.Y., 1972.
36) G. Cohen, B. Giovannini and D. Sorg, L'effet Hall extraordinaire, Comptes-rendus de la rencontre de St. Cergue du 18–20 octobre 1972, Univ. de Genève, 1973.
37) A. Fert and O. Jaoul, Phys. Rev. Letters **28**, 303, 1972.
38) R. Huguenin and D. Rivier, Helv. Phys. Acta **33**, 973, 1960.
39) R. Huguenin and D. Rivier, Helv. Phys. Acta **34**, 770, 1961.
40) R. Huguenin and D. Rivier, Helv. Phys. Acta **36**, 808, 1963.
41) R. Huguenin and D. Rivier, Helv. Phys. Acta **38**, 900, 1965.
42) D. Rivier, Helv. Phys. Acta **35**, 262, 1962.
43) D. Rivier and R. Huguenin in R. O. Davies (ed.), Proceedings of the eight international conference on low temperature physics, L.T. 8 (Queen Mary College, London 1962); Butterworths, London, 1963, p. 255.
44) A. K. Majumdar and L. Berger, Phys. Rev. **B7**, 4203, 1973.
45) J. Langlinais and J. Callaway, Phys. Rev. **B5**, 124, 1972.
46) K. J. Duff and T. P. Das, Phys. Rev. **B3**, 192, 1971.
47) S. Arajs, H. Chessin and R. V. Colvin, Phys. Stat. sol. **7**, 1009, 1964.
48) S. Arajs, F. C. Schwerer and R. M. Fisher, Phys. Stat. sol. **33**, 731, 1969.
49) C. W. Chen, Physics Letters **7**, 16, 1963.
50) M. C. Cadeville and J. Durand, Solid State Comm. **6**, 399, 1968.
51) R. A. Tawil and J. Callaway, Phys. Rev. **B7**, 4242, 1973.
52) J. Smit and J. Volger, Phys. Rev. **92**, 1576, 1953.
53) J. P. Jan and H. M. Gijsman, Physica **18**, 339, 1952.
54) L. Berger, Phys. Rev. **B2**, 4559, 1970 and Phys. Rev. **B5**, 1862, 1972.

[55]) J. Smit, Physica **24**, 39, 1958.
[56]) J. W. F. Dorleijn and A. R. Miedema, Physics Letters **55A**, 118, 1975.
[57]) J. J. M. Franse, Thesis, Univ. of Amsterdam, 1969.
[58]) J. J. M. Franse, G. de Vries and T. F. M. Kortekaas, Proc. Int. Conf. Magnetism Moscow, 1973, p. 84.
[59]) W. A. Reed and E. Fawcett, J. appl. Phys. **35**, 754, 1964.
[60]) R. Hultgren, P. D. Desai, D. T. Hawkins, M. M. Gleiser, K. K. Kelley and D. D. Wagman, Selected values of the thermodynamic properties of the elements, Am. Soc. Metals, 1973.
[61]) C. Kittel, Introduction to solid state physics, 4th ed., Wiley, N.Y., 1971.
[62]) E. I. Kondorskii, O. S. Galkina and L. A. Chernikova, Soviet Physics JETP **7**, 741, 1958.
[63]) J. Smit, Physica **21**, 877, 1955.
[64]) H. Chessin, S. Arajs and R. V. Colvin, J. appl. Phys. **35**, 2419, 1964.
[65]) M. C. Cadeville, F. Gautier, C. Robert and J. Roussel, Solid State Comm. **7**, 1701, 1969.
[66]) J. A. Dreesen and E. M. Pugh, Phys. Rev. **120**, 1218, 1960.
[67]) F. C. Schwerer and L. J. Cuddy, J. appl. Phys. **41**, 1419, 1970.
[68]) A. Fert, Thesis, Univ. de Paris-Sud, Centre d'Orsay, France, 1970.
[69]) A. Fert and I. A. Campbell, J. Phys. F: Metal Phys. **6**, 849, 1976.
[70]) D. Greig and J. A. Rowlands, J. Phys. F: Metal Phys. **4**, 232, 1974.
[71]) F. C. Schwerer, J. appl. Phys. **40**, 2705, 1969.
[72]) A. S. Joseph and A. C. Thorsen, Phys. Rev. Letters **11**, 554, 1963.
[73]) J. R. Anderson and A. V. Gold, Phys. Rev. Letters **10**, 227, 1963.
[74]) L. Berger and A. R. de Vroomen, J. appl. Phys. **36**, 2777, 1965.
[75]) F. C. Schwerer and J. Silcox, Phys. Rev. Letters **20**, 101, 1968 and J. appl. Phys. **39**, 2047, 1968.
[76]) J. A. Osborn, Phys. Rev. **67**, 351, 1945.
[77]) M. Kohler, Annalen der Physik, 5. Folge, **32**, 211, 1938.
[78]) J. W. F. Dorleijn and A. R. Miedema, J. Phys. F: Metal Phys. **5**, 487, 1975.
[79]) R. Hooke and T. A. Jeeves, J. ACM **8**, 212, 1961.
[80]) M. Bell and M. C. Pike, Comm. ACM **9**, 684, 1966.
[81]) A. Fert, J. Phys. C: Solid St. Phys. **2**, 1784, 1969.
[82]) M. F. Collins and G. G. Low, Proc. Phys. Soc. (London) **86**, 535, 1965.
[83]) G. G. Low, J. appl. Phys. **39**, 1174, 1968.
[84]) C. Demangeat, Annales de Physique **8**, 107, 1973–1974.
[85]) I. A. Campbell and A. A. Gomès, Proc. Phys. Soc. (London) **91**, 319, 1967.
[86]) J. O. Linde, Thesis, Technological University Stockholm, 1939.
[87]) R. Caudron, R. Caplain, J. Meunier and P. Costa, Phys. Rev. **B8**, 5247, 1973.
[88]) R. Caudron, J. Meunier and P. Costa, Solid State Comm. **14**, 975, 1974.
[89]) I. P. Gregory and D. E. Moody, J. Phys. F: Metal Phys. **5**, 36, 1975.
[90]) J. Durand, Thesis, Univ. de Strasbourg, France, 1969.
[91]) T. M. Holden, J. B. Comly and G. G. Low, Proc. Phys. Soc. (London) **92**, 726, 1967.
[92]) J. B. Comly, T. M. Holden and G. G. Low, J. Phys. C, **1**, Ser. 2, 458, 1968.
[93]) I. A. Campbell, Proc. Phys. Soc. (London) **89**, 71, 1966.
[94]) M. B. Stearns, Phys. Rev. **B9**, 2311, 1974.
[95]) T. R. McGuire, 20th Conf. on Magnetism and Magnetic Materials 1974, A.I.P. Conf. Proc. **24**, 435, 1974.
[96]) L. Berger, Phys. Rev. **177**, 790, 1969.
[97]) R. I. Potter, Phys. Rev. **B10**, 4626, 1974.
[98]) L. Hodges, D. R. Stone and A. V. Gold, Phys. Rev. Letters **19**, 655, 1967.
[99]) A. V. Gold, J. appl. Phys. **39**, 768, 1968.
[100]) R. W. Stark and D. C. Tsui, J. appl. Phys. **39**, 1056, 1968.
[101]) M. B. Stearns, Phys. Rev. **B13**, 1183, 1976.
[102]) F. C. Schwerer and J. Silcox, Phys. Rev. **B1**, 2391, 1970.
[103]) O. Jaoul, I. A. Campbell and A. Fert, preprint.
[104]) A. Fert, I. A. Campbell and M. Ribault, J. appl. Phys. **41**, 1428, 1970.
[105]) J. P. Jan, in F. Seitz and D. Turnbull (eds), Solid state physics, Vol. 5, Academic Press Inc., New York, 1957.
[106]) J. Crangle and D. Parsons, Proc. Royal Soc. (London) A **255**, 509, 1960.
[107]) E. I. Kondorskii, Soviet Physics JETP **28**, 291, 1969.
[108]) G. C. Carter and E. M. Pugh, Phys. Rev. **152**, 498, 1966.
[109]) R. Karplus and J. M. Luttinger, Phys. Rev. **95**, 1154, 1954.

[110]) J. Smit, Phys. Rev. **B8**, 2349, 1973.
[111]) L. Berger, Phys. Rev. **B8**, 2351, 1973.
[112]) N. V. Ryzhanova and A. N. Voloshinskiy, Physics of metals and metallogr. **35**, no. 2, 39, 1973.
[113]) S. K. Lyo and T. Holstein, Phys. Rev. Letters **29**, 423, 1972.
[114]) M. Hansen and K. Anderko, Constitution of binary alloys, 2nd ed., McGraw-Hill Book Company, New York, 1958 and Supplements by R. P. Elliot, 1965 and F. A. Shunk, 1969.
[115]) J. W. F. Dorleijn and A. R. Miedema, J. Phys. F: Metal Phys. **5**, 1543, 1975.

Summary

Experiments are reported on the electrical-conduction properties of a large number of binary and ternary alloys based on either nickel or iron. The solutes represent the elements that can be dissolved in nickel or iron at a concentration of 3 at %. At 4.2 K the resistivity, the resistivity anisotropy, the normal and the anomalous Hall effect have been measured.

The results were analysed in terms of a two-current model. In this model two mutually independent currents are associated with the two possible directions of the electron spin, viz. the majority- and the minority-spin direction. For 17 solutes in nickel and 20 solutes in iron we determined the two specific residual resistivities corresponding to the two currents. The trends among the specific resistivities found can be explained in terms of existing data on magnetic-moment disturbances around solute metals in the ferromagnetic matrix.

It was found that a simple phenomenological description of the resistivity anisotropy in nickel- or iron-based alloys can be given in terms of the two-current model. It appears that the anisotropy effect is mainly due to one of the two bands, viz. the majority-spin band in nickel and the minority-spin band in iron.

In nickel-based alloys the anomalous Hall effect, too, can satisfactorily be described in terms of the two-current model, taking into account the mechanisms of skew scattering and of side displacement. The skew-scattering angles and the coefficients for side displacement in the two bands were determined for different solutes in nickel. In the majority-spin band of nickel both the skew-scattering term and the side-displacement term are negative, in the minority-spin band of nickel both terms are found to be positive.

The limits of validity of the two-current model were observed in a study of the normal Hall effect in nickel-based alloys. It was found that within the majority-spin band of nickel the Hall coefficient varies systematically with the mean free path of the current carriers.

Samenvatting

In dit proefschrift worden experimentele resultaten weergegeven betreffende de elektrische geleidingseigenschappen van een groot aantal binaire en ternaire legeringen met nikkel of ijzer als meerderheidselement. De opgeloste elementen zijn representatief voor die elementen uit het periodiek systeem welke in nikkel of ijzer kunnen worden opgelost tot een concentratie van 3 at %. Bij een temperatuur van 4.2 K is de weerstand, de weerstandsanisotropie, het normale en het anomale Halleffect gemeten.

De resultaten zijn geanalyseerd in termen van het tweestromenmodel. In dit model wordt de totale elektrische stroom opgebouwd gedacht uit twee onderling onafhankelijke componenten die geassocieerd worden met de twee mogelijke richtingen van de elektronenspin, d.w.z. de meerderheids- en de minderheids-elektronenspin-richting. We hebben de specifieke restweerstand voor elk van de twee deelstromen bepaald voor 17 verschillende in nikkel opgeloste elementen en voor 20 verschillende in ijzer opgeloste elementen. Globaal kunnen de gevonden specifieke restweerstanden verklaard worden in termen van bestaande gegevens over de verstoring, rondom opgeloste atomen, van het magnetisch moment van de ferromagnetische matrix.

We hebben gevonden dat de weerstandsanisotropie in nikkel of ijzer legeringen phenomenologisch eenvoudig beschreven kan worden in termen van het tweestromenmodel. Het blijkt dat het anisotropie-effect voornamelijk te wijten is aan één van de twee stromen, en wel aan die welke hoort bij de meerderheids-spin-richting in nikkel en die welke hoort bij de minderheidsspin-richting in ijzer.

In nikkellegeringen kan het anomale Halleffect eveneens bevredigend beschreven worden in termen van het tweestromen-model. Hierbij moet rekening worden gehouden met de mechanismen van scheve verstrooiing ("skew scattering") en zijwaartse verplaatsing ("side displacement"). De hoeken voor scheve verstrooiing en de coefficienten voor zijwaartse verplaatsing zijn bepaald voor verschillende in nikkel opgeloste elementen voor beide deelstromen. Voor nikkellegeringen blijkt dat in de deelstroom met de meerderheidsspin-richting zowel de scheve verstrooiing als de zijwaartse verplaatsing negatief is, in de deelstroom met de minderheidsspin-richting hebben beide bijdragen tot het anomale Halleffect het positieve teken.

Een grensgeval voor wat betreft de geldige toepassing van het tweestromen-model blijkt het normale Halleffect in nikkellegeringen te zijn. We hebben gevonden dat de Hallcoefficient van de meerderheidsspin-richting systematisch varieert met de gemiddelde vrije weglengte van de ladingsdragers.

List of frequently used symbols

b	side-displacement coefficient in mrad/$\mu\Omega$cm
B	magnetic induction in G
c_A	concentration of solute element A in at %
e	electron charge in C
H	magnetic field in Oe
H_{ext}	external magnetic field in Oe
H_{dem}	demagnetization field in Oe
i	current density in A/cm^2
k	wave number of electrons in cm^{-1}
$\bar{l}$	mean free path of electrons in cm
m^*	effective electron mass in kg
M_s	saturation magnetization in G
n	density of electrons in cm^{-3}
$n(\varepsilon_F)$	density of states at the Fermi energy
N	demagnetization coefficient
R_0	normal Hall coefficient in Ωcm/G
T	temperature in K
V_H	Hall voltage in V
x	coefficient denoting solute concentration (e.g. $Ni_{99}Co_{1-x}Rh_x$)
α	ratio of sub-band resistivities ($\alpha_A = \varrho_A{}^{\downarrow}/\varrho_A{}^{\uparrow}$)
β	fraction of the total current carried by the majority-spin band ($\beta = i^{\uparrow}/i_{total}$)
γ	coefficient for the electronic specific heat in J/mol K^2
Δy	side displacement in cm
$\Delta\varrho/\varrho_{\parallel}$	resistivity anisotropy in %
ϑ_D	Debije temperature in K
μ	impurity magnetic moment in Bohr magnetons μ_B
$\varrho_{\parallel}$	electrical resistivity in the configuration with $M_s \parallel i$ at $B = 0$ in $\mu\Omega$cm
$\varrho_{\perp}$	electrical resistivity in the configuration with $M_s \perp i$ at $B = 0$ in $\mu\Omega$cm
ϱ_0	electrical resistivity at $B = 0$ in $\mu\Omega$cm
ϱ_A	specific residual resistivity due to solute A in $\mu\Omega$cm/at %
$\varrho^{\uparrow\downarrow}$	spin-flip resistivity in $\mu\Omega$cm
ϱ_T	resistivity due to thermal excitations (phonons and spin waves) in $\mu\Omega$cm
ϱ_H	total Hall resistivity in Ωcm
ϱ_{aH}	anomalous Hall resistivity in Ωcm
ϱ_{nH}	normal Hall resistivity in Ωcm
σ	electrical conductivity in ($\mu\Omega$cm)$^{-1}$
τ	characteristic time for scattering in s

φ_H	total Hall angle in mrad
φ_{aH}	anomalous Hall angle in mrad
φ_{nH}	normal Hall angle in mrad
φ_{sk}	Hall angle due to skew scattering in mrad
$\uparrow$	symbol for indicating electrons with the majority-spin direction
$\downarrow$	symbol for indicating electrons with the minority-spin direction

STELLINGEN

J. W. F. Dorleijn

2 maart 1977

I

Indien bij het vermelden van de Hallcoefficient van zuivere metalen bij lage temperatuur, in het bijzonder voor wat betreft de Hallcoefficient in de laag veld benadering, naast de zuiverheid van het metaal niet tevens vermeld wordt welke elementen als onzuiverheid voorkomen, verliest deze informatie veel van haar betekenis.

C. M. Hurd, The Hall effect in metals and alloys, Plenum-press, New York, 1972.

II

Bij de berekening van de verdeling van de elektrische stroom in complexe structuren van ferromagnetische metalen, zoals de "barber pole" voor het uitlezen van magneetbanden, dient rekening gehouden te worden met het tweestromenmodel.

III

De in sommige leerboeken gestelde regel dat atomen in legeringen gekenmerkt kunnen worden door een voor elk element karakteristiek atomair volume is niet algemeen geldig.

IV

Het is onwaarschijnlijk dat het door Coldea en Pop waargenomen NMR spectrum gedeeltelijk afkomstig is van Cu atomen op een niet-kubische roosterplaats.

M. Coldea en I. Pop, Magnetism Letters **1**, 11, 1976.

V

Het verschijnsel dat de specifieke lichtstroom van een TL-lamp afneemt met toenemende kwikdruk, wordt door Waymouth toegeschreven aan herhaalde absorptie en emissie van fotonen, door hem "imprisonment" van de straling genoemd. Deze verklaring is al te eenvoudig.

J. F. Waymouth, Electric discharge lamps, The M.I.T. Press, Cambridge, Massachusetts, 1971.

VI

De methode van Hooke en Jeeves ter minimalisatie van een funktie van N variabelen zonder nevenvoorwaarden vormt een compromis tussen enerzijds eenvoud en inzichtlijkheid der methode en anderzijds snelheid van convergentie.

R. Hooke en T. A. Jeeves, J. ACM **8**, 212, 1961.

VII

De fiscale scheiding, volgens artikel 5 van de wet op de inkomstenbelasting van 1964, van inkomstenbestanddelen van echtgenoten, is in strijd met het grondbeginsel dat belasting geheven dient te worden naar draagkracht.

VIII

De zinspreuk "Door meten tot weten", geponeerd door H. Kamerlingh Onnes, wordt ten onrechte door velen als verouderd beschouwd.

H. Kamerlingh Onnes, Redevoering uitgesproken bij de aanvaarding van het hoogleraarsambt aan de Rijks-Universiteit te Leiden, E. J. Brill, 1882.

IX

In het licht van het tweestromenmodel voor de elektrische geleiding in ferromagnetische metalen, bieden verschijnselen aan het grensvlak tussen een ferromagnetisch metaal en een tweede metaal een boeiend en geheel onontgonnen terrein van onderzoek.